ABSTRACT

Title of Dissertation:	ON THE PERFORMANCE OF
	MULTI-ANTENNA TECHNIQUES FOR
	SPATIALLY AND TEMPORALLY
	CORRELATED WIRELESS CHANNELS

Larry T. Younkins, Doctor of Philosophy, 2004

Dissertation directed by:	Professor K.J. Ray Liu
	Department of Electrical and Computer Engineering

As the demand for advanced wireless services continues to grow, system designers must employ innovative signal processing techniques to increase data throughput and maintain reliablity under adverse channel conditions. Multi-antenna techniques, such as space-time coding and beamforming, have shown promise in realizing these goals. As these and other techniques are introduced, understanding their performance in realistic scattering environments is of paramount importance.

This thesis contributes to the field of wireless communications by determining the performance of multi-antenna techniques for spatially and temporally correlated wireless channels. First, we propose a general space-time covariance model that is applicable to arbitrary scatterer geometry, arbitrary array geometry at the

base station and the mobile, and includes Doppler effects due to mobile motion. We then apply this model, in conjunction with a two-dimensional Gaussian scatterer model based on recent field measurements, to evaluate the exact pairwise error probability for arbitrary space-time block codes and determine an upper bound on the probability of a block error. In addition, we derive exact closed-form expressions for the symbol error probability for orthogonal space-time block coding, maximum ratio transmission, and beamsteering for spatially correlated quasi-static wireless channels. Finally, we present extensive numerical results that illustrate the performance of these techniques for varying degrees of spatial and temporal correlation. We also provide a comparative performance assessment of beamforming and orthogonal space-time block coding and determine the channel conditions for which one technique is favored over the other.

ON THE PERFORMANCE OF

MULTI-ANTENNA TECHNIQUES FOR

SPATIALLY AND TEMPORALLY

CORRELATED WIRELESS CHANNELS

by

Larry T. Younkins

Dissertation submitted to the Faculty of the Graduate School of the
University of Maryland, College Park in partial fulfillment
of the requirements for the degree of
Doctor of Philosophy
2004

Advisory Committee:

        Professor K.J. Ray Liu, Chairman/Advisor
        Professor Steven A. Tretter
        Professor Haralabos Papadopoulos
        Professor Min Wu
        Professor Carlos Berenstein

DEDICATION

This thesis is dedicated to my parents, Thomas D. and Shirley A. Younkins.

ACKNOWLEDGEMENTS

I would especially like to acknowledge my thesis advisor, Prof. K.J. Ray Liu. Prof. Liu's boundless energy and enthusiasm have been an inspiration for me. His dedication to students is unparalleled. Despite his prominence in the field of signal processing, commitments to many IEEE organizations, his commitment to his students is unwavering. The support and guidance he has given me during the completion of this research are truly appreciated.

I would also like to acknowledge the support of the CSPL group members. In particular, my collaboration with Dr. Weifeng Su has proven to be most beneficial.

I would be remiss without acknowledging the steadfast support of my wife and children. Their encouragement has boosted my spirits when I needed it most. Finally, I would like to acknowledge my parents. They are the ones who got me started down this road. All I need to do is complete the journey!

TABLE OF CONTENTS

LIST OF FIGURES

Chapter 1

Introduction

1.1 Motivation

Designers of modern wireless communication systems are faced with the challenge of achieving reliable communication at high data rates over a wide range of channel conditions. In addition, this must be accomplished with limited bandwidth allocation. As the demand for advanced wireless services and the number of wireless users grows, system designers must employ innovative strategies to achieve these goals.

The primary impediment to achieving reliable communication over wireless channels is multipath fading. Fading results when replicas of the transmitted signal experience slightly different propagation delays and interfere constructively or destructively at the receiver. Motion of the mobile causes fading to be time-varying, resulting in large variations in the received signal power. In order to combat the effects of multipath fading, various diversity techniques have been devised. The basic concept is to introduce redundancy in the transmitted signal and in so doing increase the probability that the signal level at the receiver, on average, is sufficient to reliably recover the transmitted data. One such diversity technique,

which has been employed at the base station of wireless systems for many years, uses multiple antennas at the receiver to capture statistically independent copies of the transmitted signal. By using a technique known as maximum ratio combining, these signal copies are combined in an appropriate fashion at the receiver to achieve diversity gain. The receive antennas must be sufficiently separated in space to ensure that the fading at each antenna is independent, otherwise, losses in diversity performance result. In addition to the spatial diversity technique just described, other approaches such as frequency, polarization or delay diversity have been considered [2]. Historically, receive diversity techniques have been implemented at the base station of a wireless system. Multiple antennas at the mobile have not found practical application, due largely to the substantial cost associated with multiple RF chains and the potential for antenna coupling.

Recently, there has been interest in the use of transmit diversity techniques at the base station. A simple delay diversity technique was proposed by Seshadri and Winters [3],[4]. This technique consists of transmitting delayed versions of the signal from multiple antennas at the base station. The delay value must be chosen such that the signals transmitted at each antenna are uncorrelated. The approach is tantamount to repetition coding and while it is capable of achieving diversity gain, the coding rate is low, since only one information symbol is transmitted over a number of time slots equal to the number of transmit antennas. A simple transmit diversity technique using two antennas, two time slots, and achieving a code rate of 1 was proposed by Alamouti [32]. This work motivated research on coding schemes for more than two transmit antennas and resulted in the seminal work of Tarokh et al. on space-time coding. [33],[34].

1.2 Space-Time Block Coding

Space-time block coding is a technique for achieving transmit diversity by coding the information symbols redundantly in space and in time. Tarokh et al. proposed space-time block code designs for PSK and QAM signal constellations for an arbitrary number of transmit antennas. These designs are based upon the mathematics of number theory, in particular, the theory of orthogonal designs. The proposed space-time block codes achieve a code rate of 1/2 for more than 4 transmit antennas and a code rate of 3/4 for designs employing 3 and 4 transmit antennas. The code design criteria is based on the pairwise error probability and the key concepts of *coding gain* and *diversity gain*. Diversity gain describes the slope of the pairwise error probability curve versus signal to noise ratio expressed in decibels. Coding gain is measured as the reduction in the signal to noise ratio required to achieve the same error probability as an uncoded system operating with the same diversity gain. A key feature of orthogonal space-time block codes is that the receiver implementation of maximum likelihood decoding can be accomplished by decoding the transmitted symbols individually and not jointly. However, it is assumed that the channel remains invariant over the space-time code block and that the receiver has complete knowledge of the complex path gains between each transmit and receive antenna pair.

Since this initial work, there has been a tremendous amount of research on the design of space-time block codes. Some of this research has focused on improving the achievable code rate for designs with more than 4 transmit antennas. See [35],[39],[40] and the references therein, for examples. Other research has addressed eliminating the requirement of channel state information at the receiver by differential code design at the transmitter. See [36],[37],[38] for additional details.

A common characteristic of all space-time code designs discussed so far is that channel information is not used at the transmitter of the wireless system.

1.3 Beamforming

Beamforming, as described herein, refers to techniques that employ channel state information at the transmitter in some fashion. Typically, reciprocity of the channel is assumed, and estimates of the channel state, as determined by the receiver, are fed back and applied at the transmitter. The channel state information can take many forms. For example, the complex path gains between each transmit and receive antenna pair may be estimated by the use of training sequences. Since the wireless channel is in general time-varying, these estimates must be updated periodically. If the channel varies quickly it may be infeasible to estimate the instantaneous complex path gains. In such cases the average channel response may be estimated, or the second-order channel statistics may be estimated. In general, both approaches have inferior performance compared to the ideal case of perfect knowledge of the instantaneous path gains of the channel. Additional information on various beamforming approaches and techniques that combine space-time coding and beamforming can be found in [27],[28],[29],[30], [31]. Since the main topic of this dissertation is the performance evaluation of transmit diversity techniques, including space-time coding and beamforming, the reader can find additional discussion on previous and related work in Chapters 2 and 3.

1.4 Overview and Contributions

The goal of this thesis is to provide a realistic evaluation of the performance of multi-antenna techniques for wireless communication systems with emphasis on the effects of spatial and temporal correlation. To achieve this goal we propose a general space-time covariance model and use it to evaluate the performance of several space-time block coding and beamforming techniques. This thesis consolidates the work presented in [65]-[68].

In Chapter 2, we present the details of the proposed space-time covariance model. The model is applicable to arbitrary array geometry at the mobil and base station, arbitrary scatterer geometry, and includes temporal effects due to mobile motion. We consider approximations to the general covariance model that are applicable when the signal from the mobile is not significantly spread in angle due to multipath. We consider applications of the proposed space-time covariance model based on several geometry-based scatterer models. The well-known 'circular ring' scatterer geometry is considered as well as a two-dimensional Gaussian scatterer model that is based on recent field measurements. Special cases of the proposed space-time covariance model are also considered, including the spatial-only case in which the temporal aspects of the model are ignored.

In Chapters 3 and 4, we evaluate the performance of several transmit diversity techniques with the aid of the proposed space-time covariance model. We consider the union bound on the block error probability for arbitrary space-time block codes based upon the exact pairwise error probability. We develop closed-form expressions for the symbol error probability for orthogonal space-time block coding, maximum ratio transmission and beamsteering for quasi-static channels with arbitrary spatial correlation. We present extensive numerical results that illustrate

the error performance of the transmit diversity techniques for the two-dimensional Gaussian scatterer model and varying degrees of temporal and spatial correlation. We consider the comparative error performance of orthogonal space-time block coding and beamforming and determine the channel conditions for which one technique is favored over the other.

In Chapter 5, we consider spatial-only processing techniques with emphasis on the reduction of co-channel interference on the uplink of a wireless communication system. With the aid of the spatial covariance model developed in Chapter 2, we evaluate the array gain of several spatial processing techniques with emphasis on the effects of multipath angular spread.

In Chapter 6, we summarize the results of this research and present some ideas for future research.

Chapter 2

Space-Time Covariance Model for Wireless Channels

2.1 Introduction

As new coding and modulation schemes are introduced to satisfy the demand for reliable communication at high data rates, understanding the performance of such techniques in realistic scattering environments is of paramount importance. In general, for diversity-based coding schemes, the best-case wireless channel is uncorrelated in space and time. These ideal conditions may be difficult to achieve in practice due to space restrictions on the placement of antennas, for example. Thus, it is important to understand the effects of non-ideal scattering environments, in particular the effects of spatial and temporal correlation, on the performance of proposed techniques.

Early research that characterized the spatial and temporal characteristics of the mobile radio channel was performed by Jakes [2] and Clarke [5]. In these works a geometric scattering model was employed that places scatterers uniformly on a circular ring a fixed distance from the mobile. More recently, Chen et al. [6]

7

extended this 'circular ring' scatterer model to include multiple antennas at the base station, a single antenna at the mobile and Doppler effects due to motion of the mobile. An example illustrating the effects of spatial and temporal correlation on antenna spacing and interleaving depth was given for a simple space-time repetition code. Shiu et al. [7] investigated the effects of fading correlation on the capacity of multiple-antenna wireless systems by employing the Jakes model to multiple antennas at the base station as well as the mobile. However, Doppler effects due to mobile motion were not considered. Abdi [8] developed at space-time correlation model for multiple antenna wireless systems by employing the 'circular ring' scattering geometry but allowing a non-uniform distribution of scatterers. Specifically, the von Mises density was used to describe the angle of arrival of the multipath with respect to the mobile. Doppler effects are included in this model. Independently, Safar [9] derived a special case of this model in which the angle of arrival was uniformly distributed.

A recent measurement campaign conducted by Pedersen et al. [10],[11],[12] has characterized the temporal and azimuth dispersion of multipath in urban wireless environments. The study found that the power azimuth spectrum was accurately modeled using a truncated Laplacian function and the power delay spectrum was well-approximated by a negative-exponential function. Recent work by Janaswamy [13] concluded that the measurements reported by Pedersen et al. were consistent with a two-dimensional Gaussian model for the scatterer locations surrounding the mobile receiver.

In this chapter we introduce a general space-time covariance model based upon scatterer geometry, transmit and receive antenna geometry and a linear motion model for the mobile. The model is applicable to arbitrary scatterer geometry

and includes Doppler effects due to mobile motion. The space-time covariance model is evaluated for the Jakes 'circular ring' scatterer geometry and the two-dimensional Gaussian scatterer geometry based on the measurements of Pedersen et al. [10],[11],[12].

This chapter is organized as follows. In Section 2.2 the development of the space-time covariance model is presented including approximations that apply for the case of small angular spread. Section 2.3 presents some applications of the proposed space-time covariance model for specific scattering geometries. Additionally, applications are presented for the spatial-only case including the uniform, Gaussian, and Laplacian angle of arrival probability density functions.

2.2   Development

The complex path gain between the pth antenna at the base and the qth antenna at the mobile is denoted by $h_{p,q}(t)$. It consists of contributions from K discrete scatterers with the mth scatterer characterized by its amplitude A_m, phase ψ_m and spatial location $\vec{x}_m$. All scatterers are assumed to be coplanar with the mobile and base station. The spatial locations of the array phase centers for the mobile and base are $\vec{x}_{mobile}$ and $\vec{x}_{base}$, respectively. The spatial location of the pth antenna at base is denoted by $\vec{x}_{base}^{p}$ and the spatial location of the qth antenna at the mobile is denoted by $\vec{x}_{mobile}^{q}$. Figure 2.1 illustrates the geometry for the scattering model. Assuming a plane wave with frequency f_c is transmitted by the base, the expression
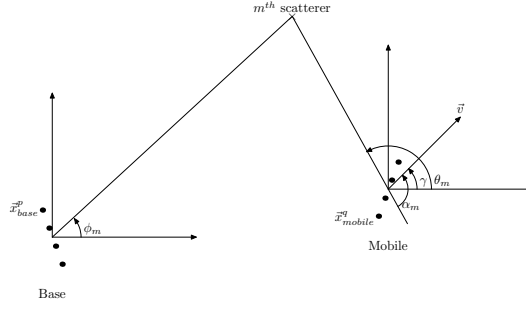
Figure 2.1: Scattering Model Geometry

for the complex path gain $h_{p,q}(t)$ is:

$$h_{p,q}(t) = \sum_{m=0}^{K-1} A_m \exp\left(j\psi_m\right) \exp\left[-j2\pi f_c \tau_m(t)\right] \tag{2.1}$$

$$\times \exp\left[+j\vec{k}_{base}^m \cdot \vec{x}_{base}^p + j\vec{k}_{mobile}^m \cdot \vec{x}_{mobile}^q\right]$$

In the previous expression $\tau_m(t)$ denotes the path delay associated with the mth scatterer and

$$\vec{k}_{mobile}^m = \frac{2\pi}{\lambda}\left(\cos\theta_m, \sin\theta_m, 0\right) \tag{2.2}$$

$$\vec{k}_{base}^m = \frac{2\pi}{\lambda}\left(\cos\phi_m, \sin\phi_m, 0\right) \tag{2.3}$$

with λ denoting the transmitted wavelength. The angle θ_m corresponds to the angle of arrival at the mobile associated with the signal re-radiated from the mth scatterer. The angle ϕ_m corresponds to the angle of departure from the base associated with the mth scatterer. The expression for the correlation between the transmission paths associated with the signal received at the qth element of the mobile array and transmitted from the pth element of the base array and the signal received by the sth element of the mobile array and transmitted from the

10

r^{th} element of the base array at time lag Δt is

$$E\left\{h_{p,q}(t)h_{r,s}^*(t+\Delta t)\right\} = E\left\{\sum_{m=0}^{K-1}\sum_{n=0}^{K-1} A_m A_n \exp\left(j\psi_m - j\psi_n\right)\right. \tag{2.4}$$

$$\times \exp\left[j2\pi f_c\left(-\tau_m(t) + \tau_n(t+\Delta t)\right)\right]$$

$$\times \exp\left[+j\vec{k}_{base}^m \cdot \vec{x}_{base}^p + j\vec{k}_{mobile}^m \cdot \vec{x}_{mobile}^q\right]$$

$$\left.\times \exp\left[-j\vec{k}_{base}^n \cdot \vec{x}_{base}^r - j\vec{k}_{mobile}^n \cdot \vec{x}_{mobile}^s\right]\right\}$$

Assuming the phases associated with the mth and n^{th} scatterers, ψ_m and ψ_n, are independent and uniformly distributed on $(-\pi, \pi)$ and independent of all other random quantities, we have

$$E\left\{h_{p,q}(t)h_{r,s}^*(t+\Delta t)\right\} = E\left\{\sum_{m=0}^{K-1} A_m^2 \exp\left[j2\pi f_c\left(-\tau_m(t) + \tau_m(t+\Delta t)\right)\right]\right. \tag{2.5}$$

$$\times \exp\left[+j\vec{k}_{base}^m \cdot (\vec{x}_{base}^p - \vec{x}_{base}^r)\right]$$

$$\left.\times \exp\left[+j\vec{k}_{mobile}^m \cdot (\vec{x}_{mobile}^q - \vec{x}_{mobile}^s)\right]\right\}$$

In order to specify the path delay associated with the mth scatterer, $\tau_m(t)$, some assumptions about the motion of the mobile must be made. In what follows we assume a linear motion model. Specifically, the spatial location of the mobile as a function of time is given by

$$\vec{x}_{mobile}(t) = \vec{x}_{mobile}^0 + \vec{v}t \tag{2.6}$$

with $\vec{x}_{mobile}^0$ denoting the initial location of the mobile and $\vec{v} = |\vec{v}|\cos\left(\gamma\right)$ denoting the velocity vector. The quantity $|\vec{v}|$ is the magnitude of velocity vector and γ is the angle the vector makes with the x-axis of the coordinate system. Using this model, the expression for the path delay is

$$\tau_m(t) = \frac{|\vec{x}_{base} - \vec{x}_m| + |\vec{x}_m - \vec{x}_{mobile}|}{c} \tag{2.7}$$

$$= \frac{|\vec{x}_{base} - \vec{x}_m| + |\vec{x}_m - (\vec{x}_{mobile}^0 + \vec{v}t)|}{c}$$

In this expression c denotes the speed of light and $|\vec{x}|$ denotes the norm of the vector $\vec{x}$. If $|\vec{x}_{mobile}^0 - \vec{x}_m| \gg |\vec{v}t|$, the path delay can be approximated by

$$\tau_m(t) \approx \tau_m^0 + \frac{|\vec{v}|t}{c} \cos \alpha_m \tag{2.8}$$

where τ_m^0 corresponds to the static (time-invariant) portion of the path delay and α_m is the angle between the mobile velocity vector $\vec{v}$ and the line joining the initial mobile location and the location of the mth scatterer. In other words, the approximation to the path delay is appropriate if the distance traveled by the mobile at time t is much less than the distance between the initial mobile location and the location of the mth scatterer.

Returning to the evaluation of the space-time correlation function (2.5) and employing the linear motion model for the mobile and the approximation developed for the path delay, we have

$$E\left\{h_{p,q}(t)h_{r,s}^*(t+\Delta t)\right\} = \exp\left(-j2\pi f_c \Delta t\right) \tag{2.9}$$
$$E\left\{\sum_{m=0}^{K-1} A_m^2 \exp\left[j2\pi f_c \left(\frac{|\vec{v}|\Delta t}{c} \cos \alpha_m\right)\right]\right.$$
$$\times \exp\left[+j\vec{k}_{base}^m \cdot (\vec{x}_{base}^p - \vec{x}_{base}^r)\right]$$
$$\left.\times \exp\left[+j\vec{k}_{mobile}^m \cdot (\vec{x}_{mobile}^q - \vec{x}_{mobile}^s)\right]\right\}$$

Define

$$\vec{x}_{base}^p - \vec{x}_{base}^r = d_{base}^{pr} \left(\cos \xi_{base}^{pr}, \sin \xi_{base}^{pr}, 0\right) \tag{2.10}$$

and

$$\vec{x}_{mobile}^q - \vec{x}_{mobile}^s = d_{mobile}^{qs} \left(\cos \xi_{mobile}^{qs}, \sin \xi_{mobile}^{qs}, 0\right) \tag{2.11}$$

The term d_{base}^{pr} corresponds to the distance between the pth and r^{th} array elements at the base and ξ_{base}^{pr} corresponds to the angle between the line joining the array

elements and the x-axis. Similarly, d_{mobile}^{qs} corresponds to the distance between the qth and s^{th} array elements at the mobile and ξ_{mobile}^{qs} corresponds to the angle between the line joining the array elements and the x-axis.

Utilizing (2.2) and (2.3) and $\cos \alpha_m = -\cos(\gamma - \theta_m)$, (2.9) becomes

$$E\left\{h_{p,q}(t)h_{r,s}^*(t + \Delta t)\right\} = \exp\left(-j2\pi f_c \Delta t\right) \qquad (2.12)$$

$$E\left\{\sum_{m=0}^{K-1} A_m^2 \exp\left[-j2\pi f_d \Delta t \cos(\theta_m - \gamma)\right]\right.$$

$$\times \exp\left[+j2\pi \frac{d_{base}^{pr}}{\lambda} \cos(\phi_m - \xi_{base}^{pr})\right]$$

$$\left.\times \exp\left[+j2\pi \frac{d_{base}^{pr}}{\lambda} \cos(\theta_m - \xi_{mobile}^{qs})\right]\right\}$$

where $f_d = f_c \frac{|\vec{v}|}{c}$ corresponds to the maximum Doppler shift associated with the mobile. Given the array geometry at the mobile and the base station, the velocity vector associated with the mobile, and the joint probability density for A_m, ϕ_m, and θ_m, (2.12) can be used to compute the desired space-time correlation.

2.2.1 Small Angular Spread Approximation

A special case of the previous result is of interest. Consider the case for which most of the scatterers are in the vicinity of the mobile. From the perspective of the base station, the angular spread of the multipath is small. Define $d = |\vec{x}_{mobile}^0 - \vec{x}_{base}|$ and $R_m = |\vec{x}_{mobile}^0 - \vec{x}_m|$. d is the distance between the mobile and the base and R_m corresponds to the scattering radius associated with the mth scatterer. If $d \gg R_m$, then the angle ϕ_m can be approximated by

$$\phi_m \approx \frac{R_m}{d} \sin \theta_m \qquad (2.13)$$

and

$$\cos \phi_m \approx 1 \tag{2.14}$$

$$\sin \phi_m \approx \frac{R_m}{d} \sin \theta_m$$

Evaluating (2.12) for the special case of *small angular spread* yields

$$E\left\{h_{p,q}(t)h_{r,s}^*(t+\Delta t)\right\} = \exp\left(-j2\pi f_c\Delta t\right)\,\exp\left[j2\pi\left(\frac{d_{base}^{pr}}{\lambda}\cos\xi_{base}^{pr}\right)\right] \tag{2.15}$$

$$E\left\{\sum_{m=0}^{K-1} A_m^2 \exp\left[j2\pi\left(\frac{d_{mobile}^{qs}}{\lambda}\cos\xi_{mobile}^{qs} - f_d\Delta t\cos\gamma\right)\cos\theta_m\right]\right.$$

$$\times \exp\left[j2\pi\left(\frac{d_{base}^{pr}}{\lambda}\frac{R_m}{d}\sin\xi_{base}^{pr}\right)\sin\theta_m\right]$$

$$\left.\times \exp\left[j2\pi\left(\frac{d_{mobile}^{qs}}{\lambda}\sin\xi_{mobile}^{qs} - f_d\Delta t\sin\gamma\right)\sin\theta_m\right]\right\}$$

In this result the scattering geometry is specified by the joint probability distribution of the scattering radius about the mobile, R_m, and the angle θ_m associated with the mth scatterer. The equation is applicable to arbitrary scattering geometry subject to the small angular spread approximation, $d \gg \max\{R_m\}_{m=0}^{K-1}$.

Equation (2.15) describes the correlation between the transmission path from the pth transmit antenna to the qth receive antenna and the transmission path from the rth transmit antenna to the sth receive antenna with time separation Δt. In order to apply this result the mobile velocity vector and initial distance from the base must be specified as well as the array geometry at the base and the mobile. Additionally, the joint probability distribution of the scatterer amplitude A_m, radius R_m and angle θ_m with respect to the mobile must be given. In most cases of practical interest (2.15) must be numerically integrated to yield a result. We consider now simplifications that result by ignoring the temporal aspects of the path correlation and considering single antennas at either the base or mobile.

2.2.2   Spatial-Only Case, Single Mobile Antenna

Evaluating (2.12) for the case of zero time lag, i.e. $\Delta t = 0$, and a single antenna at the mobile we have

$$E\left\{h_{p,1}(t)h_{r,1}^*(t)\right\} = E\left\{\sum_{m=0}^{K-1} A_m^2 \exp\left[j2\pi\frac{d_{base}^{pr}}{\lambda}\cos\left(\phi_m - \xi_{base}^{pr}\right)\right]\right\} \qquad (2.16)$$

Employing the generating function for the nth order Bessel function of the first kind [1]

$$\exp\left(jz\cos\phi\right) = \sum_{n=-\infty}^{\infty} \exp\left[jn\left(\phi + \frac{\pi}{2}\right)\right] J_n(z) \qquad (2.17)$$

on (2.16), we have

$$E\left\{h_{p,1}(t)h_{r,1}^*(t)\right\} = E\left\{\sum_{m=0}^{K-1} A_m^2 \sum_{n=-\infty}^{\infty} \exp\left[jn\left(\phi_m - \xi_{base}^{pr} + \frac{\pi}{2}\right)\right] J_n\left(2\pi\frac{d_{base}^{pr}}{\lambda}\right)\right\}$$

$$(2.18)$$

$$= \sum_{n=-\infty}^{\infty} \exp\left[jn\left(-\xi_{base}^{pr} + \frac{\pi}{2}\right)\right] J_n\left(2\pi\frac{d_{base}^{pr}}{\lambda}\right) E\left\{\sum_{m=0}^{K-1} A_m^2 \exp\left(jn\phi_m\right)\right\}$$

If the mth scatterer amplitude A_m and angle of arrival ϕ_m are assumed to be independent of each other and identically distributed, with $E(A_m^2) = \frac{A^2}{K}$ and $\phi_m = \phi$

$$E\left\{h_{p,1}(t)h_{r,1}^*(t)\right\} = A^2 \sum_{n=-\infty}^{\infty} \exp\left[jn\left(-\xi_{base}^{pr} + \frac{\pi}{2}\right)\right] J_n\left(2\pi\frac{d_{base}^{pr}}{\lambda}\right) E\left\{\exp\left(jn\phi\right)\right\} \qquad (2.19)$$

Equation (2.19) depends on the array geometry at the base station and the characteristic function of the angle ϕ. In practice, the infinite sum appearing in (2.19) is truncated to obtain a finite-term approximation suitable for computation. The number of terms retained in the approximation depend on the rate of decay of the Bessel function and the characteristic function of the angle of arrival ϕ with

increasing n. An upper bound for the nth order Bessel function of the first kind is given by [1]

$$|J_n(u)| \leq \frac{|u/2|^n}{n!} \tag{2.20}$$

2.2.3 Spatial-Only Case, Single Base Antenna

Evaluating (2.12) for the case of zero time lag, i.e. $\Delta t = 0$, and a single antenna at the base we have

$$E\left\{h_{1,q}(t)h_{1,s}^*(t)\right\} = E\left\{\sum_{m=0}^{K-1} A_m^2 \exp\left[j2\pi \frac{d_{mobile}^{qs}}{\lambda} \cos\left(\theta_m - \xi_{mobile}^{qs}\right)\right]\right\} \tag{2.21}$$

Pursuing a development similar to that presented in the previous section with $E(A_m^2) = \frac{A^2}{K}$ and $\theta_m = \theta$, we have

$$E\left\{h_{1,q}(t)h_{1,s}^*(t)\right\} = A^2 \sum_{n=-\infty}^{\infty} \exp\left[jn\left(-\xi_{mobile}^{qs} + \frac{\pi}{2}\right)\right] J_n\left(2\pi \frac{d_{mobile}^{qs}}{\lambda}\right) E\left\{\exp\left(jn\theta\right)\right\} \tag{2.22}$$

2.3 Applications

In this section we present some applications of the proposed space-time covariance model. We provide numerical results based on the 'circular ring' scatterer geometry due to Jakes [2] and the two-dimensional Gaussian scatterer geometry motivated by the measurements of Pedersen et al. [10],[11],[12]. In addition, we present numerical results for the spatial-only case for the uniform, Gaussian and Laplacian angle of arrival probability density functions.

2.3.1 Jakes 'circular ring' scatterer model

For the case of the 'circular ring' scattering model attributed to Jakes [2] a closed-form expression for the complex path correlation can be obtained. This result is useful for validating the proposed space-time covariance model since it can be compared with previously published results. For the Jakes model the radius of each scatterer is fixed, i.e. $R_m = R$, and the angle of arrival θ_m is independent for each scatterer and uniformly distributed on $(-\pi, \pi)$. It is further assumed that the scatterer amplitude A_m is independent of the angle θ_m and $E(A_m^2) = \frac{A^2}{K}$ for all m. With these assumptions, evaluating the expectation in (2.15) yields

$$E\left\{h_{p,q}(t)h_{r,s}^*(t+\Delta t)\right\} = A^2 \exp\left(-j2\pi f_c \Delta t\right) \exp\left[j2\pi\left(\frac{d_{base}^{pr}}{\lambda}\cos\xi_{base}^{pr}\right)\right] \quad (2.23)$$

$$\times J_0\left(2\pi\left[\left(\frac{d_{base}^{pr}}{\lambda}\frac{R}{d}\sin\xi_{base}^{pr} + \frac{d_{mobile}^{qs}}{\lambda}\sin\xi_{mobile}^{qs} - f_d\Delta t\sin\gamma\right)^2\right.\right.$$

$$\left.\left. + \left(\frac{d_{mobile}^{qs}}{\lambda}\cos\xi_{mobile}^{qs} - f_d\Delta t\cos\gamma\right)^2\right]^{1/2}\right)$$

where $J_0(\cdot)$ denotes the zeroth-order Bessel function. This result is in agreement with that derived earlier in [8] for the special case of isotropic scattering and in [9].

To gain insight into the characteristics of the complex path correlation due to spatial and temporal effects for the Jakes model, consider the following special cases:

Case1 $d_{base}^{pr} = 0 = d_{mobile}^{qs}$. This case corresponds to single transmit and receive antennas and considers only temporal correlation. The magnitude of the complex path correlation for this case is proportional to $|J_0\left(2\pi f_d \Delta t\right)|$. Uncorrelated space-time symbols result for normalized Doppler frequency $f_d\Delta t = 0.383$.

Case2 $d_{mobile}^{qs} = 0$ and $\Delta t = 0$. This case corresponds to a single receive antenna and considers spatial correlation due to the spacing of the transmit antennas. Temporal effects are not considered. For this case the magnitude of the complex path correlation is proportional to $|J_0 \left(2\pi \frac{d_{base}^{pr}}{\lambda} \frac{R}{d} \right)|$. Note that the transmit antenna spacing required to achieve uncorrelated paths depends on the ratio of the scattering radius to the distance between the transmitter and receiver, R/d. For the (unrealistic) case of $R/d = 1$, uncorrelated paths result for $d_{base}^{pr} = 0.383\lambda$. If $R/d = 0.01$ then a transmit antenna spacing of 38.3λ is required to achieve uncorrelated paths.

Case3 $d_{base}^{pr} = 0$ and $\Delta t = 0$. This case corresponds to a single transmit antenna and considers spatial correlation due to the spacing of the receive antennas. Temporal effects are not considered. For this case the magnitude of the complex path correlation is proportional to $|J_0 \left(2\pi \frac{d_{mobile}^{qs}}{\lambda} \right)|$. The receive antenna spacing required to achieve uncorrelated paths is $d_{mobile}^{qs} = 0.383\lambda$ and does not depend on the scattering radius.

These special cases are in agreement with previous results due to Jakes and Clarke [2],[5].

In order to give additional insight into the space-time correlation for the Jakes scattering model, we present some numerical results. We consider a pair of antennas at the base station oriented such that the mobile is located at an angle ϕ_0 relative to the perpendicular of the line joining the antennas. The mobile speed was fixed at 100km/hr and the carrier frequency was $f_c = 850$MHz resulting in a

maximum Doppler frequency of $f_d = 78$Hz. The mobile direction was along the perpendicular of the line joining the pair of antennas. Three values were considered for the scatterer radius, $R = 10, 50, 200$m, and the distance between the base antenna array (phase center) and the initial mobile location was fixed at d=1000m. The smallest value for the scattering radius yields a ratio $R/d = 0.01$ and corresponds to an angular spread of approximately $1°$ from the perspective of the base station. The largest value for the scattering radius yields a ratio $R/d = 0.2$ and corresponds to an angular spread of approximately $20°$. Figures 2.2-2.4 show the magnitude of the path correlation for $R/d = 0.01, 0.05, 0.2$, respectively, and for $\phi_0 = 0°$. In addition, each figure shows the path correlation for four values of normalized Doppler frequency: $f_d \Delta t = 0.0, 0.1, 0.2, 0.3$. With reference to Figure 2.2 it is seen that the element spacing required for zero path correlation is approximately 38λ for $R/d = 0.01$ and $f_d \Delta t = 0.0$. Figures 2.3 and 2.4 illustrate that the element spacing required for zero path correlation decreases as the scattering radius, or equivalently, the angular spread is increased. With reference to these figures note the general oscillatory nature of the path correlation for the Jakes model for large element separation ($> 5\lambda$). This is associated with the behavior of the Bessel function $J_0(z)$ and is due to the (unrealistic) assumption that all multipath scatterers lie on a circular ring of radius R around the mobile. Figures 2.2- 2.4 also illustrate that the most significant temporal effects occur for small scattering radius and small antenna spacing.

Figures 2.5-2.7 show the magnitude of the path correlation for $R/d = 0.01, 0.05, 0.2$, respectively, and for $\phi_0 = 45°$. For this case the mobile is $45°$ off of broadside of the two-element array. Comparing Figures 2.2 and 2.5 it can be observed that the element spacing required for zero path correlation is increased for $\phi_0 = 45°$ compared
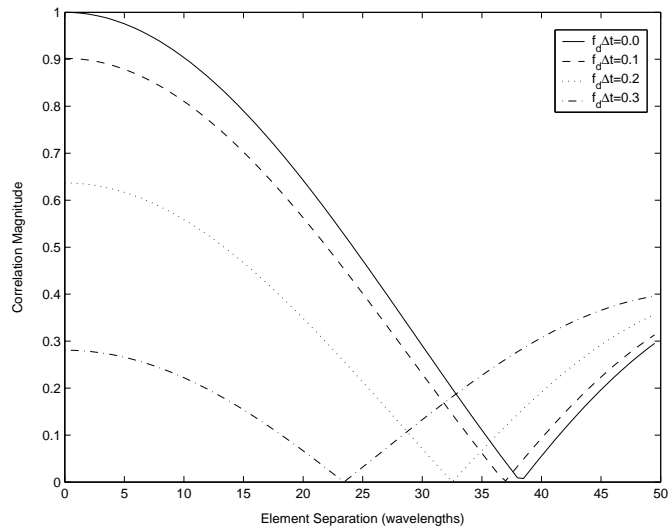
Figure 2.2: Magnitude of the path correlation for the Jakes 'circular ring' model, $R/d = 0.01$, $\phi_0 = 0°$

to the broadside case, $\phi_0 = 0°$. These observations highlight the influence of array geometry on the behavior of the path correlation. For linear array geometry the angle between a pair of array elements and the mean angle of arrival is constant for all element pairs. For a circular array, however, this angle varies with each element pair resulting in a combination of effects due to element separation and orientation with respect to the mean angle of arrival.

2.3.2   2D Gaussian scatterer model

The motivation for the two-dimensional Gaussian scattering model is due to a recent measurement campaign conducted by Pedersen et al. [10],[11],[12] in which the temporal and azimuth dispersion of multipath in urban wireless environments was characterized. The study found that the power azimuth spectrum was accurately modeled using a truncated Laplacian function and the power delay spectrum was

20
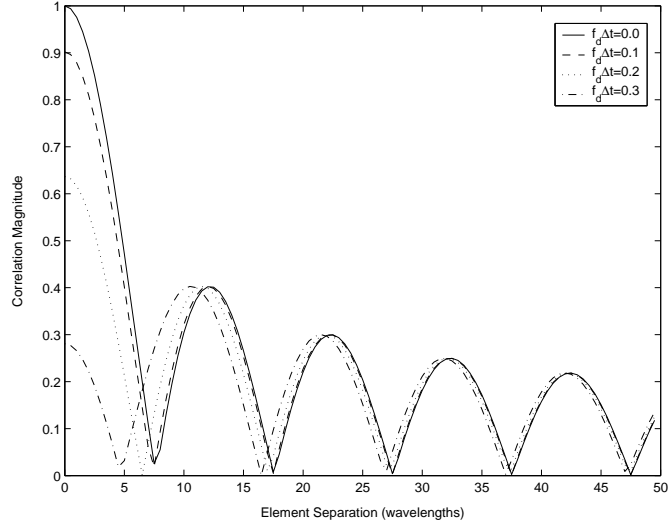
Figure 2.3: Magnitude of the path correlation for the Jakes 'circular ring' model, $R/d = 0.05$, $\phi_0 = 0°$
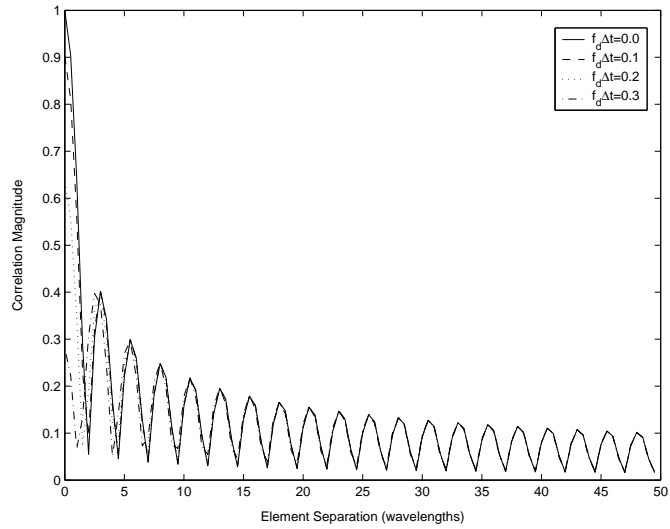
Figure 2.4: Magnitude of the path correlation for the Jakes 'circular ring' model, $R/d = 0.2$, $\phi_0 = 0°$
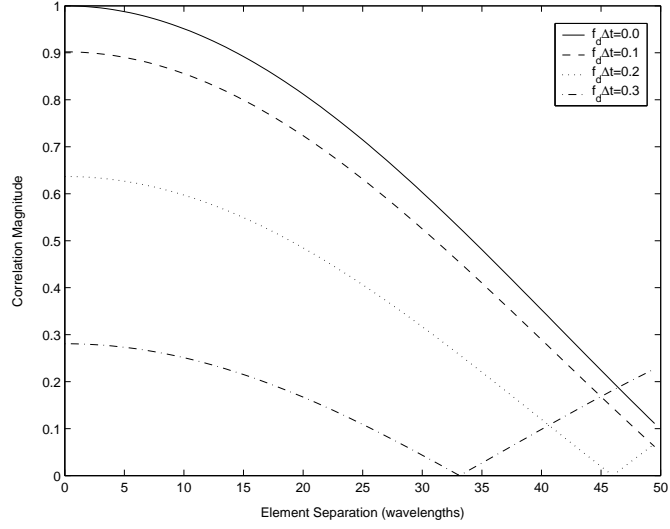
Figure 2.5: Magnitude of the path correlation for the Jakes 'circular ring' model, $R/d = 0.01$, $\phi_0 = 45°$
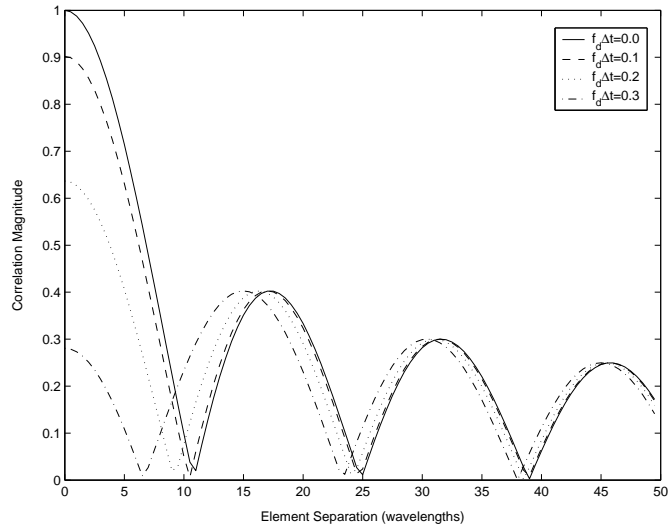
Figure 2.6: Magnitude of the path correlation for the Jakes 'circular ring' model, $R/d = 0.05$, $\phi_0 = 45°$
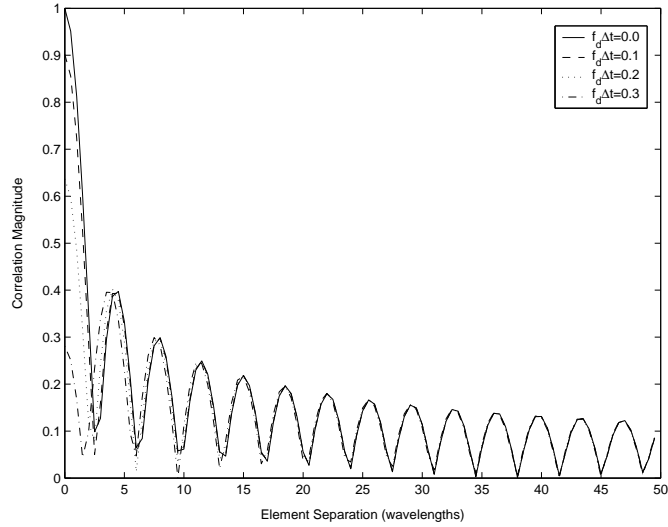
Figure 2.7: Magnitude of the path correlation for the Jakes 'circular ring' model, $R/d = 0.2$, $\phi_0 = 45°$

well-approximated by a negative-exponential function. Recent work by Janaswamy [13] concluded that the measurements reported by Pedersen et al. were consistent with a two-dimensional Gaussian model for the scatterer locations surrounding the mobile receiver.

For the two-dimensional Gaussian model the expression for the path correlation, (2.15) for the case of small angular spread, must be numerically integrated to yield a result. The scatterer radius R_m associated with the mth scatterer has a Rayleigh density and the scatterer angle θ_m is uniformly distributed on $(-\pi, \pi)$. It is assumed that (R_m, θ_m) are independent and identically distributed for each m. It is further assumed that the scatterer amplitude A_m is independent of the scatterer radius R_m and angle θ_m and that $E(A_m^2) = \frac{A^2}{K}$ for all m. The two-dimensional Gaussian model is parameterized by σ_R which specifies the radius about the mobile for which approximately 68 percent of the scatterers are contained.

We present some numerical results for the path correlation associated with the two-dimensional Gaussian scatterer model. The setup is the same as that for the Jakes 'circular ring' scatterer model and is repeated here for the convenience of the reader. We consider a pair of antennas at the base station oriented such that the mobile is located at an angle ϕ_0 relative to the perpendicular of the line joining the antennas. The mobile speed was fixed at 100km/hr and the carrier frequency was $f_c = 850$MHz resulting in a maximum Doppler frequency of $f_d = 78$Hz. The mobile direction was along the perpendicular of the line joining the pair of antennas. Three values were considered for the scatterer radius standard deviation, $\sigma_R = 10, 50, 200$m, and the distance between the base antenna array (phase center) and the initial mobile location was fixed at d=1000m. The smallest value for the scattering radius standard deviation yields a ratio $\sigma_R/d = 0.01$ and corresponds to an angular spread of approximately 1° from the perspective of the base station. The largest value for the scattering radius standard deviation yields a ratio $\sigma_R/d = 0.2$ and corresponds to an angular spread of approximately 20°.

Figures 2.8-2.10 illustrate the magnitude of the path correlation for $\sigma_R/d = 0.01, 0.05, 0.2$, respectively, and for $\phi_0 = 0°$. In addition, each figure shows the path correlation for four values of normalized Doppler frequency: $f_d\Delta t = 0.0, 0.1, 0.2, 0.3$.

Figures 2.11-2.13 show the magnitude of the path correlation for $\sigma_R/d = 0.01, 0.05, 0.2$, respectively, and for $\phi_0 = 45°$. In addition, each figure shows the path correlation for four values of normalized Doppler frequency: $f_d\Delta t = 0.0, 0.1, 0.2, 0.3$.
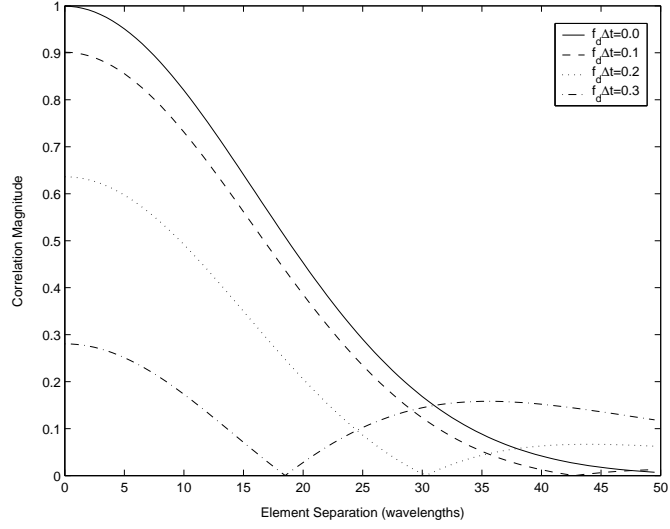
Figure 2.8: Magnitude of the path correlation for the two-dimensional Gaussian model, $\sigma_R/d = 0.01$, $\phi_0 = 0°$
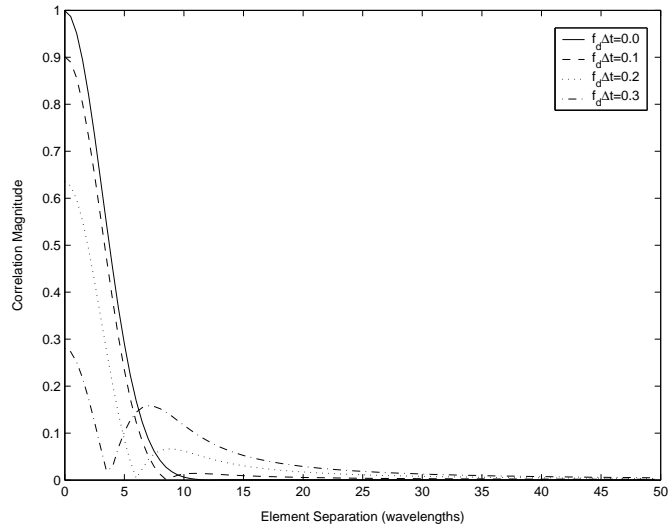
Figure 2.9: Magnitude of the path correlation for the two-dimensional Gaussian model, $\sigma_R/d = 0.05$, $\phi_0 = 0°$
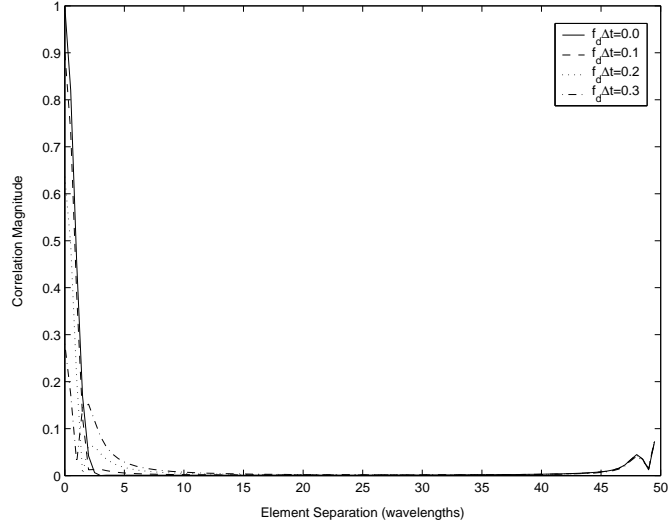
Figure 2.10: Magnitude of the path correlation for the two-dimensional Gaussian model, $\sigma_R/d = 0.2$, $\phi_0 = 0°$
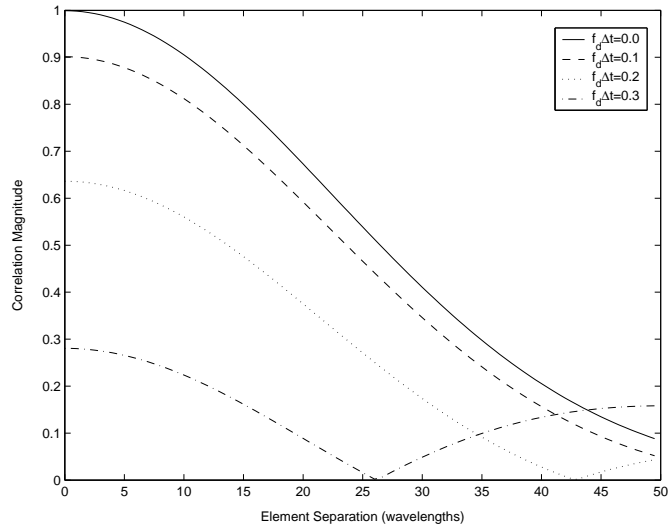
Figure 2.11: Magnitude of the path correlation for the two-dimensional Gaussian model, $\sigma_R/d = 0.01$, $\phi_0 = 45°$
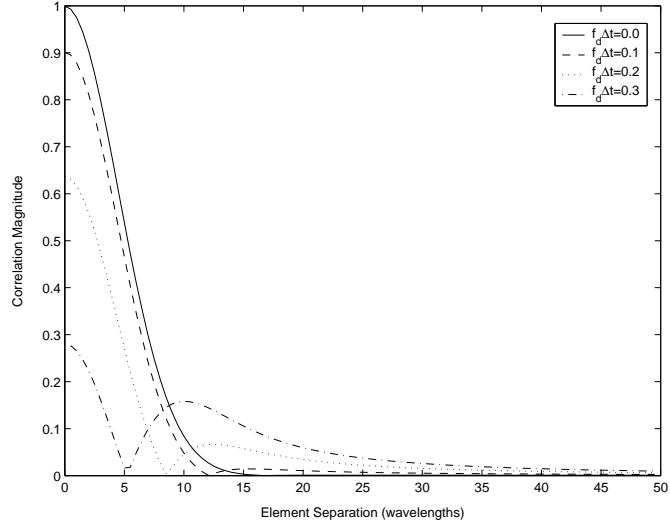
Figure 2.12: Magnitude of the path correlation for the two-dimensional Gaussian model, $\sigma_R/d = 0.05$, $\phi_0 = 45°$
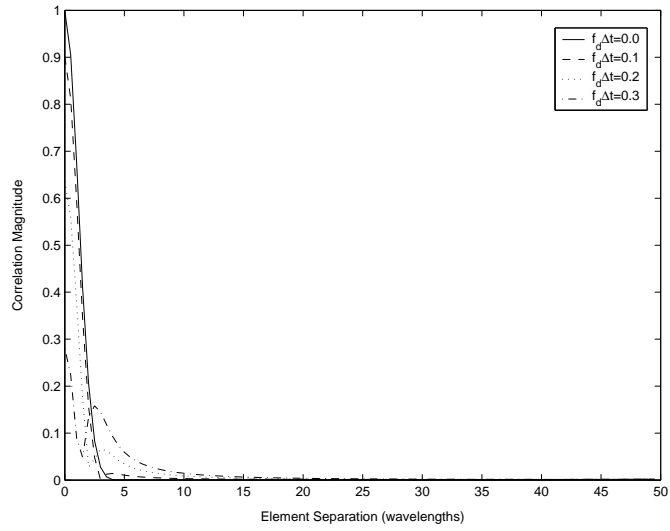
Figure 2.13: Magnitude of the path correlation for the two-dimensional Gaussian model, $\sigma_R/d = 0.2$, $\phi_0 = 45°$

2.3.3 Spatial-Only Case

We now consider applications for the spatial-only case for the uniform, Gaussian and Laplacian angle of arrival (AOA) probability density functions. Without loss of generality we consider only the case of multiple antennas at the base station and a single antenna at the mobile. With reference to the development presented in section 2.2.2, we define $h_p(t) = h_{p,1}(t)$ and $h_q(t) = h_{q,1}(t)$.

Uniform AOA

Several researchers have employed the uniform angle of arrival model in evaluating array processing techniques for wireless systems [14],[16],[17],[18]. Consider the evaluation of the path correlation for uniform angle of arrival on the interval $(\phi_0 - \Delta, \phi_0 + \Delta)$. The expectation term in (2.19) is easily determined

$$E\big\{\exp{(jn\phi)}\big\} = \exp{(jn\phi_0)}\frac{\sin{(n\Delta)}}{n\Delta} \tag{2.24}$$

and the correlation between the signals received at the pth and q^{th} base antennas is

$$E\Big\{h_p(t)h_q^*(t)\Big\} = \sum_{n=-\infty}^{\infty} \exp{(jn\phi_0)}\frac{\sin{(n\Delta)}}{n\Delta} \tag{2.25}$$
$$\times \exp\left[jn\left(-\xi_{base}^{pq} + \frac{\pi}{2}\right)\right] J_n\left(kd_{base}^{pq}\right)$$

where $k = 2\pi/\lambda$. For the special case of a linear array on the y-axis with uniform element spacing d

$$E\Big\{h_p(t)h_q^*(t)\Big\} = \sum_{n=-\infty}^{\infty} \exp{(jn\phi_0)}\frac{\sin{(n\Delta)}}{n\Delta}(-1)^n J_n\left(kd\left(p - q\right)\right) \tag{2.26}$$

This result agrees with that published by Salz and Winters [18]. The general expression derived here, 2.25, is not restricted to a linear array, however. Note

also the special case of $\Delta = \pi$ for which

$$E\{\exp{(jn\phi)}\} = \begin{cases} 1, & n = 0 \\ \\ 0, & n \neq 0 \end{cases} \tag{2.27}$$

and

$$E\left\{h_p(t)h_q^*(t)\right\} = J_0\left(kd_{base}^{pq}\right) \tag{2.28}$$

This well-known result corresponds to the spatial correlation function for cylindrically isotropic noise [19],[20].

Figures 2.14 and 2.15 illustrate the path correlation versus antenna spacing for the uniform AOA model and $\phi_0 = 0, 45°$, respectively.

Gaussian AOA

Trump [24] employed a Gaussian density for the angle of arrival when investigating approaches for estimating the direction of arrival and angular spread for wireless systems. If the angle of arrival is Gaussian distributed with mean ϕ_0 and standard deviation σ_ϕ

$$E\{\exp{(jn\phi)}\} = \exp\left(jn\phi_0 - \frac{n^2\sigma_\phi^2}{2}\right) \tag{2.29}$$

The correlation between the signals received at the pth and q^{th} base antennas is

$$E\left\{h_p(t)h_q^*(t)\right\} = \sum_{n=-\infty}^{\infty} \exp\left(jn\phi_0 - \frac{n^2\sigma_\phi^2}{2}\right) \tag{2.30}$$
$$\times \exp\left[jn\left(-\xi_{base}^{pq} + \frac{\pi}{2}\right)\right] J_n\left(kd_{base}^{pq}\right)$$

and for the special case of a linear array on the y-axis with uniform element spacing d

$$E\left\{h_p(t)h_r^*(t)\right\} = \sum_{n=-\infty}^{\infty} \exp\left(jn\phi_0 - \frac{n^2\sigma_\phi^2}{2}\right)(-1)^n J_n\left(kd\left(p-q\right)\right) \tag{2.31}$$
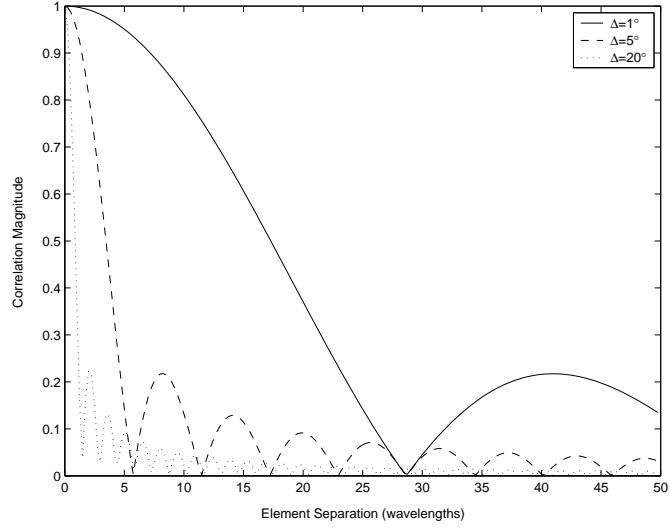
Figure 2.14: Magnitude of the path correlation for uniform angle of arrival, $\Delta = 1, 5, 20°$, $\phi_0 = 0°$
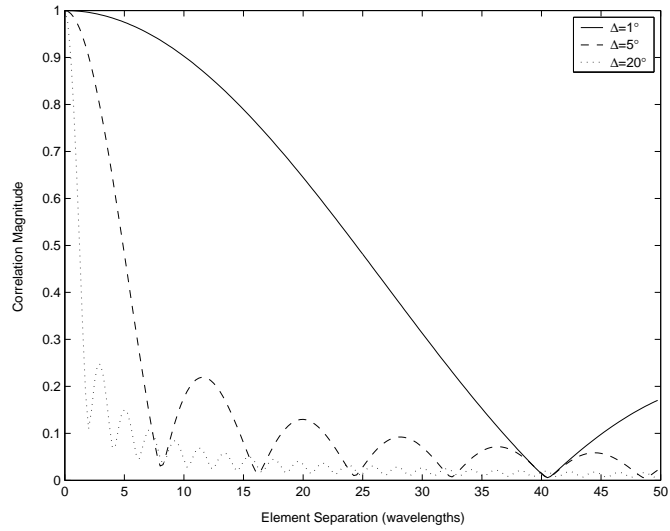
Figure 2.15: Magnitude of the path correlation for uniform angle of arrival, $\Delta = 1, 5, 20°$, $\phi_0 = 45°$
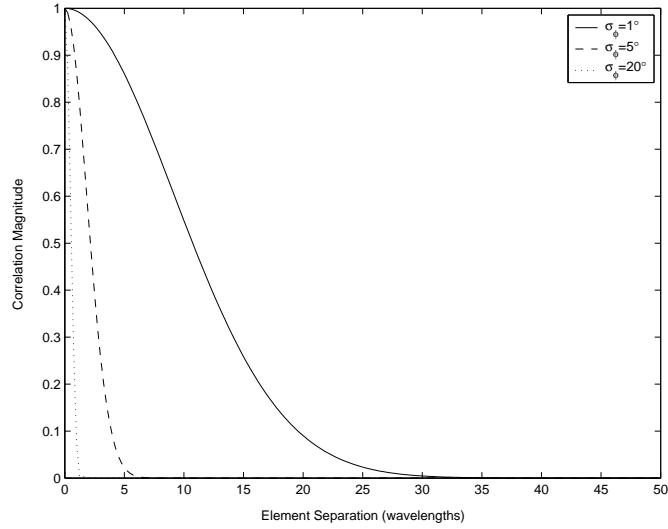
Figure 2.16: Magnitude of the path correlation for Gaussian angle of arrival, $\sigma_\phi = 1, 5, 20°$, $\phi_0 = 0°$

The approach presented here assumes $(-\infty < \phi < \infty)$, that is, the angular nature of the angle of arrival is not accounted for. Fuhl et al. [16] proposed a truncated normal distribution which results in a modified expression for the path correlation. The von Mises distribution was proposed by Fleury [21] as an alternative to the truncated Gaussian function. This distribution has found wide application in the analysis of directional data.

Figures 2.16 and 2.17 illustrate the path correlation versus antenna spacing for the Gaussian AOA model and $\phi_0 = 0, 45°$, respectively.

Laplacian AOA

The use of the truncated Laplacian probability density function for the angle of arrival is considered next. This model is motivated by the field measurements of Pedersen et al. [10],[11],[12] who determined that the power azimuth spectrum for
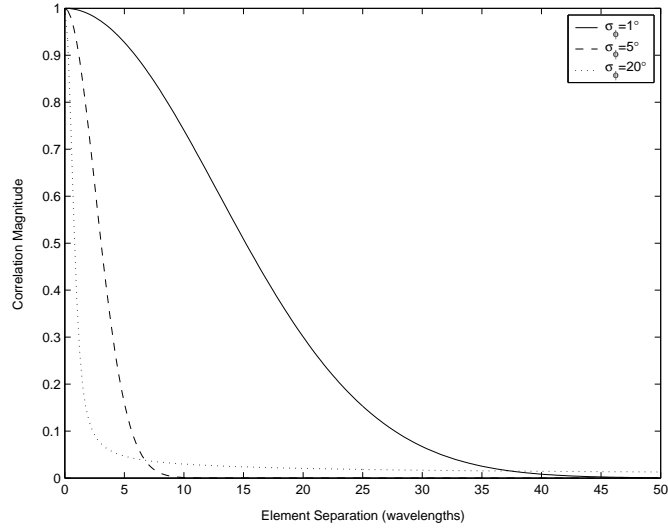
Figure 2.17: Magnitude of the path correlation for Gaussian angle of arrival, $\sigma_\phi = 1, 5, 20°$, $\phi_0 = 45°$

an urban wireless environment was accurately modeled using a truncated Laplacian function.

The Laplacian probability density is

$$f(\phi) = \frac{\exp\left(-\frac{\sqrt{2}|\phi-\phi_0|}{\sigma_A}\right)}{\sigma_A\sqrt{2}\left[1 - \exp\left(-\frac{\sqrt{2}\pi}{\sigma_A}\right)\right]} \quad \phi_0 - \pi \leq \phi \leq \phi_0 + \pi \quad (2.32)$$

with mean angle of arrival ϕ_0 and angular spread parameter σ_A. The expectation appearing in (2.19) is

$$E\{\exp(jn\phi)\} = \exp(jn\phi_0)\frac{2}{n^2\sigma_A^2 + 2}\left[\frac{1 - (-1)^n \exp\left(-\frac{\sqrt{2}\pi}{\sigma_A}\right)}{1 - \exp\left(-\frac{\sqrt{2}\pi}{\sigma_A}\right)}\right] \quad (2.33)$$

The correlation between the signals received at the pth and q^{th} base antennas is

$$E\{h_p(t)h_q^*(t)\} = \sum_{n=-\infty}^{\infty} \exp(jn\phi_0)\frac{2}{n^2\sigma_A^2 + 2}\left[\frac{1 - (-1)^n \exp\left(-\frac{\sqrt{2}\pi}{\sigma_A}\right)}{1 - \exp\left(-\frac{\sqrt{2}\pi}{\sigma_A}\right)}\right] \quad (2.34)$$

$$\times \exp\left[jn\left(-\xi_{base}^{pq} + \frac{\pi}{2}\right)\right] J_n(kd_{base}^{pq})$$

32
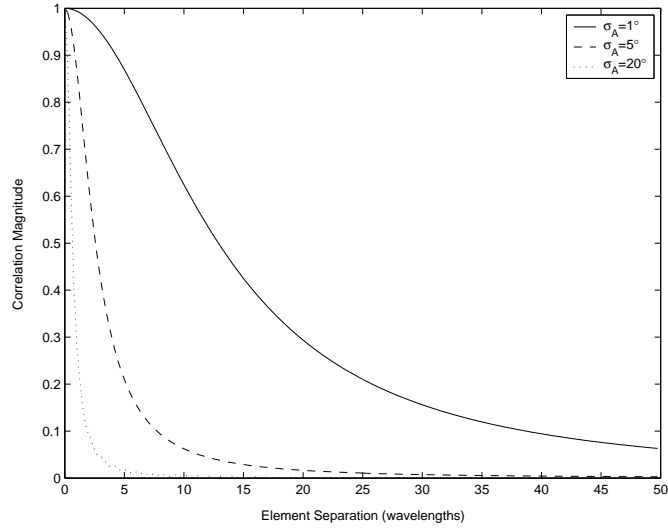
Figure 2.18: Magnitude of the path correlation for Laplacian angle of arrival, $\sigma_\phi = 1, 5, 20°$, $\phi_0 = 0°$

For the special case of a linear array on the y-axis with uniform element spacing d and mean angle of arrival $\phi_0 = 0$, we have

$$E\left\{h_p(t)h_q^*(t)\right\} = J_0\left(kd\left(p-q\right)\right) \qquad (2.35)$$
$$+ \sum_{m=1}^{\infty} \frac{2}{2m^2\sigma_A^2 + 1} J_{2m}\left(kd\left(p-q\right)\right)$$

This result differs slightly from that published by Fleury et al. [23]. The general expression derived here applies for arbitrary array geometery and arbitrary mean angle of arrival ϕ_0.

Figures 2.18 and 2.19 illustrate the path correlation versus antenna spacing for the Laplacian AOA model and $\phi_0 = 0, 45°$, respectively.
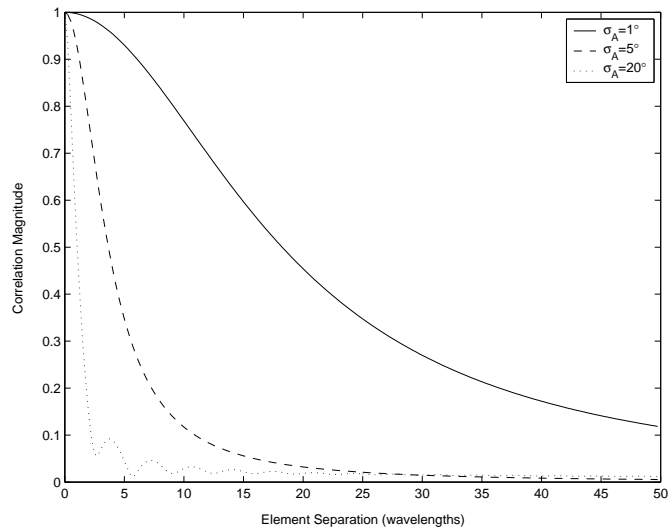
Figure 2.19: Magnitude of the path correlation for Laplacian angle of arrival, $\sigma_\phi = 1, 5, 20°$, $\phi_0 = 45°$

Approximations for Small Angular Spread

If the angular spread due to multipath is small, simple approximations for the path correlation may be developed. Aside from reduced computation, these approximations have the advantage of separating the correlation between a pair of array elements into two distinct factors. One factor is due to the mean angle of arrival and the remaining factor is due to angular spread. This, in turn, allows the array covariance matrix to be written as a Hadamard (element-by-element) product of two matrices, one depending only on the angle of arrival and the second depending only on the angular spread. Besson and Stoica have exploited this decoupling in developing estimators for the angle of arrival and angular spread for a linear array using the extended invariance principle [25].

Consider $\phi = \phi_0 + \delta$ with ϕ_0 corresponding to the angle of arrival of the direct path and δ small. Using small angle approximations for the sine and cosine

functions

$$\cos\left(\phi - \xi^{pq}\right) \approx \cos\left(\phi_0 - \xi^{pq}\right) - \delta \sin\left(\phi_0 - \xi^{pq}\right) \tag{2.36}$$

and

$$E\left\{h_p(t)h_q^*(t)\right\} \approx \exp\left[jkd^{pq}\cos\left(\phi_0 - \xi^{pq}\right)\right] \tag{2.37}$$
$$\times E\left\{\exp\left[-jkd^{pq}\delta\sin\left(\phi_0 - \xi^{pq}\right)\right]\right\}$$

Uniform AOA

For δ uniformly distributed on $(-\Delta, \Delta)$ and $\Delta \ll \pi$

$$E\left\{h_p(t)h_q^*(t)\right\} \approx \exp\left[jkd^{pq}\cos\left(\phi_0 - \xi^{pq}\right)\right] \tag{2.38}$$
$$\times \frac{\sin\left(kd^{pq}\Delta\sin\left(\phi_0 - \xi^{pq}\right)\right)}{kd^{pq}\Delta\sin\left(\phi_0 - \xi^{pq}\right)}$$

Figure 2.20 compares the approximation to the exact correlation for a 2-element linear array with uniform AOA and mean angle of arrival $\phi_0 = 45°$.

Gaussian AOA

For δ zero-mean Gaussian with standard deviation $\sigma_\phi \ll \pi$

$$E\left\{h_p(t)h_q^*(t)\right\} \approx \exp\left[jkd^{pq}\cos\left(\phi_0 - \xi^{pq}\right)\right] \tag{2.39}$$
$$\times \exp\left[-\left(kd^{pq}\sigma_\phi\sin\left(\phi_0 - \xi^{pq}\right)\right)^2/2\right]$$

Figure 2.21 compares the approximation to the exact correlation for a 2-element linear array with Gaussian AOA and mean angle of arrival $\phi_0 = 45°$.
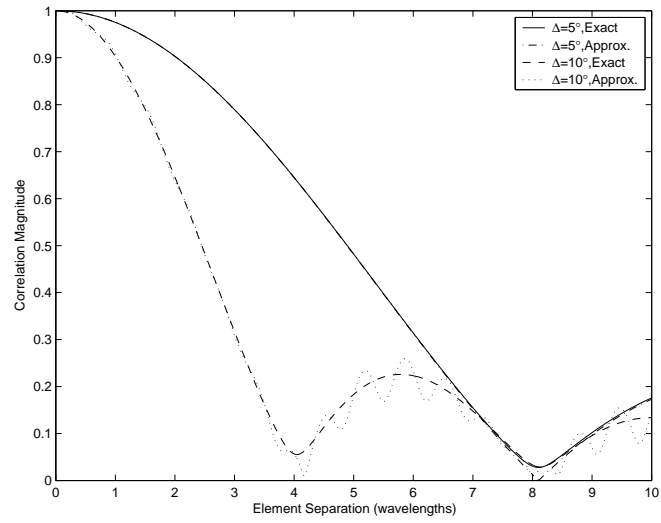
Figure 2.20: Comparison of exact and approximate correlation for Uniform AOA, $\phi_0 = 45°$
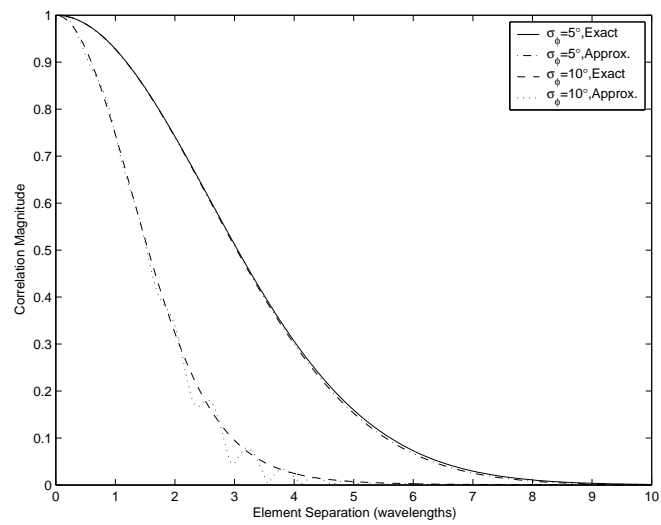
Figure 2.21: Comparison of exact and approximate correlation for Gaussian AOA, $\phi_0 = 45°$
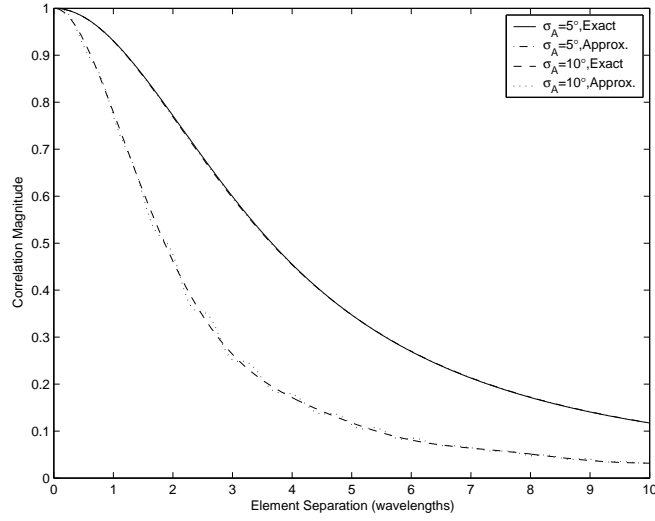
Figure 2.22: Comparison of exact and approximate correlation for Laplacian AOA, $\phi_0 = 45°$

Lapacian AOA

For δ zero-mean Laplacian with parameter $\sigma_A \ll \pi$

$$E\left\{h_p(t)h_q^*(t)\right\} \approx \exp\left[jkd^{pq}\cos\left(\phi_0 - \xi^{pq}\right)\right] \tag{2.40}$$
$$\times \frac{2}{\left[kd^{pq}\sigma_A\sin\left(\phi_0 - \xi^{pq}\right)\right]^2 + 2}$$

Figure 2.22 compares the approximation to the exact correlation for a 2-element linear array with Lapacian AOA and mean angle of arrival $\phi_0 = 45°$.

2.4   Chapter Summary

In this chapter we have introduced a general space-time covariance model that is applicable to arbitrary scatterer geometry, arbitrary array geometry at the base and mobile, and includes Doppler effects due to mobile motion. We have presented

37

applications of the proposed model based upon the 'circular ring' scatterer geometry due to Jakes [2] and the two-dimensional Gaussian scatterer geometry based upon the field measurements of Pedersen et al. [10],[11],[12]. A number of numerical examples were presented to illustrate the influence of antenna separation and effective scattering radius on the path correlation. In addition, variations in the normalized Doppler frequency were considered to illustrate the temporal aspects of the model.

Chapter 3

Evaluation of Space-Time Coding Performance with Spatial and Temporal Correlation

3.1 Introduction

In this chapter and the following chapter we evaluate the performance of several transmit diversity techniques for spatially and temporally correlated wireless channels. Diversity techniques can be broadly categorized according to whether or not channel knowledge is employed at the transmitter of the communication system. Beamforming approaches, such as maximum ratio transmission [27], rely on feedback of the channel response to the transmitter to achieve signal reinforcement and hence diversity gain. The temporal characteristics of the wireless channel determine the effectiveness of such techniques due to the senescence of the channel state information. Space-time block coding, on the other hand, encodes the information symbols redundantly in space and in time to achieve diversity gain. No channel state information is employed by the transmitter for this technique. As will be demonstrated, the error performance of both beamforming and space-time coding is significantly affected by the temporal and spatial correlation characteristics of

the wireless channel. In this chapter we analyze the performance of space-time block coding techniques and in the following chapter we analyze the performance of beamforming techniques.

The computation of the symbol error probability for arbitrary space-time block codes is, in general, analytically intractable. So, we approach the problem of analyzing the error performance through the use of the union bound and the exact pairwise error probability. It should be noted that in all cases we assume the receiver of the wireless system has perfect knowledge of the channel response. That is, we do not address the problem of channel estimation. With the aid of the space-time covariance model developed in the previous chapter, we present extensive numerical results that illustrate the error performance of several space-time block codes. We consider variations in the spatial and temporal correlation of the wireless channel and the resultant effects on the error performance of these techniques.

The chapter is organized as follows. In Section 3.2 we briefly describe the space-time block coding techniques that are investigated and related work. Section 3.3 describes the basic system model and Section 3.4 details the development of the exact pairwise error probability for arbitrary space-time block codes. Finally, numerical results are presented in Section 3.5.

3.2   Space-Time Block Coding

Wireless systems employing multiple transmit and receive antennas have the potential for tremendous gains in channel capacity through exploitation of independent transmission paths due to scattering. Transmit diversity, achieved through the use of space-time coding techniques at the base station is a recent innovation motivated

by the need for higher throughput in the wireless channel. A simple two-branch transmit diversity scheme was proposed by Alamouti [32]. It was demonstrated that this scheme provides the same diversity order as a wireless system employing a single transmit antenna and two receive antennas and utilizing maximal-ratio combining (i.e. classical receive diversity). The bit-error-rate (BER) performance of the proposed scheme was evaluated assuming that the path from each transmit antenna to each receive antenna experiences mutually uncorrelated Rayleigh amplitude fading. Abundant space-time codes to achieve transmit diversity have been proposed, for example see [33], [34], [35], [36], and the references therein. In these works a Rayleigh channel model was used to evaluate the performance of the proposed codes and the transmit antennas were assumed to be sufficiently spaced such that the transmission paths are independent.

The majority of the research to date on space-time coding techniques has employed the assumption of uncorrelated transmission paths without regard for the conditions under which this assumption is justified. The degree of correlation between channel transmission paths from a transmit antenna to a receive antenna depends significantly on the scattering environment and on the antenna separation at the transmitter and receiver. For example, if the majority of the channel scatterers are located in close proximity to the mobile then the transmission paths will be highly correlated unless the transmit antennas are sufficiently separated in space.

In recently published work Wang et al. [26] derive the exact pairwise error probability for space-time coding over quasi-static or fast-fading Rayleigh channels in the presence of spatial fading correlation. For analytical tractability, the authors assume the channel matrix can be decomposed as a product of the square roots of

the transmit and receive correlation matrices, respectively. The effects of spatial correlation on space-time coding performance are investigated for several scenarios but it is unclear how the parameters chosen relate to physical scattering parameters such as effective scattering radius, etc.

3.3   System Model

Consider a wireless system employing N_T transmit antennas and N_R receive antennas. The signal received at the qth antenna at time t is

$$y_q(t) = \sum_{p=1}^{N_T} h_{p,q}(t) c_p(t) + z_q(t) \tag{3.1}$$

where $h_{p,q}(t)$ is the complex channel response between the pth transmit antenna and the qth receive antenna at time t and is modeled as complex Gaussian with zero mean and unit variance. $c_p(t)$ denotes the space-time signal transmitted by the pth antenna at time t and $z_q(t)$ is independent complex Gaussian noise with zero mean and variance N_0.

Each space-time signal is described by a $T \times N_T$ matrix $\mathbf{C}$ with the columns corresponding to the space dimension and the rows corresponding to the time dimension

$$\mathbf{C} = \begin{pmatrix} c_1(1) & c_2(1) & \cdots & c_{N_T}(1) \\ c_1(2) & c_2(2) & \cdots & c_{N_T}(2) \\ \vdots & \vdots & \ddots & \vdots \\ c_1(T) & c_2(T) & \cdots & c_{N_T}(T) \end{pmatrix}. \tag{3.2}$$

The space-time signal $c_p(t)$ is chosen as the entry in the code matrix corresponding to the pth column and t^{th} row. The space-time signal is transmitted over T time

slots and employs N_T transmit antennas. The average signal energy is defined as

$$E_s = \mathrm{E}\left[\frac{1}{T}\sum_{t=1}^{T}\sum_{p=1}^{N_T}|c_p(t)|^2\right] \tag{3.3}$$

and the signal to noise ratio is $\rho = \frac{E_s}{N_0}$.

Equation (3.1) can be re-written in vector form as [40]

$$\mathbf{y} = \mathbf{D}\mathbf{h} + \mathbf{z} \tag{3.4}$$

where the $N_R T \times N_T N_R T$ matrix $\mathbf{D}$ is constructed from the space-time signal matrix $\mathbf{C}$ as follows

$$\mathbf{D} = \begin{pmatrix} D_1 & D_2 & \cdots & D_{N_T} & \cdots & 0 & 0 & \cdots & 0 \\ 0 & 0 & \cdots & 0 & \cdots & 0 & 0 & \cdots & 0 \\ & & \vdots & & \ddots & & & \vdots & \\ 0 & 0 & \cdots & 0 & \cdots & D_1 & D_2 & \cdots & D_{N_T} \end{pmatrix} \tag{3.5}$$

with

$$D_i = \mathrm{diag}\left(c_i(1), c_i(2), \cdots, c_i(T)\right), \quad i = 1, 2, \cdots, N_T. \tag{3.6}$$

The elements of the diagonal matrix D_i correspond to the ith column of the code matrix $\mathbf{C}$. The $N_T N_R T \times 1$ channel vector $\mathbf{h}$ is defined by

$$\mathbf{h} = \left(\mathbf{h}'_{1,1}, \cdots, \mathbf{h}'_{N_T,1}, \cdots, \mathbf{h}'_{1,N_R}, \cdots, \mathbf{h}'_{N_T,N_R},\right)' \tag{3.7}$$

with

$$\mathbf{h}_{i,j} = \left(h_{i,j}(1), h_{i,j}(2), \cdots, h_{i,j}(T)\right)' \tag{3.8}$$

and $'$ denoting the matrix transpose operation. The $N_R T \times 1$ received signal vector $\mathbf{y}$ is defined by

$$\mathbf{y} = \left(y_1(1), \cdots, y_1(T), \cdots, y_{N_R}(1), \cdots, y_{N_R}(T)\right)' \tag{3.9}$$

and the $N_R T \times 1$ noise vector $\mathbf{z}$ is given by

$$\mathbf{z} = \left(z_1(1), \cdots, z_1(T), \cdots, z_{N_R}(1), \cdots, z_{N_R}(T)\right)' \tag{3.10}$$

43

3.4   Pairwise Error Probability

In this section an expression for the exact pairwise error probability is developed for spatially and temporally correlated wireless channels. The pairwise error probability is used in conjunction with the union bound to determine an upper bound for the probability of a block error for arbitrary space-time codes.

Suppose $\mathbf{D}_\alpha$ and $\mathbf{D}_\beta$ correspond to two distinct space-time signals $\mathbf{C}_\alpha$ and $\mathbf{C}_\beta$, respectively. Assuming the channel vector $\mathbf{h}$ is known, the hypothesis test for choosing between $\mathbf{C}_\alpha$ and $\mathbf{C}_\beta$ is

$$\left(\mathbf{y} - \mathbf{D}_\alpha \mathbf{h} + \mathbf{z}\right)^\dagger \left(\mathbf{y} - \mathbf{D}_\alpha \mathbf{h} + \mathbf{z}\right) \tag{3.11}$$

$$\mathbf{C}_\beta$$
$$\overset{>}{\underset{<}{}} \left(\mathbf{y} - \mathbf{D}_\beta \mathbf{h} + \mathbf{z}\right)^\dagger \left(\mathbf{y} - \mathbf{D}_\beta \mathbf{h} + \mathbf{z}\right)$$
$$\mathbf{C}_\alpha$$

where the symbol $\dagger$ denotes the matrix conjugate transpose operation. This test corresponds to choosing between two (complex) Gaussian vectors with equal co-variance matrices and unequal mean vectors. The pairwise error probability given the channel vector $\mathbf{h}$ is [41]

$$\Pr\left(\mathbf{C}_\alpha \rightarrow \mathbf{C}_\beta \mid \mathbf{h}\right) = Q\left(\sqrt{\frac{\rho}{2N_T}\left\|\left(\mathbf{D}_\alpha - \mathbf{D}_\beta\right)\mathbf{h}\right\|^2}\right) \tag{3.12}$$

where $\|\mathbf{x}\|$ denotes the norm of the vector $\mathbf{x}$, i.e. $\|\mathbf{x}\|^2 = \mathbf{x}^\dagger \mathbf{x}$ and $Q(x)$ denotes the Gaussian Q function. An alternative form of the Gaussian Q function due to Craig [42] is employed in the sequel. It is defined as

$$Q(x) = \frac{1}{\sqrt{2\pi}} \int_x^\infty \exp\left(-t^2/2\right) dt \tag{3.13}$$
$$= \frac{1}{\pi} \int_0^{\pi/2} \exp\left(-\frac{x^2}{2\sin^2\theta}\right) d\theta$$

Considering now the expectation over the channel vector $\mathbf{h}$, we have

$$\Pr\left(\mathbf{C}_\alpha \to \mathbf{C}_\beta\right) = E\left\{Q\left(\sqrt{\frac{\rho}{2N_T}\left\|\left(\mathbf{D}_\alpha - \mathbf{D}_\beta\right)\mathbf{h}\right\|^2}\right)\right\} \tag{3.14}$$

$$= \frac{1}{\pi}\int_0^{\pi/2} E\left\{\exp\left(-\frac{\rho}{N_T}\frac{\left\|\left(\mathbf{D}_\alpha - \mathbf{D}_\beta\right)\mathbf{h}\right\|^2}{4\sin^2\theta}\right)\right\}d\theta$$

Assuming that the channel vector $\mathbf{h}$ is complex Gaussian with zero mean vector and space-time covariance matrix $\mathbf{R}$, a result due to Turin [43],[44] regarding the characteristic function of a quadratic form of a complex Gaussian vector may be used to evaluate the expectation appearing in (3.14)

$$E\left\{\exp\left(-\frac{\rho}{N_T}\frac{\left\|\left(\mathbf{D}_\alpha - \mathbf{D}_\beta\right)\mathbf{h}\right\|^2}{4\sin^2\theta}\right)\right\} = \frac{1}{\det\left(\mathbf{I} + \frac{\rho}{N_T}\frac{\left(\mathbf{D}_\alpha - \mathbf{D}_\beta\right)\mathbf{R}\left(\mathbf{D}_\alpha - \mathbf{D}_\beta\right)^\dagger}{4\sin^2\theta}\right)} \tag{3.15}$$

$$= \prod_{i=1}^K \left(1 + \frac{\rho}{N_T}\frac{\lambda_i}{4\sin^2\theta}\right)^{-1}$$

with K corresponding to the rank of the matrix

$$\left(\mathbf{D}_\alpha - \mathbf{D}_\beta\right)\mathbf{R}\left(\mathbf{D}_\alpha - \mathbf{D}_\beta\right)^\dagger \tag{3.16}$$

and $\{\lambda_i\}_{i=1}^K$ its non-zero eigenvalues. For completeness, a proof of this result is presented in Appendix A. The final expression for the pairwise error probability between $\mathbf{C}_\alpha$ and $\mathbf{C}_\beta$ is now given by

$$\Pr\left(\mathbf{C}_\alpha \to \mathbf{C}_\beta\right) = \frac{1}{\pi}\int_0^{\frac{\pi}{2}}\prod_{i=1}^K\left(1 + \frac{\rho}{N_T}\frac{\lambda_i}{4\sin^2\theta}\right)^{-1}d\theta \tag{3.17}$$

Given space-time codes $\mathbf{C}_\alpha$ and $\mathbf{C}_\beta$ and the channel space-time covariance matrix $\mathbf{R} = E\{\mathbf{h}\mathbf{h}^\dagger\}$, the pairwise error probability can be calculated from (3.17). Note that in most cases of practical interest (3.17) must be numerically integrated to determine the exact pairwise error probability.

An upper bound on the pairwise error probability can be easily deduced from the Q function definition in (3.13). Specifically, $Q(x) \leq \frac{1}{2}\exp\left(-\frac{x^2}{2}\right)$ since the

integrand in (3.13) attains its maximum value for $\theta = \pi/2$. We have

$$\Pr\left(\mathbf{C}_\alpha \to \mathbf{C}_\beta\right) \leq \prod_{i=1}^{K} \left(1 + \frac{\rho}{N_T} \frac{\lambda_i}{4}\right)^{-1} \tag{3.18}$$

$$\leq \frac{\left(\frac{\rho}{4N_T}\right)^K}{\prod_{i=1}^{K} \lambda_i}$$

Tighter upper bounds on the pairwise error probability have been found, see [44], for example.

An upper bound on the probability of incorrectly decoding a space-time block code may be obtained by employing the union bound. Specifically, let P_{block} denote the probability that the space-time block code is erroneously decoded. Then,

$$P_{\text{block}} \leq \sum_{\alpha} \Pr\left(\mathbf{C}_\alpha\right) \sum_{\alpha \neq \beta} \Pr\left(\mathbf{C}_\alpha \to \mathbf{C}_\beta\right) \tag{3.19}$$

In the sequel, the expression for the upper bound on the block error probability (3.19) is evaluated to assess space-time code performance. Define the diversity order δ as

$$\delta = \lim_{\rho \to \infty} \frac{\log P_{block}}{\log \rho} \tag{3.20}$$

The parameter δ describes the asymptotic slope of the block error probability versus signal to noise ratio. For example, a diversity order of 2 implies a reduction of 10^{-2} in the block error probability for each 10dB increase in signal to noise ratio. In the sequel, the achieved diversity order is also used to assess space-time code performance.

3.5   Numerical Results

In this section we evaluate the union bound on the block error probability (3.19) using a two-dimensional Gaussian scattering model for several space-time codes

employing two and four transmit antennas and up to three receive antennas. Linear array geometry was employed at the base and mobile for all results. Variations in both spatial and temporal correlation are considered and the results are compared to the case of an uncorrelated (space and time) channel.

The motivation for the use of the two-dimensional Gaussian scattering model is due to a recent measurement campaign conducted by Pedersen et al. [10],[11],[12] in which the temporal and azimuth dispersion of multipath in urban wireless environments was characterized. The study found that the power azimuth spectrum was accurately modeled using a truncated Laplacian function and the power delay spectrum was well-approximated by a negative-exponential function. Recent work by Janaswamy [13] concluded that the measurements reported by Pedersen et al. were consistent with a two-dimensional Gaussian model for the scatterer locations surrounding the mobile receiver.

The standard deviation of the scattering radius for the two-dimensional Gaussian model was varied from $\sigma_R = 10, 50, 200$m and the distance between the mobile and base (array phase centers) was fixed at $d = 1000$m. The parameter σ_R specifies the radius about the mobile for which approximately 68 percent of the scatterers are contained. The smallest value for σ_R yields the ratio $\sigma_R/d = 0.01$ and corresponds to angular spread due to multipath of approximately $1°$ from the perspective of the base station. The mobile location was broadside to the base antenna array and its velocity was chosen such that the maximum Doppler frequency was approximately $f_d = 78$Hz corresponding to a carrier frequency of 850MHz and a maximum speed of 100km/hr. Variations in the space-time symbol period T_s were considered to assess the effects due to temporal correlation. Specifically, values used for the normalized Doppler frequency were $f_d T_s = 0.0033, 0.01, 0.05, 0.1$.

The smallest value corresponds to a slow fading channel with a symbol to fading ratio of approximately 300:1. In other words, space-time symbols separated by 300 symbol periods are approximately uncorrelated. The largest value corresponds to a channel with a symbol to fading ratio of 10:1 and is denoted as fast fading.

The space-time block codes investigated include the orthogonal code [32],[33],[34], the orthogonal code with sphere packing [40], the diagonal algebraic code [35], and the cyclic code [36]. These codes were chosen because they resprent a wide spectrum of available space-time codes and yield reasonable performance.

For the presentation that follows, results for spatial correlation are presented first followed by the results for temporal correlation.

3.5.1 Spatial Correlation

This section presents results for the slow fading ($f_d T_s = 0.0033$) and uncorrelated wireless channels with variations in spatial correlation due to transmit antenna spacing, receive antenna spacing and scattering radius standard deviation σ_R for the two-dimensional Gaussian scattering model. Results for two transmit antennas are presented first followed by results for four transmit antennas. All results for two transmit antennas were evaluated at 10^{-2} block error probability and all results for four transmit antennas were evaluated at 10^{-4} block error probability.

2 Transmit Antennas

For 2 transmit antennas the orthogonal code due to Alamouti [32] was used with a 16-QAM symbol constellation. For the diagonal algebraic code we also chose

16-QAM symbols and the unitary rotation matrix was chosen to be

$$\frac{1}{\sqrt{2}} \begin{pmatrix} 1 & e^{j\pi/4} \\ 1 & -e^{j\pi/4} \end{pmatrix} \tag{3.21}$$

For all space-time codes the spectral efficiency was 4 bits/s/Hz.

Figure 3.1 shows the block error probability (union bound) versus signal to noise ratio and scattering radius standard deviation for 2 transmit antennas ($\lambda/2$ spacing) and 1 receive antenna. The normalized Doppler frequency for this case was $f_d T_s = 0.0033$, representing slow fading. To achieve a block error probablity of 10^{-2} for the uncorrelated channel approximately 26.4dB signal to noise ratio is required for the diagonal algebraic code. The orthogonal code and orthogonal code with sphere packing realize performance improvements of 1.4dB and 1.7dB, respectively, over the diagonal algebraic code for the uncorrelated channel. For a scattering radius standard deviation of $\sigma_R = 10$m, approximately 37.8dB signal to noise ratio is required to achieve a block error probability of 10^{-2} for the diagonal algebraic code. The orthogonal code and orthogonal code with sphere packing yield improvements of 0.4dB and 0.7dB, respectively, for this case. Thus, the channel with scattering radius standard deviation of $\sigma_R = 10$m requires an increase in signal to noise ratio of 11.4dB, relative to that required for the uncorrelated channel, to achieve a block error probability of 10^{-2} for the diagonal algebraic code. The required increase in signal-to-noise ratio for the orthogonal code and the orthogonal code with sphere packing is 12.3dB and 12.4dB, respectively. These results highlight the dependence of space-time coding performance on spatial correlation for the slow fading channel. Fractional wavelength antenna spacing at the transmitter combined with small scattering radius yield transmission paths that are highly correlated and result in degraded performance relative to the uncorrelated

channel. Increasing the spacing of the transmit antennas mitigates this effect to a certain extent as will be demonstrated next. Figure 3.1 also illustrates that a diversity order of 2 is achieved for all space-time codes investigated for both the uncorrelated channel and the two-dimensional Gaussian scatterer model for values of $\sigma_R = 10, 50, 200$m. For example, the block error probability for the orthogonal space-time code and uncorrelated channel is reduced from 10^{-3} at a signal to noise ratio of 30dB to 10^{-5} at a signal to noise ratio of 40dB.

Figure 3.2 shows the block error probability (union bound) versus signal to noise ratio and transmit antenna spacing for a single receive antenna and normalized Doppler frequency of $f_d T_s = 0.0033$ and scattering radius standard deviation of $\sigma_R = 10$m. From these results it was determined that an antenna spacing of 30λ is required to achieve performance within 0.5dB of the uncorrelated channel for 10^{-2} block error probability. For a carrier frequency of 850MHz the transmitted wavelength is $\lambda = 0.35$m and $30\lambda = 10.5$m. From Figure 3.2 it is seen that increasing the spacing of the transmit antennas from $\lambda/2$ to 5λ decreases the signal to noise ratio required to achieve a block error probability of 10^{-2} by 6.7dB for the diagonal algebraic code, 7.4dB and 7.5dB, respectively, for the orthogonal code and orthogonal code with sphere packing for a scattering radius standard deviation of $\sigma_R = 10$m.

Figure 3.3 shows the results for 2 transmit antennas (5λ spacing) and 2 receive antennas ($\lambda/2$ spacing) and $f_d T_s = 0.0033$. A signal to noise ratio of 17.3dB is required to achieve a block error probability of 10^{-2} for the diagonal algebraic code and an uncorrelated channel. The orthogonal code and orthogonal code with sphere packing achieve gains of 0.6dB and 1.1dB, respectively, over the diagonal algebraic code for the uncorrelated channel. For the channel with scattering radius standard

deviation $\sigma_R = 10$m the required signal to noise ratios to achieve 10^{-2} block error probability are 22.2, 22.1 and 22.0dB, respectively, for the diagonal algebraic code, orthogonal code, and orthogonal code with sphere packing. Comparing Figures 3.2 and 3.3 it is seen that the addition of 1 receive antenna ($\lambda/2$ spacing) reduces the signal to noise ratio required to achieve a block error probability of 10^{-2} by 9.1dB for the diagonal algebraic code, 8.3dB and 8.5dB, respectively, for the orthogonal code and orthogonal code with sphere packing for the uncorrelated channel. Figure 3.3 also illustrates that a diversity order of 4 is achieved for the uncorrelated channel and for all space-time codes investigated. For example, the block error probability for the orthogonal space-time code is reduced from 10^{-7} at a signal to noise ratio of 30dB to 10^{-11} at a signal to noise ratio of 40dB. Although not evident from the figure, it was verified that the asymptotic slope of the block error probability for the two-dimensional Gaussian scatterer model with $\sigma_R = 10, 50$m was the same as that for the uncorrelated channel and thus these cases also yield a diversity order of 4.

4 Transmit Antennas

For the case of 4 transmit antennas we investigated three space-time codes having a spectral efficiency of 2 bits/s/Hz. These codes are: the orthogonal code with sphere packing [39],[40] the cyclic code [36], and the diagonal algebraic code with unitary rotation matrix

$$\frac{1}{2}\begin{pmatrix} 1 & e^{j\pi/8} & e^{j2\pi/8} & e^{j3\pi/8} \\ 1 & -e^{j\pi/8} & e^{j2\pi/8} & -e^{j3\pi/8} \\ 1 & je^{j\pi/8} & -e^{j2\pi/8} & -je^{j3\pi/8} \\ 1 & -je^{j\pi/8} & -e^{j2\pi/8} & je^{j3\pi/8} \end{pmatrix} \tag{3.22}$$
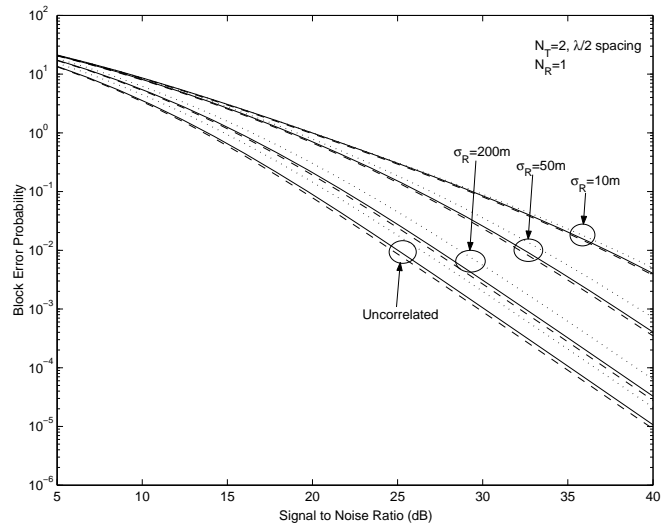
Figure 3.1: Orthogonal code with 16-QAM symbols (solid curve), orthogonal code with sphere packing (dashed curve), diagonal algebraic code (dotted curve). Block error probability (union bound) versus signal to noise ratio and scattering radius standard deviation, 2 transmit antennas ($\lambda/2$ spacing), 1 receive antenna, $f_d T_s = 0.0033$.
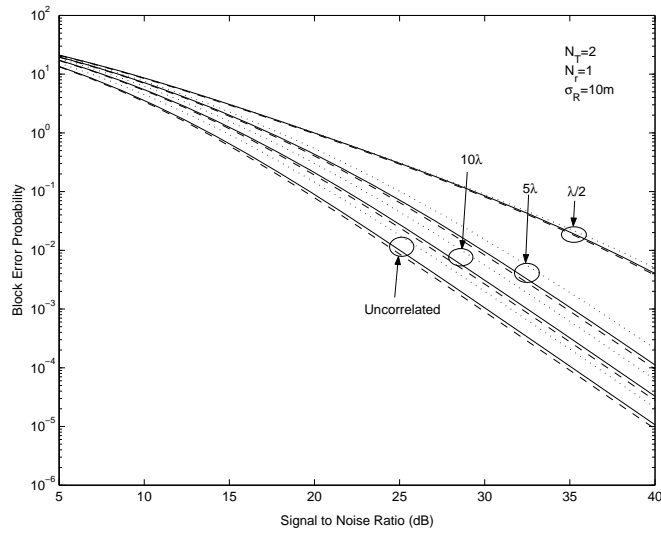
Figure 3.2: Orthogonal code with 16-QAM symbols (solid curve), orthogonal code with sphere packing (dashed curve), diagonal algebraic code (dotted curve). Block error probability (union bound) versus signal to noise ratio and transmit antenna separation, 2 transmit antennas, 1 receive antenna, $f_d T_s = 0.0033$, $\sigma_R = 10$m.
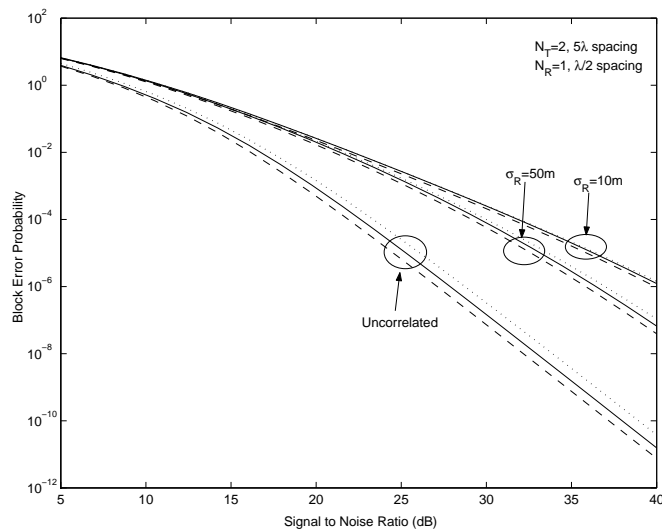
Figure 3.3: Orthogonal code with 16-QAM symbols (solid curve), orthogonal code with sphere packing (dashed curve), diagonal algebraic code (dotted curve). Block error probability (union bound) versus signal to noise ratio and scattering radius standard deviation, 2 transmit antennas (5λ spacing), 2 receive antennas ($\lambda/2$ spacing), $f_d T_s = 0.0033$.

and QPSK signal constellation. Figure 3.4 shows the block error probability (union bound) versus signal to noise ratio and scattering radius standard deviation for 4 transmit antennas ($\lambda/2$ spacing) and 1 receive antenna. The normalized Doppler frequency for this case was $f_d T_s = 0.0033$, representing slow fading. To achieve a block error probablity of 10^{-4} for the uncorrelated channel a signal to noise ratio of approximately 22.6dB is required for the cyclic code. The diagonal algebraic and the orthogonal code with sphere packing realize performance improvements of 2.2dB and 3.0dB, respectively, over the cyclic code for the uncorrelated channel. For a scattering radius standard deviation of $\sigma_R = 10$m, approximately 41.7dB signal to noise ratio is required to achieve a block error probability of 10^{-4} for the cyclic code. The diagonal algebraic and the orthogonal code with sphere packing yield improvements of 0.4dB and 2.0dB, respectively, for this case. With reference to Figure 3.4 note that 19.1dB additional signal to noise ratio is required to maintain a block error probability of 10^{-4} for a scattering radius standard deviation of $\sigma_R = 10$m compared with the uncorrelated channel for the cyclic code. The diagonal algebraic code and orthogonal code with sphere packing require an additional signal to noise ratio of 20.9dB and 20.1dB, respectively, for the same conditions. Figure 3.4 also illustrates that a diversity order of 4 is achieved for the uncorrelated channel and for all space-time codes investigated. For example, the block error probability for the orthogonal space-time code with sphere packing is reduced from 10^{-8} at a signal to noise ratio of 30dB to 10^{-12} at a signal to noise ratio of 40dB. Although not evident from the figure, it was verified that the asymptotic slope of the block error probability for the two-dimensional Gaussian scatterer model with $\sigma_R = 10, 50, 200$m was the same as that for the uncorrelated channel and thus these cases also yield a diversity order of 4.

Figure 3.5 shows the block error probability (union bound) versus signal to noise ratio and transmit antenna spacing for scattering radius standard deviation $\sigma_R = 10$m and normalized Doppler frequency $f_d T_s = 0.0033$. It was found that a transmit antenna spacing of 40λ (14.0m) is required to achieve performance within 0.5dB of that for the uncorrelated channel at a block error probability of 10^{-4}. From Figure 3.5 it is seen that increasing the spacing of the transmit antennas from $\lambda/2$ to 5λ decreases the signal to noise ratio required to achieve a block error probability of 10^{-4} by 11.3dB for the cyclic code, 11.9dB and 10.9dB, respectively, for the diagonal algebraic code and orthogonal code with sphere packing for a scattering radius standard deviation of $\sigma_R = 10$m.

Figures 3.6 and 3.7 show the results for 2 and 3 receive antennas ($\lambda/2$ spacing), respectively, and 4 transmit antennas (5λ spacing) for $f_d T_s = 0.0033$ and scattering radius standard deviation $\sigma_R = 10$m and the uncorrelated channel. For the case of 2 receive antennas the cyclic code achieves a block error probability of 10^{-4} at a signal to noise ratio of 14.4dB for the uncorrelated channel. A performance improvement of 1.8dB and 2.0dB, respectively, is observed for the diagonal algebraic code and orthogonal code with sphere packing for the uncorrelated channel. For the case of 3 receive antennas the cyclic code achieves a block error probability of 10^{-4} at a signal to noise ratio of 10.9dB for the uncorrelated channel. A performance improvement of 1.3dB and 1.4dB, respectively, is observed for the diagonal algebraic code and orthogonal code with sphere packing for the uncorrelated channel. Comparing Figures 3.5, 3.6 and 3.7 it is seen that a system with 2 receive antennas requires 8.2dB less signal to noise ratio to achieve a block error probability of 10^{-4} than a system with 1 receive antenna for the cyclic code and uncorrelated channel. It was found that a system with 3 receive antennas further

Figure 3.4: Orthogonal code with sphere packing (dashed curve), diagonal algebraic code (dotted curve), cyclic code (dash-dotted curve). Block error probability (union bound) versus signal to noise ratio and scattering radius standard deviation, 4 transmit antennas ($\lambda/2$ spacing), 1 receive antenna, $f_dT_s = 0.0033$.

reduces the required signal to noise ratio by 3.5dB compared with the case of 2 receive antennas for the same conditions. Also, results for 4 receive antennas (not shown) demonstrate a further reduction of 2.1dB compared with the case of 3 receive antennas. Although these comparisons were made for the cyclic code, comparable results were obtained for the diagonal algebraic code and orthogonal code with sphere packing. From these results it appears that the benefit realized by adding multiple receive antennas diminishes with increasing numbers of antennas.

3.5.2   Temporal Correlation

This section investigates the space-time block code error performance due to variations in temporal correlation. Four cases for the normalized Doppler frequency

Figure 3.5: Orthogonal code with sphere packing (dashed curve), diagonal algebraic code (dotted curve), cyclic code (dash-dotted curve). Block error probability (union bound) versus signal to noise ratio and transmit antenna spacing, 4 transmit antennas ($\lambda/2$ spacing), 1 receive antenna, $f_d T_s = 0.0033$, $\sigma_R = 10$m.

Figure 3.6: Orthogonal code with sphere packing (dashed curve), diagonal algebraic code (dotted curve), cyclic code (dash-dotted curve). Block error probability (union bound) versus signal to noise ratio and scattering radius standard deviation, 4 transmit antennas (5λ spacing), 2 receive antennas ($\lambda/2$ spacing), $f_d T_s = 0.0033$.

Figure 3.7: Orthogonal code with sphere packing (dashed curve), diagonal alge-braic code (dotted curve), cyclic code (dash-dotted curve). Block error probability (union bound) versus signal to noise ratio and scattering radius standard deviation, 4 transmit antennas (5λ spacing), 3 receive antennas ($\lambda/2$ spacing), $f_d T_s = 0.0033$.

were considered, $f_d T_s = 0.0033, 0.01, 0.05, 0.1$. The smallest value corresponds to a slow fading wireless channel and the largest value corresponds to the case of fast fading. The symbol to fading ratios for the slow fading and fast fading cases are 300:1 and 10:1, respectively. All results for two transmit antennas were evaluated at 10^{-2} block error probability and all results for four transmit antennas were evaluated at 10^{-4} block error probability.

2 Transmit Antennas

Figure 3.8 shows the block error probability (union bound) versus signal to noise ratio and normalized Doppler frequency for 2 transmit antennas ($\lambda/2$ spacing), 1 receive antenna and scattering radius standard deviation $\sigma_R = 10$m. For the fast fading channel ($f_d T_s = 0.1$) the orthogonal code with sphere packing requires 31.9dB signal to noise ratio to achieve a block error probability of 10^{-2}. The orthogonal code and diagonal algebraic code yield improvements of 1.0dB and 2.1dB, respectively, over the orthogonal code with sphere packing for the fast fading channel. This case corresponds to space-time symbols with low temporal correlation but high spatial correlation due to the fractional wavelength spacing at the transmitter and small scattering radius. For the slow fading channel ($f_d T_s = 0.0033$) the diagonal algebraic code requires 37.8dB signal to noise ratio to achieve a block error probability of 10^{-2}. The orthogonal code and the orthogonal code with sphere packing yield improvements of 0.5dB and 0.7dB, respectively, over the diagonal algebraic code for this case. With reference to Figure 3.8 and considering a block error probability of 10^{-2}, the best performing space-time code for the fast fading channel is the diagonal algebraic code. However, this code yields the worst performance among all codes investigated for the slow fading channel and the un-

correlated (space and time) channel. Also from Figure 3.8 it can be seen that the space-time code yielding the best performance for a fixed value of normalized Doppler frequency depends on the signal to noise ratio. For the fast fading channel, for example, the best code for signal to noise ratios less than 19.7dB is the orthogonal code with sphere packing while the best code for signal to noise ratios greater than 19.7dB is the diagonal algebraic code. Similar effects can be observed for the channel with normalized Doppler frequency of $f_d T_s = 0.05$. It was verified that all space-time codes exhibit the same asymptotic slope of block error probability versus signal to noise ratio for all values of normalized Doppler frequency investigated and thus have the same diversity order. Evidently, the differences in performance are due to differences in coding gain among the various space-time codes.

Figure 3.9 shows the block error probability (union bound) versus signal to noise ratio and normalized Doppler frequency for 2 transmit antennas (5λ spacing), 1 receive antenna, scattering radius standard deviation $\sigma_R = 200$m and the uncorrelated channel. From Figure 3.9 it is seen that increasing the spacing of the transmit antennas from $\lambda/2$ to 5λ combined with an increase in scattering radius standard deviation from $\sigma_R = 10$m to $\sigma_R = 200$m produces a channel with low spatial correlation and results in error performance indistinguishable from the uncorrelated (space and time) channel for all variations of normalized Doppler frequency that were investigated. With reference to Figure 3.9, the diagonal algebraic code requires 26.4dB signal to noise ratio to achieve a block error probability of 10^{-2} and the orthogonal code and orthogonal code with sphere packing provide improvements of 1.4dB and 1.7dB, respectively, over the diagonal algebraic code.
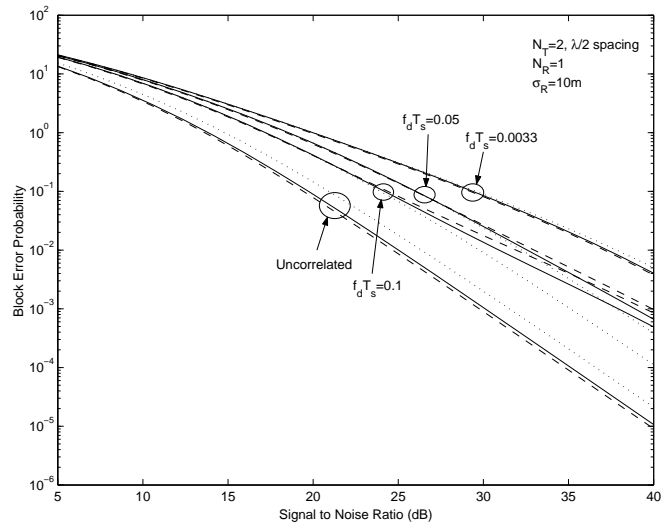
Figure 3.8: Orthogonal code with 16-QAM symbols (solid curve), orthogonal code with sphere packing (dashed curve), diagonal algebraic code (dotted curve). Block error probability (union bound) versus signal to noise ratio and normalized Doppler frequency, 2 transmit antennas ($\lambda/2$ spacing), 1 receive antenna, $\sigma_R = 10$m.
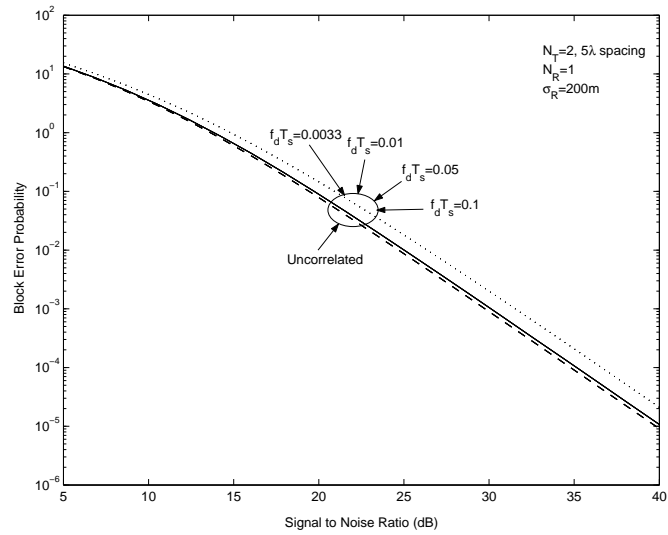
Figure 3.9: Orthogonal code with 16-QAM symbols (solid curve), orthogonal code with sphere packing (dashed curve), diagonal algebraic code (dotted curve). Block error probability (union bound) versus signal to noise ratio and normalized Doppler frequency, 2 transmit antennas (5λ spacing), 1 receive antenna, $\sigma_R = 200$m.

4 Transmit Antennas

Figure 3.10 shows the block error probability (union bound) versus signal to noise ratio and normalized Doppler frequency for 4 transmit antennas ($\lambda/2$ spacing), 1 receive antenna, scattering radius standard deviation $\sigma_R = 10$m and the uncorrelated channel. For the fast fading channel ($f_d T_s = 0.1$) the cyclic code requires 29.3dB signal to noise ratio to achieve a block error probability of 10^{-4}. The orthogonal code with sphere packing and the diagonal algebraic code yield improvements of 0.7dB and 1.0dB, respectively, over the cyclic code for the fast fading channel. This case corresponds to space-time symbols with low temporal correlation but high spatial correlation due to the fractional wavelength spacing at the transmitter and small scattering radius. For the slow fading channel ($f_d T_s = 0.0033$) the cyclic code requires 41.7dB signal to noise ratio to achieve a block error probability of 10^{-4}. The diagonal algebraic code and the orthogonal code with sphere packing yield improvements of 0.4dB and 2.0dB, respectively, over the cyclic code for this case. With reference to Figure 3.10, it can be seen that the space-time code yielding the best performance for a fixed value of normalized Doppler frequency depends on the signal to noise ratio. For the fast fading channel, for example, the best code for signal to noise ratios less than 34.8dB is the diagonal algebraic code while the best code for signal to noise ratios greater than 34.8dB is the orthogonal code with sphere packing. Similar effects can be observed for the channel with normalized Doppler frequency of $f_d T_s = 0.05$. It was verified that all space-time codes exhibit the same asymptotic slope of block error probability versus signal to noise ratio for all values of normalized Doppler frequency investigated and thus have the same diversity order.

Figure 3.11 shows the block error probability (union bound) versus signal to
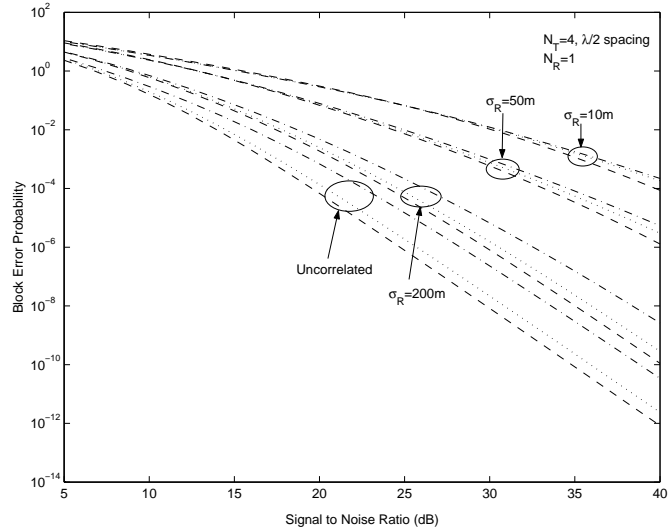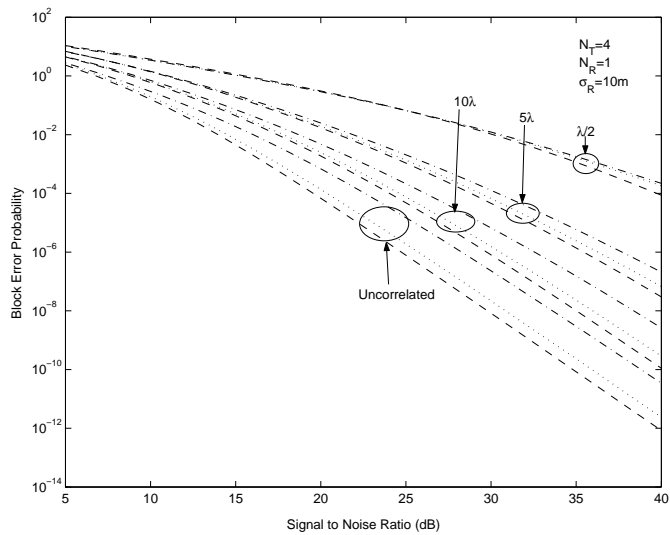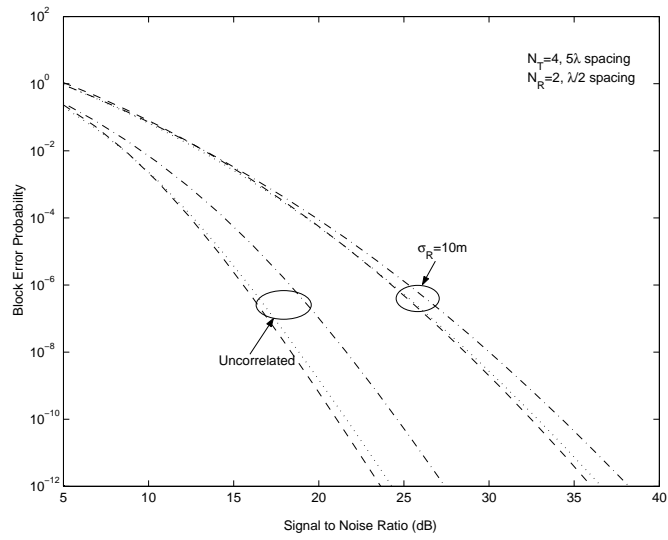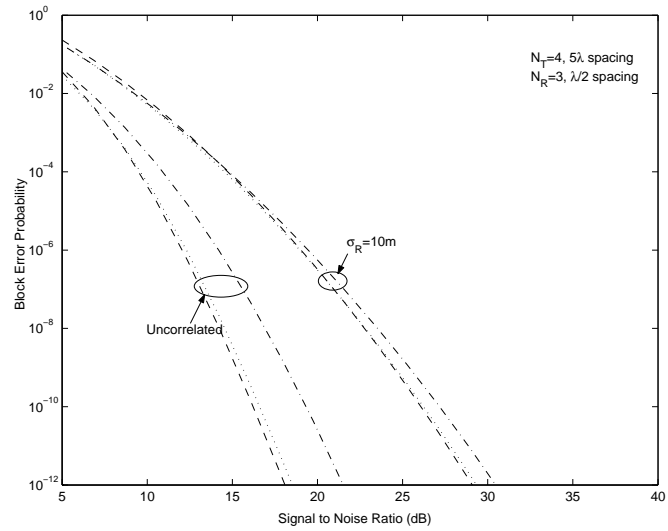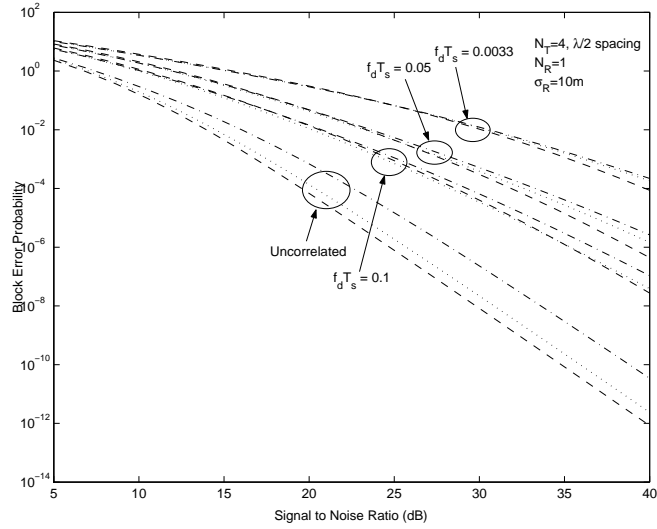
Figure 3.10: Orthogonal code with sphere packing (dashed curve), diagonal algebraic code (dotted curve), cyclic code (dash-dotted curve). Block error probability (union bound) versus signal to noise ratio and normalized Doppler frequency, 4 transmit antennas ($\lambda/2$ spacing), 1 receive antenna, $\sigma_R = 10$m.

noise ratio and normalized Doppler frequency for 4 transmit antennas (5λ spacing), 1 receive antenna, scattering radius standard deviation $\sigma_R = 200$m and the uncorrelated channel. Comparing Figures 3.10 and 3.11 it can be seen that increasing the transmit antenna separation and increasing the scattering radius standard deviation produces a channel with low spatial correlation and results in performance virtually indistinguishable from the uncorrelated (space and time) channel despite variations in the normalized Doppler frequency. With reference to Figure 3.11 the cyclic code requires 22.7dB signal to noise ratio to achieve a block error probability of 10^{-4}, the diagonal algebraic code and orthogonal code with sphere packing provide improvements of 2.1dB and 2.9dB, respectively, over the cyclic code.
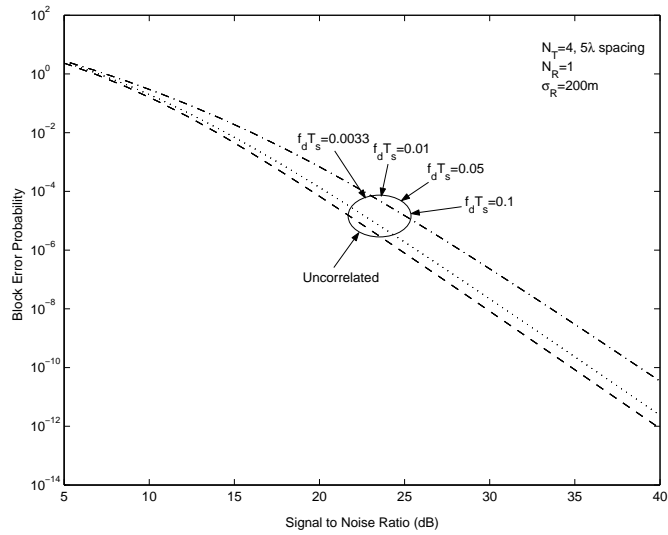
Figure 3.11: Orthogonal code with sphere packing (dashed curve), diagonal algebraic code (dotted curve), cyclic code (dash-dotted curve). Block error probability (union bound) versus signal to noise ratio and normalized Doppler frequency, 4 transmit antennas (5λ spacing), 1 receive antenna, $\sigma_R = 200$m.

3.6 Chapter Summary

In this chapter we analyzed the performance of several space-time block coding techniques for spatially and temporally correlated wireless channels. An upper bound on the probability of a block error was found using the exact pairwise error probability for arbitrary space-time block codes. Using the general space-time covariance model derived in the previous chapter, we presented extensive numerical results that illustrate the performance of the proposed transmit diversity techniques for the two-dimensional Gaussian scatterer model. The numerical results are summarized in the following.

For the slow fading wireless channel ($f_d T_s = 0.0033$), spatial correlation caused by fractional wavelength spacing at the transmitter or scatterers located in close proximity to the mobile, resulted in significant performance degradation relative to the uncorrelated (space and time) channel. For example, for the case of 2 transmit antennas there was roughly a 12dB difference in signal to noise ratio required (averaged over all space-time codes) to achieve 10^{-2} block error probability for the uncorrelated channel compared to the channel with scattering radius standard deviation $\sigma_R = 10$m for $\lambda/2$ transmit antenna spacing. It was found that increasing the spacing of transmit antennas to 30λ (10.5m) yielded performance within 0.5dB of that for the uncorrelated channel for all space-time codes. For the case of 4 transmit antennas there was roughly a 20dB difference in signal to noise ratio required (averaged over all space-time codes) to achieve 10^{-4} block error probability for the uncorrelated channel compared to the channel with scattering radius standard deviation $\sigma_R = 10$m for $\lambda/2$ transmit antenna spacing. For this case it was found that increasing the spacing of transmit antennas to 40λ (14.0m) yielded performance within 0.5dB of that for the uncorrelated channel for all space-time

codes. In some scenarios it may impractical, due to physical constraints, for example, to achieve the transmit antenna spacing required for performance comparable to the uncorrelated channel. In such cases some performance loss is inevitable and the results presented allow the performance degradation to be quantified.

Effects due to temporal correlation between adjacent space-time symbols resulting from mobile motion were also investigated. If the transmission paths are spatially correlated a significant performance degradation is observed for slow fading ($f_d T_s = 0.0033$) compared to fast fading ($f_d T_s = 0.1$). For the case of 2 transmit antennas there was roughly a 6.5dB difference (averaged over all space-time codes) in the signal to noise ratio required to achieve 10^{-2} block error probability for the fast fading channel compared to slow fading for scattering radius standard deviation $\sigma_R = 10$m and $\lambda/2$ transmit antenna spacing. For the case of 4 transmit antennas there was roughly a 12dB difference in the signal to noise ratio required (averaged over all space-time codes) to achieve 10^{-4} block error probability for the fast fading channel compared to the slow fading channel for scattering radius standard deviation $\sigma_R = 10$m and $\lambda/2$ transmit antenna spacing. If the transmission paths are spatially uncorrelated, however, there is virtually no performance difference between the slow fading and fast fading channels. In fact, all variations in the normalized Doppler frequency that were investigated yield performance virtually indistinguishable to that observed for the uncorrelated (space and time) channel for this case.

The numerical results presented indicate that there exists a tradeoff between spatial correlation and temporal correlation effects in determining the performance of systems employing space-time block codes. The best-case wireless channel was found to be uncorrelated in both space and time. However, it was also determined

that the effects of high spatial correlation may be compensated to a certain extent by low temporal correlation and vice versa to achieve performance comparable to the uncorrelated channel.

Chapter 4

Comparison of Space-Time Coding and Beamforming Techniques

4.1 Introduction

In this chapter we evaluate the performance of orthogonal space-time block coding and beamforming techniques for spatially and temporally correlated wireless channels.

For the special case of orthogonal space-time block codes, closed-form expressions for the symbol error probability have been developed for spatially uncorrelated wireless channels [45]. We extend these results to include spatially correlated channels and in addition develop closed-form expressions for the symbol error probability for maximum ratio transmission [27] and beamsteering. It should be noted that in all cases we assume the receiver of the wireless system has perfect knowledge of the channel response. That is, we do not address the problem of channel estimation.

With the aid of the space-time covariance model developed in the previous chapter, we present extensive numerical results that illustrate the error perfor-

mance of these techniques for varying degrees of spatial and temporal correlation of the wireless channel. Since beamforming and space-time coding are competing transmit diversity techniques, we present numerical results that illustrate the tradeoff in performance between these approaches.

The chapter is organized as follows. In Section 4.2 we briefly describe the beamforming techniques that are investigated and related work. Section 4.3 describes the basic system model. The derivation of the exact symbol error probability for orthogonal space-time block coding, maximum ratio transmission, and beamsteering is presented in Section 4.4. Finally, numerical results are presented in Section 4.5.

4.2   Beamforming

Beamforming refers generically to techniques that employ channel state information at the transmitter in some fashion. For example, the receiver may estimate and feed back to the transmitter the mean channel response between each transmit and receive antenna. This approach is referred to as mean-feedback beamforming. A special case of mean-feedback beamforming occurs when the averaging time is zero and the instantaneous channel response is fed back to the transmitter. If the channel response varies rapidly it may be difficult to estimate the mean and consequently the channel covariance is estimated by the receiver and fed back to the transmitter. This approach is referred to as covariance-feedback beamforming. Another approach, which requires only the direction of the mobile relative to the base station may also be considered. We refer to this approach as beamsteering since the transmitter employs directional information to create a spatially selective array response which 'steers' transmitted energy in the direction of the

mobile. Beamsteering does not provide diversity gain but can provide power gain due to the directional nature of the transmitted energy. Additionally, co-channel interference may be reduced since energy is transmitted primarily in the direction of the desired mobile thus minimizing interference. The approach is simple to implement since only the direction of the mobile relative to the base is required. This information can be obtained from positioning devices such as Global Positioning System (GPS) receivers, for example.

In [27] the concept of maximum ratio transmission (MRT) was introduced. With MRT the instantaneous channel response is employed by the transmitter to create array weights that produce signal reinforcement, i.e. diversity gain, at the receiver. This approach can be considered as a special case of mean-feedback beamforming in which the averaging time is reduced to zero and is analogous to the well-known technique of maximum ratio combining (MRC) at the base station [2]. Cavers [28] investigated the performance of MRT where decorrelation of the channel response between the uplink and downlink was considered. Channel decorrelation is due to the time delay and/or frequency offset between the uplink and downlink channels. The bit error rate performance of MRT was determined analytically for binary modulation and a spatially uncorrelated wireless channel.

Jongren et al. [29] investigated combining beamforming and orthogonal space-time coding to exploit channel state information. A pre-determined orthogonal space-time code was linearly transformed to create a new space-time codeword. In order to find the optimal linear transformation the solution of a complicated optimization problem is required. A simplified scenario was considered in which the channel coefficients were assumed to be independent, identically distributed complex Gaussian random variables. Simulation results illustrating the performance

of the proposed scheme were presented for this simplified scenario. Related work on mean-feedback beamforming and covariance-feedback beamforming appears in [30], [31].

4.3   System Model

We employ the system model presented in Section 3.3 except that the channel response is assumed to be constant over the transmission of the space-time code block. The channel response may vary from block to block. Specifically, $h_{p,q}(1) = h_{p,q}(2) = \ldots = h_{p,q}(T) \equiv h_{p,q}$.

Define the $N_T \times N_R$ channel response matrix $\mathbf{H}$ as

$$\mathbf{H} = \begin{pmatrix} h_{1,1} & h_{1,2} & \cdots & h_{1,N_R} \\ h_{2,1} & h_{2,2} & \cdots & h_{2,N_R} \\ \vdots & \vdots & \ddots & \vdots \\ h_{N_T,1} & h_{N_T,2} & \cdots & h_{N_T,N_R} \end{pmatrix} . \tag{4.1}$$

The $N_T \times 1$ vector $\mathbf{h}_q$ is defined as the qth column of $\mathbf{H}$. This vector represents the channel response between all N_T transmit antennas and the qth receive antenna. Also, define the $N_T N_R \times 1$ vector $\mathbf{h}$ obtained by stacking the columns of the channel response matrix $\mathbf{H}$

$$\mathbf{h} = \text{vec}\,(\mathbf{H}) \tag{4.2}$$

$$= \begin{pmatrix} \mathbf{h}_1' & \mathbf{h}_2' & \ldots & \mathbf{h}_{N_R}' \end{pmatrix}'$$

where the symbol $'$ denotes the vector transpose operation.

4.4 Exact Symbol Error Probability

In this section closed-form expressions for the probability of a symbol error are developed for orthogonal space-time block coding, maximum ratio transmission and beamsteering for spatially correlated channels.

4.4.1 Orthogonal Space-Time Block Coding

Li et al. [47] demonstrated that a multiple-input multiple-output (MIMO) system employing orthogonal space-time block coding is equivalent to a single-input single-output (SISO) system assuming the channel response is constant over the space-time code block. Shin and Lee [45],[46] utilized this result to derive the exact symbol error probability for orthogonal space-time block codes with M-ary PSK or QAM symbols and transmitted over spatially uncorrelated channels. In this subsection, we extend this result to include spatially correlated channels.

The instantaneous signal to noise ratio (per symbol) at the output of the maximum likelihood decoder of the equivalent SISO system is given by

$$\gamma = \sum_{p=1}^{N_T} \sum_{q=1}^{N_R} |h_{p,q}|^2 \frac{E_s}{N_T R N_0} = \|\mathbf{H}\|^2 \bar{\gamma}_s \tag{4.3}$$

where $\bar{\gamma}_s = \frac{E_s}{N_T R N_0}$, R is the code rate and

$$\|\mathbf{H}\|^2 = \sum_{p=1}^{N_T} \sum_{q=1}^{N_R} |h_{p,q}|^2 = \mathbf{h}^\dagger \mathbf{h} \, . \tag{4.4}$$

The symbol † denotes the conjugate transpose operation. Due to the random nature of the channel response matrix $\mathbf{H}$, γ is a random variable.

For M-ary PSK symbols, the exact symbol error probability for orthogonal space-time block coding is given by [45]

$$P_{symbol}^{PSK} = \frac{1}{\pi} \int_0^{(M-1)\frac{\pi}{M}} \phi_\gamma \left(-\frac{g_{PSK}}{\sin^2 \theta} \right) d\theta \tag{4.5}$$

with $g_{PSK} = \sin^2\left(\frac{\pi}{M}\right)$ and where

$$\phi_\gamma(s) = \mathrm{E}\left[\exp(s\gamma)\right] \tag{4.6}$$

is the characteristic function of the random variable γ. For the case of $h_{p,q}$ independent and identically distributed complex Gaussian random variables, γ has a χ^2 distribution with $2N_T N_R$ degrees of freedom and

$$\phi_\gamma(s) = \frac{1}{(1 - s\bar{\gamma}_s)^{N_T N_R}} \, . \tag{4.7}$$

Consider now the case of $h_{p,q}$ complex Gaussian and correlated and let

$$\mathbf{R} = \mathrm{E}\left[\mathbf{h}\mathbf{h}^\dagger\right] \tag{4.8}$$

represent the spatial covariance matrix of the channel. We have

$$\phi_\gamma(s) = \mathrm{E}\left[\exp(s\gamma)\right] \tag{4.9}$$

$$= \mathrm{E}\left[\exp(s\mathbf{h}^\dagger\mathbf{h}\bar{\gamma}_s)\right] \, .$$

It can be shown that

$$\phi_\gamma(s) = \frac{1}{\det\left(\mathbf{I} - s\mathbf{R}\bar{\gamma}_s\right)} \tag{4.10}$$

$$= \frac{1}{\prod_{n=1}^{N_T N_R}\left(1 - s\lambda_n\bar{\gamma}_s\right)}$$

where λ_n is the nth eigenvalue of the matrix $\mathbf{R}$. For completeness, a proof of this result is presented in Appendix A. Let N denote the number of distinct eigenvalues and let δ_n denote the multiplicity of the nth eigenvalue. A partial fraction expansion may be performed on (4.10) to yield [48]

$$\phi_\gamma(s) = \sum_{n=1}^{N}\sum_{m=1}^{\delta_n} \frac{\alpha_{n,m}}{\left(1 - s\lambda_n\bar{\gamma}_s\right)^m} \, . \tag{4.11}$$

Substituting this result into (4.5), a closed-form expression for the exact symbol error probability may be obtained by expanding the integral in terms of hypergeometric functions. Specifically,

$$P_{symbol}^{PSK} = \frac{1}{\pi} \int_0^{(M-1)\frac{\pi}{M}} \sum_{n=1}^{N} \sum_{m=1}^{\delta_n} \frac{\alpha_{n,m}}{\left(1 + \frac{g_{PSK}}{\sin^2 \theta} \lambda_n \bar{\gamma}_s\right)^m} \, d\theta \qquad (4.12)$$

$$= \sum_{n=1}^{N} \sum_{m=1}^{\delta_n} \alpha_{n,m} \Psi^{PSK} (m; \lambda_n \bar{\gamma}_s)$$

where

$$\Psi^{PSK} (m; \gamma_s) = \frac{1}{\pi} \int_0^{(M-1)\frac{\pi}{M}} \frac{1}{\left(1 + \frac{g_{PSK}}{\sin^2 \theta} \gamma_s\right)^m} \, d\theta . \qquad (4.13)$$

According to calculations in [45], $\Psi^{PSK} (m; \gamma_s)$ can be specified as

$$\Psi^{PSK} (m; \gamma_s) = \frac{1}{2\sqrt{\pi}} \frac{1}{(1 + \gamma_s g_{PSK})^m} \frac{\Gamma \left(m + \frac{1}{2}\right)}{\Gamma (m + 1)} \, {}_2F_1 \left(m, \frac{1}{2}; m + 1; \frac{1}{1 + \gamma_s g_{PSK}}\right)$$

$$\qquad (4.14)$$

$$+ \frac{1}{\pi} \frac{1}{(1 + \gamma_s g_{PSK})^m} \sqrt{1 - g_{PSK}} \, F_1 \left(\frac{1}{2}; m; \frac{1}{2} - m; \frac{3}{2}; \frac{1 - g_{PSK}}{1 + \gamma_s g_{PSK}}; 1 - g_{PSK}\right)$$

where ${}_2F_1 (a, b; c; z)$ and $F_1 (a, b_1; b_2; c; z_1, z_2)$ are the Gauss and Appell hypergeometric functions, respectively, and $\Gamma(z)$ denotes the Gamma function [1].

A similar development may be followed for the case of M-ary QAM baseband symbols. The details are not presented here but are summarized as follows. The probability of a symbol error for orthogonal space-time block coding with M-ary QAM baseband symbols and $h_{p,q}$ complex Gaussian and correlated can be written as

$$P_{symbol}^{QAM} = \sum_{n=1}^{N} \sum_{m=1}^{\delta_n} \alpha_{n,m} \Psi^{QAM} (m; \lambda_n \bar{\gamma}_s) \qquad (4.15)$$

where

$$\Psi^{QAM}(m;\gamma_s) = \frac{2q}{\sqrt{\pi}} \frac{1}{(1+\gamma_s g_{QAM})^m} \frac{\Gamma\left(m+\frac{1}{2}\right)}{\Gamma(m+1)} \, {}_2F_1\left(m,\frac{1}{2};m+1;\frac{1}{1+\gamma_s g_{QAM}}\right)$$

(4.16)

$$- \frac{2q^2}{\pi} \frac{1}{2m+1} \frac{1}{(1+2\gamma_s g_{QAM})^m} F_1\left(1;m;1;m+\frac{3}{2};\frac{1+\gamma_s g_{QAM}}{1+2\gamma_s g_{QAM}};\frac{1}{2}\right)$$

with $q = 1 - \frac{1}{\sqrt{M}}$ and $g_{QAM} = \frac{3}{2(M-1)}$ [46].

We have derived exact expressions for the symbol error probability for orthogonal space-time block coding for spatially correlated channels. Note that for the special case of a spatially uncorrelated channel, i.e. $\mathbf{R} = \mathbf{I}$ and $\lambda_n = 1$, $n = 1,\ldots,N_T N_R$, (4.12) and (4.15) reduce to the results presented in [45]. If the eigenvalues of the spatial covariance matrix $\mathbf{R}$ are distinct, the expressions for the symbol error probability simplify to

$$P_{symbol}^{PSK} = \sum_{n=1}^{N_T N_R} \alpha_{n,1} \Psi^{PSK}(1;\lambda_n \bar{\gamma}_s)$$

(4.17)

and

$$P_{symbol}^{QAM} = \sum_{n=1}^{N_T N_R} \alpha_{n,1} \Psi^{QAM}(1;\lambda_n \bar{\gamma}_s)$$

(4.18)

for M-ary PSK and M-ary QAM symbols, respectively.

4.4.2   Maximum Ratio Transmission

For maximum ratio transmission the array weight applied to the pth transmit antenna is

$$w_p = \frac{\tilde{h}_{p,1}^*}{\sqrt{\sum_{p=1}^{N_T} |\tilde{h}_{p,1}|^2}}$$

(4.19)

where $\tilde{h}_{p,1}$ is the estimated channel response between the pth transmit antenna and the single receive antenna. The signal $c_p(t)$ in (3.1) is given by

$$c_p(t) = w_p \, s(t)$$

(4.20)

where w_p is the array weight applied to the pth transmit antenna and $s(t)$ represents the M-PSK or M-QAM baseband symbol transmitted at time t. The array weights are normalized such that

$$\sum_{p=1}^{N_T} |w_p|^2 = 1 \,. \tag{4.21}$$

In our work it is assumed that the receiver estimates the channel response perfectly but there is a delay in the application of the estimated channel response by the transmitter. That is,

$$\tilde{h}_{p,1}(t) = h_{p,1}(t - \Delta t) \tag{4.22}$$

where Δt represents the feedback time delay. Define ρ as the correlation between the estimated and actual channel response, i.e.,

$$\rho = \frac{\mathrm{E}\left[h_{p,1}(t)\tilde{h}_{p,1}^*(t)\right]}{\sigma_h^2} \tag{4.23}$$
$$= \frac{\mathrm{E}\left[h_{p,1}(t)h_{p,1}^*(t - \Delta t)\right]}{\sigma_h^2}$$

where

$$\sigma_h^2 = \mathrm{E}\left[|h_{p,1}(t)|^2\right] \,. \tag{4.24}$$

ρ depends on the temporal correlation characteristics of the wireless channel. This parameter can be computed from the space-time covariance model developed in the previous chapter. For zero time delay, i.e. $\Delta t = 0$, corresponding to the case of perfect feedback ($\rho = 1$), the instantaneous signal to noise ratio at the receive antenna is

$$\gamma = \sum_{p=1}^{N_T} |h_{p,1}|^2 \frac{E_s}{N_0} \tag{4.25}$$

Noting the similarity between (4.25) and (4.3) for $N_R = 1$ and upon redefining $\bar{\gamma}_s = \frac{E_s}{N_0}$, the results of the previous section may be applied to determine the

symbol error probability for this case. Specifically,

$$P_{symbol}^{PSK} = \sum_{n=1}^{N} \sum_{m=1}^{\delta_n} \alpha_{n,m} \Psi^{PSK} (m; \lambda_n \bar{\gamma}_s) \qquad (4.26)$$

for M-ary PSK and

$$P_{symbol}^{QAM} = \sum_{n=1}^{N} \sum_{m=1}^{\delta_n} \alpha_{n,m} \Psi^{QAM} (m; \lambda_n \bar{\gamma}_s) \qquad (4.27)$$

for M-ary QAM with λ_n corresponding to the nth eigenvalue of the spatial co-variance matrix $\mathbf{R}$, δ_n its multiplicity, N the number of distinct eigenvalues, and $\bar{\gamma}_s = \frac{E_s}{N_0}$.

For the case of non-zero time delay, corresponding to imperfect feedback ($\rho \neq 1$), an analytical approach for determining the symbol error probability does not appear to be tractable. In the sequel Monte Carlo simulations are used to determine the error probability for this case.

4.4.3 Beamsteering

For the case of beamsteering the array weights are given by

$$w_p = \frac{\exp(j\phi_p)}{\sqrt{N_T}} \qquad (4.28)$$

where the angle ϕ_p is determined by the array geometry and the direction in which the beam is steered. The signal $c_p(t)$ in (3.1) is given by

$$c_p(t) = w_p \, s(t) \qquad (4.29)$$

where w_p is the array weight applied to the pth transmit antenna and $s(t)$ represents the M-PSK or M-QAM baseband symbol transmitted at time t. The array weights are normalized such that

$$\sum_{p=1}^{N_T} |w_p|^2 = 1 \, . \qquad (4.30)$$

For simplicity we assume that the mobile is broadside to a linear antenna array with N_T elements at the base station. The instantaneous signal to noise ratio at the receive antenna is

$$\gamma = \left| \sum_{p=1}^{N_T} h_{p,1} \right|^2 \frac{E_s}{N_T N_0} \; . \tag{4.31}$$

The quantity $\left| \sum_{p=1}^{N_T} h_{p,1} \right|^2$ is χ^2 distributed with 2 degrees of freedom. Upon re-defining

$$\bar{\gamma}_s = \mathrm{E} \left[\left| \sum_{p=1}^{N_T} h_{p,1} \right|^2 \right] \frac{E_s}{N_T N_0} \tag{4.32}$$

$$= \sum_{r=1}^{N_T} \sum_{s=1}^{N_T} \mathrm{E} \left[h_{r,1} h_{s,1}^* \right] \frac{E_s}{N_T N_0} \tag{4.33}$$

the results of the previous section may also be used to determine the symbol error probability for this case. Specifically,

$$P_{symbol}^{PSK} = \Psi^{PSK} \left(1; \bar{\gamma}_s \right) \tag{4.34}$$

for M-ary PSK and

$$P_{symbol}^{QAM} = \Psi^{QAM} \left(1; \bar{\gamma}_s \right) \tag{4.35}$$

for M-ary QAM baseband symbols.

4.4.4 Comparison of Exact Symbol Error Probability with Monte Carlo Simulations

We have verified the expressions developed for the exact symbol probability with Monte Carlo simulations. The results of these comparisons are presented in this section.

The simulations used a two-dimensional Gaussian model for the scatterer geometry and the standard deviation of the scattering radius was varied from $\sigma_R =$

$10, 50, 200$m. The distance between the mobile and base (array phase center) was fixed at $d = 1000$m and the mobile location was broadside to the base antenna array.

Figures 4.1 and 4.2 show the comparison of the Monte Carlo simulations with the exact symbol error probability for orthogonal space-time block coding for 2 and 4 transmit antennas, respectively. The space-time block codes used were the G_2 and H_4 codes due to Tarokh [33],[34].

Figures 4.3 and 4.4 show the comparison of the Monte Carlo simulations with the exact symbol error probability for maximum ratio transmission for 2 and 4 transmit antennas, respectively, and perfect feedback correlation, i.e. $\rho = 1$.

Figures 4.5 and 4.6 show the comparison of the Monte Carlo simulations with the exact symbol error probability for beamsteering for 2 and 4 transmit antennas, respectively.

In all cases, excellent agreement between the Monte Carlo simulations and the exact calculation of the symbol error probability is observed.

4.5 Numerical Results

In this section we compare the error performance of orthogonal space-time block coding, maximum ratio transmission and beamsteering using a two-dimensional Gaussian scattering model. Linear array geometry was employed at the base station for all results.

The standard deviation of the scattering radius for the two-dimensional Gaussian model was varied from $\sigma_R = 10, 50, 200$m and the distance between the mobile and base (array phase center) was fixed at $d = 1000$m. The parameter σ_R specifies the radius about the mobile for which approximately 68 percent of the
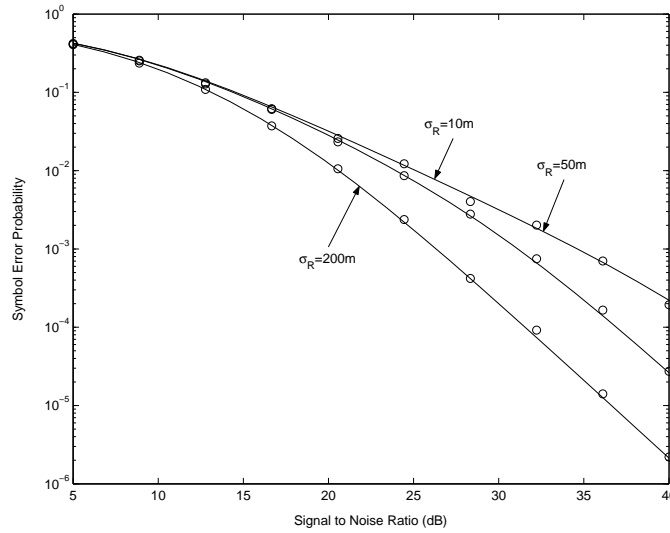
Figure 4.1: Comparison of exact symbol error probability with Monte Carlo simulations for orthogonal space-time block coding. 2 transmit antennas ($\lambda/2$ spacing), 1 receive antenna, 3 bits/s/Hz spectral efficiency and σ_R=10,50,200m.
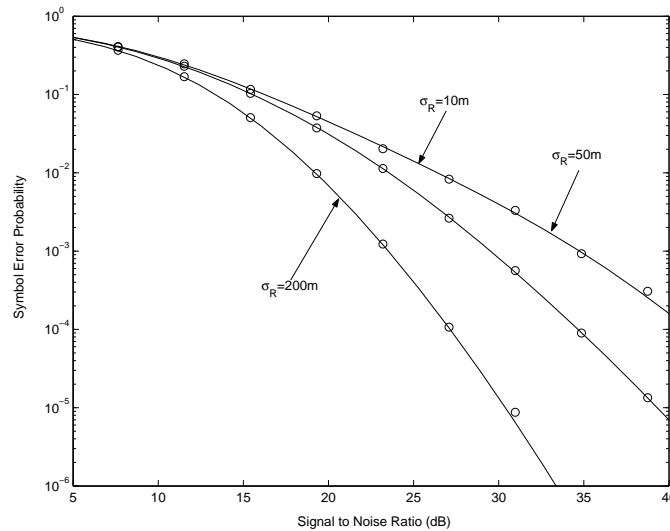
Figure 4.2: Comparison of exact symbol error probability with Monte Carlo simulations for orthogonal space-time block coding. 4 transmit antennas ($\lambda/2$ spacing), 1 receive antenna, 3 bits/s/Hz spectral efficiency and σ_R=10,50,200m.
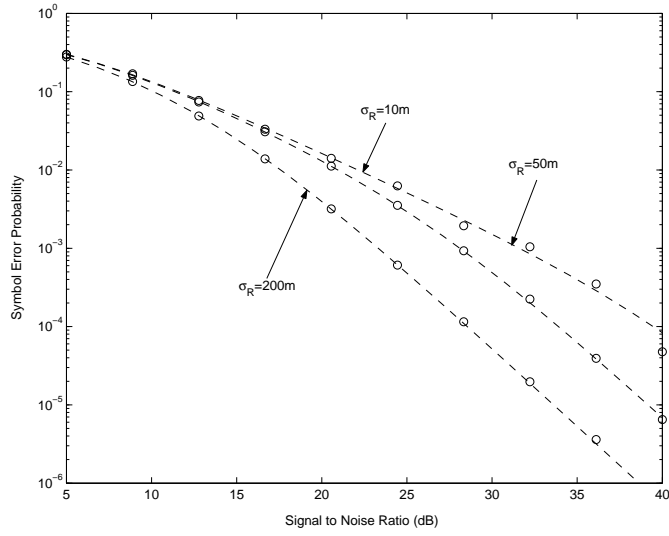
Figure 4.3: Comparison of exact symbol error probability with Monte Carlo simulations for maximum ratio transmission, $\rho = 1$. 2 transmit antennas ($\lambda/2$ spacing), 1 receive antenna, 3 bits/s/Hz spectral efficiency and σ_R=10,50,200m.
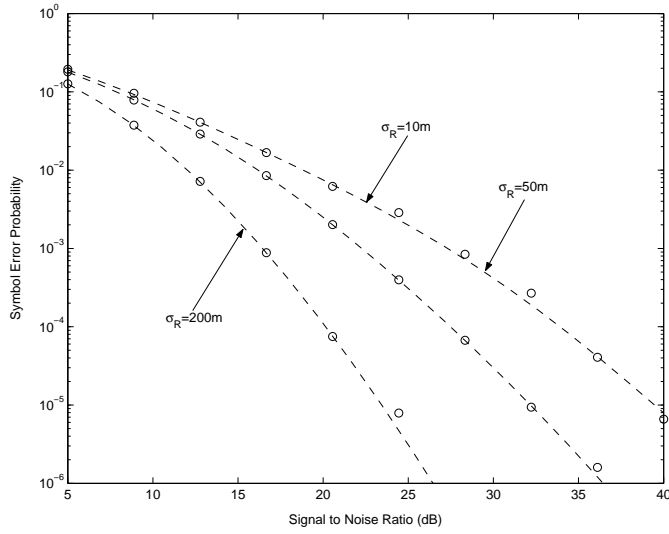
Figure 4.4: Comparison of exact symbol error probability with Monte Carlo simulations for maximum ratio transmission, $\rho = 1$. 4 transmit antennas ($\lambda/2$ spacing), 1 receive antenna, 3 bits/s/Hz spectral efficiency and σ_R=10,50,200m.
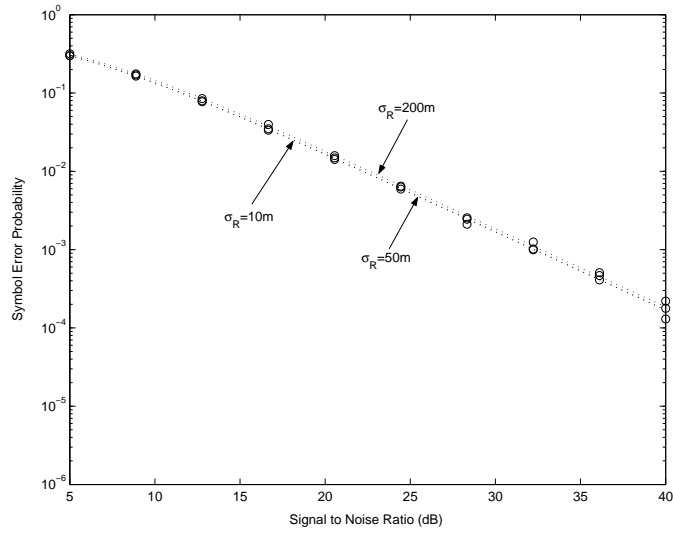
Figure 4.5: Comparison of exact symbol error probability with Monte Carlo simulations for beamsteering. 2 transmit antennas ($\lambda/2$ spacing), 1 receive antenna, 3 bits/s/Hz spectral efficiency and σ_R=10,50,200m.
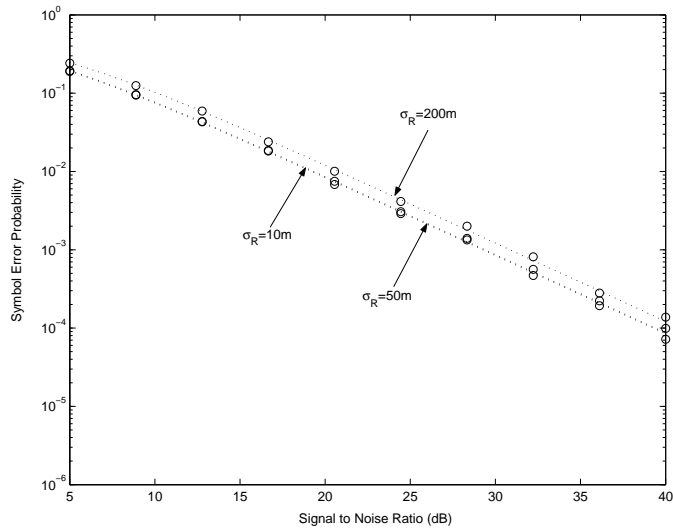
Figure 4.6: Comparison of exact symbol error probability with Monte Carlo simulations for beamsteering. 4 transmit antennas ($\lambda/2$ spacing), 1 receive antenna, 3 bits/s/Hz spectral efficiency and σ_R=10,50,200m.

scatterers are contained. The smallest value for σ_R yields the ratio $\sigma_R/d = 0.01$ and corresponds to angular spread due to multipath of approximately $1°$ from the perspective of the base station. The largest value for σ_R corresponds to an angular spread of approximately $20°$. The mobile location was broadside to the base antenna array and its velocity was chosen such that the maximum Doppler frequency was approximately $f_d = 78\text{Hz}$ corresponding to a carrier frequency of 850MHz and a maximum speed of 100km/hr. The normalized Doppler frequency was $f_d T_s = 0.0033$ and corresponds to a slow fading channel with a symbol to fading ratio of approximately 300:1. In other words, space-time symbols separated by 300 symbol periods are approximately uncorrelated. Four values for the feedback correlation parameter were considered: $\rho = 1.0, 0.99, 0.95, 0.9$. For a normalized Doppler frequency of $f_d T_s = 0.0033$, these values correspond to feedback time delays of $\Delta t = 0, 0.4, 0.9, 1.3$ milliseconds, respectively.

The orthogonal space-time block codes employed in this work are due to Alamouti and Tarokh [32],[33],[34]. We consider code designs for 2 and 4 transmit antennas. For 2 transmit antennas, the space-time code G_2 with code rate 1 was used.

$$G_2(x_1, x_2) = \begin{pmatrix} x_1 & x_2 \\ -x_2^* & x_1^* \end{pmatrix} \tag{4.36}$$

For this case we employed a 8PSK signal constellation yielding a spectral efficiency of 3 bits/s/Hz. For 4 transmit antennas the space-time code H_4 with code rate

3/4 was used.

$$H_4(x_1, x_2, x_3) = \tag{4.37}$$

$$\begin{pmatrix} x_1 & x_2 & \frac{x_3}{\sqrt{2}} & \frac{x_3}{\sqrt{2}} \\ -x_2^* & x_1^* & \frac{x_3}{\sqrt{2}} & -\frac{x_3}{\sqrt{2}} \\ \frac{x_3^*}{\sqrt{2}} & \frac{x_3^*}{\sqrt{2}} & \frac{(-x_1-x_1^*+x_2-x_2^*)}{2} & \frac{(-x_2-x_2^*+x_1-x_1^*)}{2} \\ \frac{x_3^*}{\sqrt{2}} & -\frac{x_3^*}{\sqrt{2}} & \frac{(x_2+x_2^*+x_1-x_1^*)}{2} & -\frac{(x_1+x_1^*+x_2-x_2^*)}{2} \end{pmatrix}$$

For this case a 16QAM signal constellation was used and resulted in a spectral efficiency of 3 bits/s/Hz.

The symbol error probability was computed using (4.12) for M-ary PSK symbols or (4.15) for M-ary QAM symbols for orthogonal space-time block coding, (4.34) or (4.35) for beamsteering and (4.26) or (4.27) for maximum ratio transmission with $\rho = 1.0$. For maximum ratio transmission with $\rho = 0.99, 0.95, 0.9$ the symbol error probability was determined from Monte Carlo simulations. 8PSK signal constellations were used for both beamsteering and maximum ratio transmission resulting in a spectral efficiency of 3 bits/s/Hz. In the following performance results for 2 transmit antennas are presented first followed by results for 4 transmit antennas.

Figure 4.7 shows the symbol error probability versus signal to noise ratio for 2 transmit antennas ($\lambda/2$ spacing), 1 receive antenna and scattering radius standard deviation $\sigma_R = 200$m. With reference to Figure 4.7 we observe that maximum ratio transmission (MRT) uniformly outperforms orthogonal space-time block coding (OSTBC) by 3dB for perfect feedback correlation, i.e. $\rho = 1.0$. However, the results for $\rho = 0.99, 0.95, 0.9$ demonstrate that the performance of MRT degrades rapidly for a slight reduction in the feedback correlation parameter. The primary effects observed are an apparent loss of diversity order and reduced coding gain

compared with the case of perfect feedback correlation. Furthermore, for the case of imperfect feedback ($\rho \neq 1$) it can be seen that OSTBC outperforms MRT above a certain threshold value of signal to noise ratio. As will be demonstrated, the threshold value of signal to noise ratio depends on the feedback correlation parameter as well as the scattering radius and will be quantified later in this section.

Figures 4.8 and 4.9 show the results for scattering radius standard deviation $\sigma_R = 50, 10m$, respectively. Several observations may be made from these figures. First, the performance of both OSTBC and MRT degrade significantly as the scattering radius is reduced. Decreasing the scattering radius increases the correlation between the signals transmitted from each antenna and reduces performance. In contrast, the performance of beamsteering is not significantly affected by decreasing the scattering radius. Since the distance between the mobile and base station is fixed, decreasing the scattering radius corresponds to decreasing the angular spread of the multipath from the perspective of the base station. Second, it can be seen by comparing Figures 4.7,4.8 and 4.9 that the performance of MRT approaches that of beamsteering as the scattering radius is reduced. Also, in some cases beamsteering outperforms OSTBC below a certain threshold value of signal to noise ratio. The performance tradeoff between beamsteering and OSTBC is quantified later in this section.

Figure 4.10 shows the symbol error probability versus signal to noise ratio for 4 transmit antennas ($\lambda/2$ spacing), 1 receive antenna and scattering radius standard deviation $\sigma_R = 200$m. With reference to Figure 4.10 we observe that maximum ratio transmission (MRT) uniformly outperforms orthogonal space-time block coding (OSTBC) by about 7dB for perfect feedback correlation, i.e. $\rho = 1.0$.

It is also apparent from the figure that MRT provides the same diversity order as beamsteering for $\rho = 0.95, 0.9$, i.e. diversity order 1. Figures 4.11 and 4.12 show the results for scattering radius standard deviation $\sigma_R = 50, 10m$, respectively. Comparing Figures 4.10,4.11 and 4.12 it is seen that the performance of MRT approaches that of beamsteering as the scattering radius is reduced. For $\sigma_R = 10m$, both MRT and beamsteering outperform OSTBC over the range of signal to noise ratio from 5-40dB. The performance tradeoff between MRT, OSTBC and beamsteering is quantified next.

The results presented illustrate that the relative performance of MRT, OSTBC and beamsteering depends on the value of the feedback correlation parameter ρ, as well as the scattering radius standard deviation σ_R. For example, in comparing beamsteering and OSTBC it was determined that the performance of OSTBC exceeds that of beamsteering above a certain threshold value of signal to noise ratio. This value of signal to noise ratio may be determined analytically by equating the expressions for the symbol error probability for beamsteering and OSTBC as developed in a previous section. Numerical search techniques may be used to quickly find the value of signal to noise ratio that yields equal symbol error probabilities. Figure 4.13 illustrates the results for beamsteering and 3 orthogonal space-time codes: the G_2 code for 2 transmit antennas, the H_3 code for 3 transmit antennas and the H_4 code for 4 transmit antennas [33],[34]. The horizontal axis of this figure shows the threshold value of signal to noise ratio and the vertical axis shows the scattering radius standard deviation. With reference to Figure 4.13 it is observed that the threshold value of signal to noise ratio increases as the scattering radius is reduced. Thus, beamsteering is favored over OSTBC over a large range of signal to noise ratios at small values of scattering radius.

Since no analytical formulas are available for the symbol error probability of MRT for $\rho \neq 1$, the threshold values of signal to noise ratio were determined empirically from the results of Monte Carlo simulations. Figures 4.14 and 4.15 illustrate the results for 2 transmit antennas ($\lambda/2$ spacing) and 4 transmit ($\lambda/2$ spacing) antennas, respectively. From these figures it is observed that for a fixed value of ρ the threshold value of signal to noise ratio increases as the scattering radius is decreased. As a result, MRT is favored over OSTBC for a large range of signal to noise ratios at small values of scattering radius. Considering variations in the feedback correlation ρ for a fixed value of scattering radius, it is observed that the threshold value of signal to noise ratio increases as $\rho \to 1$. Thus, as the quality of the feedback improves MRT provides superior performance to OSTBC over a broader range of signal to noise ratios.

The results presented in this section apply primarily for vehicular applications. For the case of pedestrian users the requirements for timely feedback of channel state information to the transmitter are considerably relaxed. For example, if the maximum speed is assumed to be 1km/hr then the time delays corresponding to feedback correlation values of $\rho = 1.0, 0.99, 0.95, 0.9$ are $\Delta t = 0, 40, 90, 130$ milliseconds, respectively.

4.6   Chapter Summary

In this chapter we analyzed the performance of orthogonal space-time block coding and beamforming techniques for spatially and temporally correlated wireless channels. For the case of orthogonal space-time block codes and quasi-static channel response, a closed-form expression was derived for the symbol error probability for spatially correlated channels, extending previously known results for uncor-
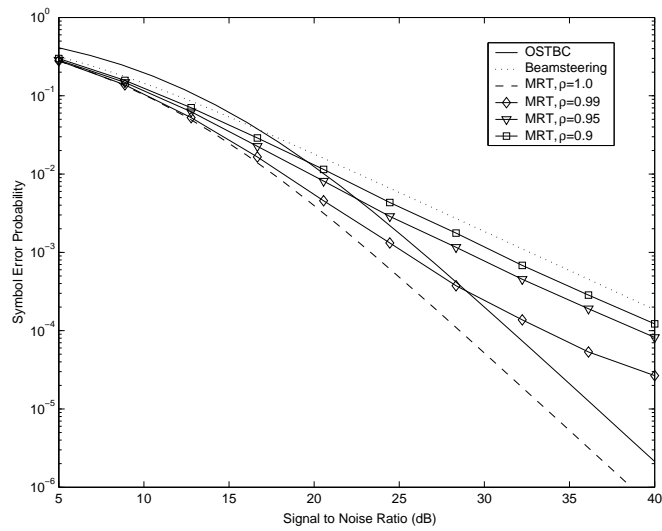
Figure 4.7: Symbol error probability versus signal to noise ratio for orthogonal space-time block coding, beamsteering and maximum ratio transmission. 2 transmit antennas ($\lambda/2$ spacing), 1 receive antenna, 3 bits/s/Hz spectral efficiency and σ_R=200m.
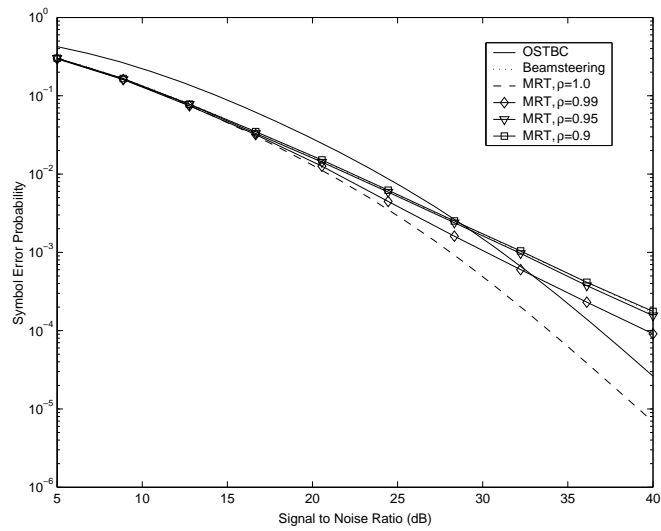
Figure 4.8: Symbol error probability versus signal to noise ratio for orthogonal space-time block coding, beamsteering and maximum ratio transmission. 2 transmit antennas ($\lambda/2$ spacing), 1 receive antenna, 3 bits/s/Hz spectral efficiency and σ_R=50m.
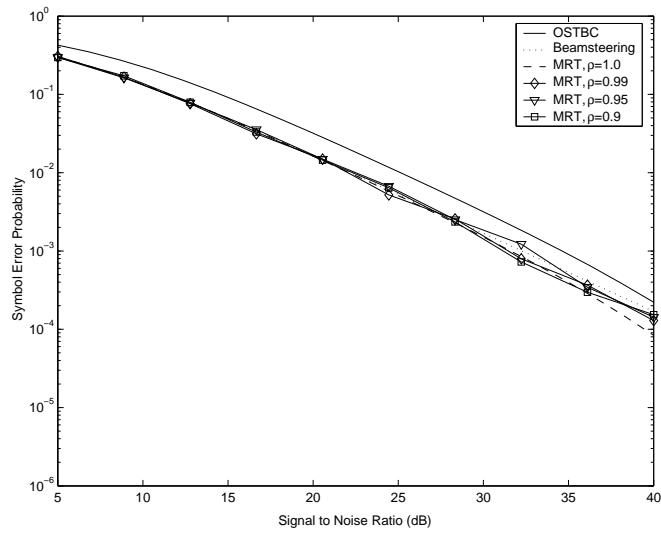
Figure 4.9: Symbol error probability versus signal to noise ratio for orthogonal space-time block coding, beamsteering and maximum ratio transmission. 2 transmit antennas ($\lambda/2$ spacing), 1 receive antenna, 3 bits/s/Hz spectral efficiency and σ_R=10m.
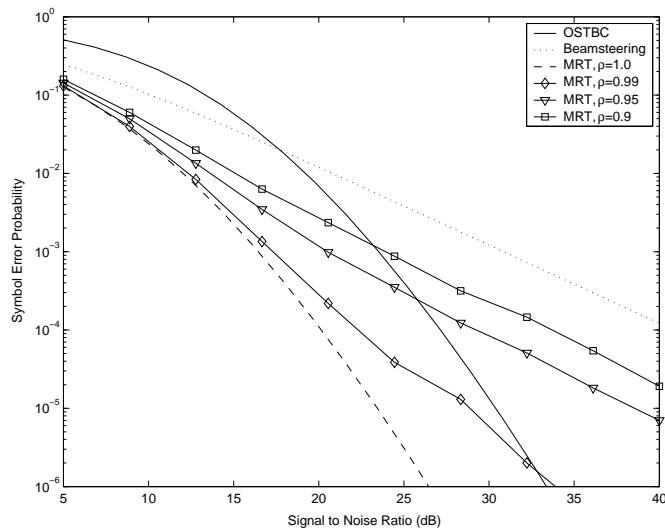
Figure 4.10: Symbol error probability versus signal to noise ratio for orthogonal space-time block coding, beamsteering and maximum ratio transmission. 4 transmit antennas ($\lambda/2$ spacing), 1 receive antenna, 3 bits/s/Hz spectral efficiency and σ_R=200m.
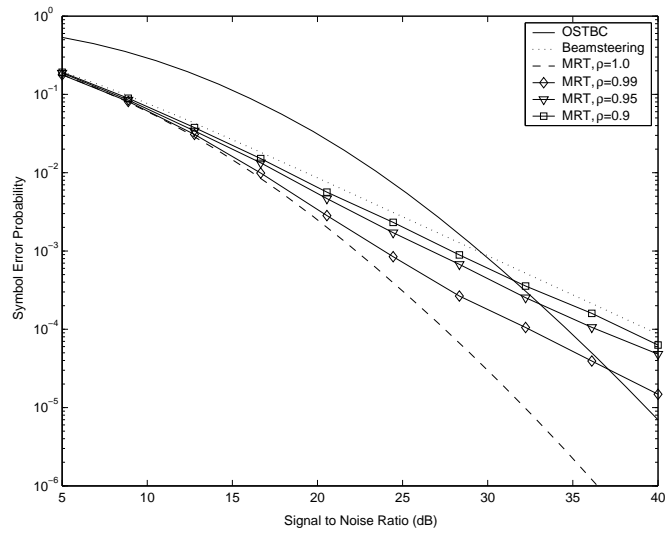
Figure 4.11: Symbol error probability versus signal to noise ratio for orthogonal space-time block coding, beamsteering and maximum ratio transmission. 4 transmit antennas ($\lambda/2$ spacing), 1 receive antenna, 3 bits/s/Hz spectral efficiency and σ_R=50m.
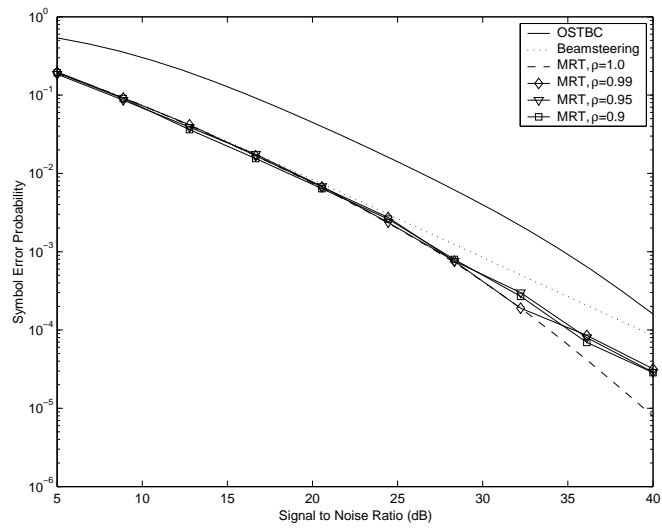
Figure 4.12: Symbol error probability versus signal to noise ratio for orthogonal space-time block coding, beamsteering and maximum ratio transmission. 4 transmit antennas ($\lambda/2$ spacing), 1 receive antenna, 3 bits/s/Hz spectral efficiency and σ_R=10m.
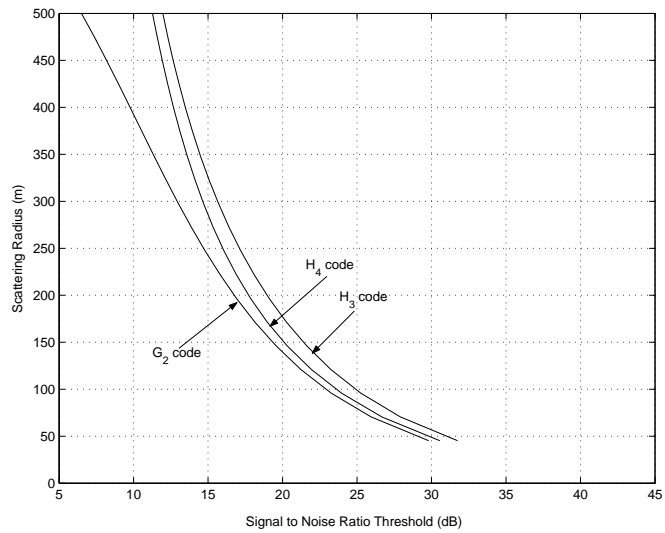
Figure 4.13: Signal to noise ratio threshold for switching between orthogonal space-time block coding and beamsteering versus scattering radius standard deviation. 2,3 and 4 transmit antennas ($\lambda/2$ spacing), 1 receive antenna, 3 bits/s/Hz spectral efficiency.
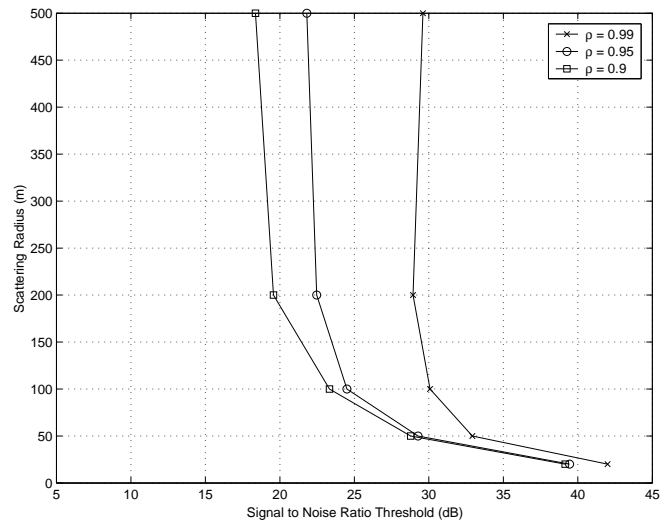
Figure 4.14: Signal to noise ratio threshold for switching between orthogonal space-time block coding and maximum ratio transmission versus scattering radius standard deviation and feedback correlation parameter. 2 transmit antennas ($\lambda/2$ spacing), 1 receive antenna, 3 bits/s/Hz spectral efficiency.
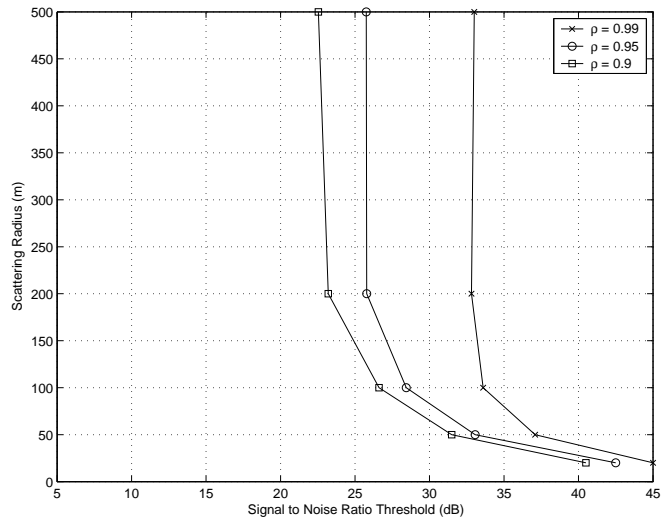
Figure 4.15: Signal to noise ratio threshold for switching between orthogonal space-time block coding and maximum ratio transmission versus scattering radius standard deviation and feedback correlation parameter. 4 transmit antennas ($\lambda/2$ spacing), 1 receive antenna, 3 bits/s/Hz spectral efficiency.

related channels. Closed-form expressions for the symbol error probability were also derived for maximum ratio transmission and beamsteering. Using the general space-time covariance model derived in the previous chapter, we presented extensive numerical results that illustrate the performance of the proposed transmit diversity techniques for the two-dimensional Gaussian scatterer model. The numerical results are summarized in the following.

In the case of perfect channel feedback maximum ratio transmission was shown to yield superior performance over orthogonal space-time block coding and beamsteering. However, it was demonstrated that the performance degrades rapidly with imperfect channel feedback. The primary effects observed were loss of diversity gain and loss of coding gain. The performance of maximum ratio transmission also depends on the angular spread of the channel and it was shown that the technique yields performance comparable to beamsteering when the angular spread due to multipath is small. It was demonstrated that simple beamsteering can provide performance superior to orthogonal space-time block coding in some cases. The performance tradeoff between beamsteering and orthogonal space-time block coding was quantified in terms of signal to noise ratio and scattering radius or equivalently angular spread. In addition, the performance tradeoff between maximum ratio transmission and orthogonal space-time block coding was quantified in terms of signal to noise ratio, scattering radius and feedback correlation.

Chapter 5

Spatial Processing Techniques for Wireless Systems

5.1 Introduction

In this chapter we investigate spatial processing techniques employing multiple receive antennas on the uplink of a wireless communications system. The emphasis here is on the reduction of co-channel interference through the use of such techniques and the effects of multipath angular spread. With the aid of the spatial covariance models developed in a previous chapter we determine the array gain for several common spatial processing techniques. The array gain for the signal, interference and signal+interference are each evaluated so the effects of interference reduction and possible signal degradation may be determined.

The chapter is organized as follows. The spatial processing techniques investigated are described in Section 5.2 and numerical results are presented in Section 5.3.

5.2 Spatial Processing Techniques

5.2.1 Beamsteering

Beamsteering shapes the array response to enhance signals arriving from a particular direction. No other constraints are imposed. For example, to create a response that enhances signals arriving from the direction (θ, ϕ), the components of the array weight vector $\mathbf{w}$ are given by

$$w_p = \exp\left(j\vec{k}\left(\theta, \phi\right) \cdot \vec{x}_p\right) \quad p = 0, \ldots, P-1 \tag{5.1}$$

with the wavenumber vector

$$\vec{k}\left(\theta, \phi\right) = k\left(\sin\theta\cos\phi, \sin\theta\sin\phi, \cos\theta\right) \tag{5.2}$$

$\vec{x}_p$ is the spatial location of the pth array element and $k = 2\pi/\lambda$ with λ the transmitted wavelength. Interference reduction for beamsteering is achieved by reduced sidelobe levels and nulls in the array response since only the desired steering direction is required to determine the array weights.

5.2.2 Linearly-Constrained Minimum Variance

The linearly-constrained minimum variance (LCMV) approach minimizes the output power of the array subject to fixed gain in the desired pointing direction [52]. The optimization problem that underlies the LCMV approach can be stated as finding the array weight vector $\mathbf{w}$ that minimizes the quantity $\mathbf{w}^\dagger \mathbf{R}\mathbf{w}$ subject to the linear constraint $\mathbf{e}^\dagger \mathbf{w} = 1$. The vector $\mathbf{e} = \mathbf{e}\left(\theta, \phi\right)$ determines the pointing direction and its components are given by

$$e_p = \exp\left(j\vec{k}\left(\theta, \phi\right) \cdot \vec{x}_p\right) \quad p = 0, \ldots, P-1 \tag{5.3}$$

with the wavenumber vector

$$\vec{k}(\theta, \phi) = k(\sin\theta\cos\phi, \sin\theta\sin\phi, \cos\theta) \tag{5.4}$$

and $\vec{x}_p$ the spatial location of the pth array element. $\mathbf{R}$ is the estimated spatial covariance matrix (signal, noise and interference combined). The solution to this problem is well-known and the optimum array weight vector is given by

$$\mathbf{w} = \frac{\mathbf{R}^{-1}\mathbf{e}}{\mathbf{e}^{\dagger}\mathbf{R}^{-1}\mathbf{e}} \tag{5.5}$$

The power output of the array using the LCMV algorithm is given by

$$P_{LCMV}(\theta, \phi) = \frac{1}{\mathbf{e}^{\dagger}\mathbf{R}^{-1}\mathbf{e}} \tag{5.6}$$

Note that the optimum weight vector and the output power of the array both depend on the pointing direction (θ, ϕ) through the vector $\mathbf{e}$.

5.2.3 Maximizing the Signal-to-Interference plus Noise Ratio

This approach determines the array weight vector that maximizes the ratio

$$\frac{\mathbf{w}^{\dagger}\mathbf{R}_S\mathbf{w}}{\mathbf{w}^{\dagger}\mathbf{R}_{N+I}\mathbf{w}} \tag{5.7}$$

The numerator of this expression represents the array output power due to the desired signal with spatial covariance matrix $\mathbf{R}_S$. The denominator represents the output power for the noise and interference combined with covariance matrix $\mathbf{R}_{N+I}$. Depending on the application $\mathbf{R}_S$ and $\mathbf{R}_{N+I}$ may be separately estimated from the array data itself, an approach which requires signal training, or may be created based upon models for the signal and interference.

The solution to maximizing the ratio of quadratic forms is given by Rayleigh's theorem [50]. Let the generalized eigenvalues and eigenvectors of the matrix pair $[\mathbf{R}_S, \mathbf{R}_{N+I}]$ be given by $(\lambda_i, \mathbf{v}_i)$ $\quad i = 0, \ldots, P-1$ sorted such that $\lambda_i \leq \lambda_j$ for $i > j$. The array weight vector that maximizes the signal-to-interference ratio is equal to the eigenvector corresponding to the largest eigenvalue, i.e. $\mathbf{w} = \mathbf{v}_1$. The eigenvalue is the maximizing SINR.

5.2.4 Nulling of Interference Sources

This approach creates an array response with nulls (i.e. zero response) in the directions corresponding to sources of interference while minimizing the deviation of the achieved array response from a nominal response. The nominal response is often taken to be the beamsteering response when the array is steered in the direction of the desired signal. Two cases are considered: 0th order nulling in which the array response only is constrained to be zero and 1st order nulling in which both the array response at its derivative are constrained to be zero at the angles where nulls are to be placed.

Define the array response for weight vector $\mathbf{w} = (w_0, w_1, \ldots, w_{P-1})$ to be

$$A\left(\theta, \phi\right) = \sum_{p=0}^{P-1} w_p \exp\left(j\vec{k}\left(\theta, \phi\right) \cdot \vec{x}_p\right) \tag{5.8}$$

The mean-square deviation between the nominal response $A_0(\theta, \phi)$ and the achieved response $A(\theta, \phi)$ is given by

$$\epsilon = \frac{1}{2\pi^2} \int_{-\pi}^{\pi} \int_{0}^{\pi} |A_0\left(\theta, \phi\right) - A\left(\theta, \phi\right)|^2 \, d\theta \, d\phi \tag{5.9}$$

and the nulling constraints are

$$A\left(\theta_q, \phi_q\right) = 0 \quad q = 1, \ldots, Q \tag{5.10}$$

The solution to the problem of nulling interferers while minimizing the error of the array response from a nominal response was solved by Steyskal [51] for a linear array. The present work extends this result to the case of circular array geometry.

Consider the array response for a circular array with elements located at

$$(x_p, y_p) = \left(a \cos \left(\frac{2\pi p}{P} \right), a \sin \left(\frac{2\pi p}{P} \right) \right), \quad p = 0, \ldots, P - 1 \tag{5.11}$$

and evaluated for $(\theta = \pi/2, \phi)$

$$A(\phi) = \sum_{p=0}^{P-1} w_p \exp \left(jka \cos \left(\phi - \frac{2\pi p}{P} \right) \right) \tag{5.12}$$

With $\mathbf{w}_0 = (w_{00}, w_{01}, \ldots, w_{0P-1})$ corresponding to the nominal array weights, the mean-square error for arbitrary array weight vector $\mathbf{w}$ is

$$\epsilon = \frac{1}{2\pi} \int_{-\pi}^{\pi} \sum_{n=0}^{P-1} \sum_{m=0}^{P-1} (w_{0n} - w_n)(w_{0m}^* - w_m^*) \tag{5.13}$$

$$\times \exp \left[j2ka \sin \left(\phi - \frac{\pi(n+m)}{P} \right) \sin \left(\frac{\pi(n-m)}{P} \right) \right] d\phi$$

Using the Bessel function relation [1]

$$e^{jz \sin \psi} = \sum_{r=-\infty}^{\infty} J_r(z) e^{jr\psi} \tag{5.14}$$

we have

$$\exp \left[j2ka \sin \left(\phi - \frac{\pi(n+m)}{P} \right) \sin \left(\frac{\pi(n-m)}{P} \right) \right] = \tag{5.15}$$

$$\sum_{r=-\infty}^{\infty} J_r \left(2ka \sin \left(\frac{\pi(n-m)}{P} \right) \right) \exp \left[jr \left(\phi - \frac{\pi(n+m)}{P} \right) \right]$$

and

$$\frac{1}{2\pi} \int_{-\pi}^{\pi} \exp \left[jr \left(\phi - \frac{\pi(n+m)}{P} \right) \right] d\phi = \begin{cases} 1, & r = 0 \\ 0, & r \neq 0 \end{cases} \tag{5.16}$$

Using these results, the mean-square error is found to be

$$\epsilon = \sum_{n=0}^{P-1} \sum_{m=0}^{P-1} (w_{0n} - w_n)(w_{0m}^* - w_m^*) J_0\left(2ka\sin\left(\frac{\pi(n-m)}{P}\right)\right) \tag{5.17}$$

or, written in matrix form

$$\epsilon = (\mathbf{w}_0 - \mathbf{w})^\dagger \mathbf{Q}(\mathbf{w}_0 - \mathbf{w}) \tag{5.18}$$

with the mn^{th} element of the matrix $\mathbf{Q}$

$$q_{mn} = J_0\left(2ka\sin\left(\frac{\pi|n-m|}{P}\right)\right) \tag{5.19}$$

The 0th order nulling constraints for the circular array are

$$A(\phi_q) = \sum_{p=0}^{P-1} w_p \exp\left(jka\cos\left(\phi_q - \frac{2\pi p}{P}\right)\right) \tag{5.20}$$

$$= 0 \quad q = 1, \ldots, Q$$

Defining the vector inner product $(\mathbf{x}, \mathbf{y}) = \mathbf{y}^\dagger \mathbf{x}$, the qth constraint can be written as $(\mathbf{w}, \mathbf{y}_q) = 0$ with

$$\mathbf{y}_q = \begin{pmatrix} \exp(-jka\cos\phi_q) \\ \exp\left(-jka\cos\left(\phi_q - \frac{2\pi}{P}\right)\right) \\ \vdots \\ \exp\left(-jka\cos\left(\phi_q - \frac{2\pi(P-1)}{P}\right)\right) \end{pmatrix} \tag{5.21}$$

for $q = 1, \ldots, Q$. Define the vector $\mathbf{x} = \mathbf{w}_0 - \mathbf{w}$. The mean-square error is now

$$\epsilon = \mathbf{x}^\dagger \mathbf{Q}\mathbf{x} \tag{5.22}$$

and the qth constraint is given by $(\mathbf{x}, \mathbf{y}_q) = (\mathbf{w}_0, \mathbf{y}_q)$. Collecting the Q constraints together in matrix form as $\mathbf{A}\mathbf{x} = \mathbf{b}$ with

$$\mathbf{A} = \begin{pmatrix} \mathbf{y}_1^\dagger \\ \mathbf{y}_2^\dagger \\ \vdots \\ \mathbf{y}_Q^\dagger \end{pmatrix} \tag{5.23}$$

106

and

$$\mathbf{b} = \begin{pmatrix} \mathbf{y}_1^\dagger \mathbf{w}_0 \\ \mathbf{y}_2^\dagger \mathbf{w}_0 \\ \vdots \\ \mathbf{y}_Q^\dagger \mathbf{w}_0 \end{pmatrix} \tag{5.24}$$

The array nulling problem has been converted to the following vector optimization problem: minimize the quadratic form $\mathbf{x}^\dagger \mathbf{Q} \mathbf{x}$ subject to the linear constraint $\mathbf{A}\mathbf{x} = \mathbf{b}$. This problem has a well-known solution given by [60]

$$\mathbf{x} = \mathbf{Q}^{-1}\mathbf{A}^\dagger \left(\mathbf{A}\mathbf{Q}^{-1}\mathbf{A}^\dagger \right)^{-1} \mathbf{b} \tag{5.25}$$

and the array weight vector is $\mathbf{w} = \mathbf{w}_0 - \mathbf{x}$.

For 1st order nulling Q additional constraints are imposed on the derivative of the array response. The approach follows that outlined for 0th order nulling except that the matrix $\mathbf{A}$ and the vector $\mathbf{b}$ are augmented by additional constraint vectors. The derivative constraints are

$$\frac{\partial A\left(\phi_q\right)}{\partial \phi} = -jka \sum_{p=0}^{P-1} w_p \, sin\left(\phi_q - \frac{2\pi p}{P}\right) \exp\left(jka \cos\left(\phi_q - \frac{2\pi p}{P}\right)\right) \tag{5.26}$$

$$= 0 \quad q = 1, \ldots, Q$$

Define the augmented constraint vector $\mathbf{y}_q$ as

$$\mathbf{y}_q = \begin{pmatrix} -jka \, sin(\phi_q) \exp\left(-jka \cos \phi_q\right) \\ -jka \, sin\left(\phi_q - \frac{2\pi}{P}\right) \exp\left(-jka \cos\left(\phi_q - \frac{2\pi}{P}\right)\right) \\ \vdots \\ -jka \, sin\left(\phi_q - \frac{2\pi(P-1)}{P}\right) \exp\left(-jka \cos\left(\phi_q - \frac{2\pi(P-1)}{P}\right)\right) \end{pmatrix} \tag{5.27}$$

for , $q = Q + 1, \ldots, 2Q$ and

$$\mathbf{A} = \begin{pmatrix} \mathbf{y}_1^\dagger \\ \vdots \\ \mathbf{y}_Q^\dagger \\ \mathbf{y}_{Q+1}^\dagger \\ \vdots \\ \mathbf{y}_{2Q}^\dagger \end{pmatrix} \quad (5.28)$$

and

$$\mathbf{b} = \begin{pmatrix} \mathbf{y}_1^\dagger \mathbf{w}_0 \\ \vdots \\ \mathbf{y}_Q^\dagger \mathbf{w}_0 \\ \mathbf{y}_{Q+1}^\dagger \mathbf{w}_0 \\ \vdots \\ \mathbf{y}_{2Q}^\dagger \mathbf{w}_0 \end{pmatrix} \quad (5.29)$$

The optimal array weight vector for 1st order nulling is given as before using the newly defined matrix $\mathbf{A}$ and the vector $\mathbf{b}$. Higher order derivative constraints may be handled in a similar fashion.

The placement of a null in the array response requires one degree of freedom for 0th order nulling and two degrees of freedom for 1st order nulling. In general, an array with P elements has P degrees of freedom available for both nulling and minimizing the mean-square error of the achieved array response. Thus $P \geq Q$ for 0th order nulling and $\frac{P}{2} \geq Q$ for 1st order nulling. A practical restriction of the technique is that nulls cannot be placed within the main beam of the array response due to the severe distortion that results. Interferers with angles of arrival in the main beam of the nominal response must be eliminated prior to forming the nulling constraints. Of course, these interference sources will not be mitigated by

the technique.

5.2.5 Equivalence of Spatial Processing Techniques Under Certain Conditions

If the desired signal consists of a point source (zero angular spread) and the interference consists of point or angularly spread sources, the array weight vectors for the LCMV and maximum SINR methods agree to within a scale factor.

The following model is assumed for the array input vector

$$\mathbf{y}(t) = s(t)\mathbf{e} + n(t) \tag{5.30}$$

$s(t)$ is the signal and $n(t)$ is combined noise and interference. $n(t)$ is assumed to be zero mean and uncorrelated with $s(t)$. Without loss of generality it is assumed that $E\left\{|s(t)|^2\right\} = 1$. The vector $\mathbf{e} = \mathbf{e}(\theta, \phi)$ describes the direction of arrival of the desired signal and is given by Equations 5.3 and 5.4.

Under the assumption of a point source for the desired signal, the spatial covariance matrix (signal, noise and interference) is

$$\mathbf{R} = \mathbf{R}_S + \mathbf{R}_{N+I} \tag{5.31}$$

with

$$\mathbf{R}_S = \mathbf{e}\mathbf{e}^\dagger \tag{5.32}$$

$\mathbf{R}_{N+I}$ represents the covariance matrix for interference and noise combined and is assumed to be positive definite. Using the matrix inversion lemma

$$\mathbf{R}^{-1} = \mathbf{R}_{N+I}^{-1} - \frac{\mathbf{R}_{N+I}^{-1}\mathbf{e}\mathbf{e}^\dagger\mathbf{R}_{N+I}^{-1}}{1 + \mathbf{e}^\dagger\mathbf{R}_{N+I}^{-1}\mathbf{e}} \tag{5.33}$$

and

$$\mathbf{R}^{-1}\mathbf{e} = \frac{\mathbf{R}_{N+I}^{-1}\mathbf{e}}{1 + \mathbf{e}^\dagger\mathbf{R}_{N+I}^{-1}\mathbf{e}} \tag{5.34}$$

Consider now the LCMV method with a unity gain constraint in the direction (θ, ϕ). Using Equations 5.5 and 5.34, the array weight vector for the LCMV method assuming a point source for the desired signal is

$$\mathbf{w}_{LCMV} \propto \mathbf{R}_{N+I}^{-1}\mathbf{e} \tag{5.35}$$

Consider the maximum SINR method under the assumption of a point source for the desired signal. The optimum array weight vector is found by solving the generalized eigenvalue problem

$$\mathbf{R}_S\mathbf{v} = \lambda\mathbf{R}_{N+I}\mathbf{v} \tag{5.36}$$

and choosing the eigenvector corresponding the largest eigenvalue. This eigenvalue corresponds to the maximum SINR. Using the optimum weight vector $\mathbf{w}$ and corresponding maximizing SINR in the previous expression,

$$\mathbf{R}_S\mathbf{w} = \left(\frac{\mathbf{w}^{\dagger}\mathbf{R}_S\mathbf{w}}{\mathbf{w}^{\dagger}\mathbf{R}_{N+I}\mathbf{w}}\right)\mathbf{R}_{N+I}\mathbf{w} \tag{5.37}$$

For $\mathbf{R}_S = \mathbf{e}\mathbf{e}^{\dagger}$

$$\left(\mathbf{e}\mathbf{e}^{\dagger}\right)\mathbf{w} = \left(\frac{\mathbf{w}^{\dagger}\left(\mathbf{e}\mathbf{e}^{\dagger}\right)\mathbf{w}}{\mathbf{w}^{\dagger}\mathbf{R}_{N+I}\mathbf{w}}\right)\mathbf{R}_{N+I}\mathbf{w} \tag{5.38}$$

and

$$\mathbf{w}_{maxSINR} \propto \mathbf{R}_{N+I}^{-1}\mathbf{e} \tag{5.39}$$

Thus, under the assumption of a point source for the desired signal and point or angularly spread sources for the interference, the array weight vectors for the LCMV and maximum SINR methods agree to within a constant factor. It is important to note that the equivalence between these methods applies only to the case of a point source for the desired signal and not the general case of an angularly spread source. The next section details the performance of these methods for the general case of angularly spread signal and interference.

An extension of the results derived here applies to the case of a point source for the desired signal and interference that is both spatially uncorrelated and stationary. For this case, $\mathbf{R}_{N+I} = \mathbf{I}$, and it is easily demonstrated that the beamsteering, LCMV, and maximum SINR methods all produce equivalent array weight vectors.

5.3   Numerical Results

In this section the spatial covariance models developed in the previous chapter are applied to analyze the performance of spatial processing techniques for wireless systems. Three performance measures are used: the gain in the array interference to noise ratio (INR), the gain in the array signal to noise ratio (SNR) and the gain in the array signal to interference plus noise ratio (SINR). These measures permit analysis of how the desired signal and interference separately are affected by a candidate spatial processing algorithm. The signal from the desired mobile and a single interferer are considered and the gain in the array INR, SNR, and SINR is determined as a function of the angular separation of the desired mobile and interferer.

The spatial covariance models associated with the Jakes 'circular ring' scatterer model (spatial-only case) and the Laplacian angle of arrival (AOA) model were used. These models are described in Sections 2.3.1 and 2.3.3, respectively. The Jakes covariance model is parameterized by the angle of arrival of the direct path ϕ, the scattering radius R, and the distance between the base receiver and mobile transmitter d. For the results presented here the scattering radius was varied from $R = 0, 50, 100, 200m$ and the separation between the mobile and base fixed at $d = 1000m$. For the scattering radius of $R = 200m$ the maximum deviation of the angle of arrival from the direct path is approximately $\pm 12.6°$ for the Jakes model.

The Laplacian AOA probability density is parameterized by the angle of arrival of the direct path to the source (desired or interference) ϕ and the angular spread σ_A. Values considered for the angular spread parameter were: $\sigma_A = 0, 5, 10, 20°$. The angle of arrival of the signal from the desired mobile was fixed at $\phi_S = 0°$ and the angle of arrival for the interferer was varied between $0° \leq \phi_I \leq 180°$. For each covariance model investigated, the signal from the desired mobile and the interferer were assumed to have identical angular spread. For the Jakes model this means that the scattering radius R was identical for both the desired mobile and the interferer; for the Laplacian AOA model the angular spread parameter σ_A was identical for both sources.

Circular array geometry with $\lambda/2$ element spacing was used with the spacing measured along the circumference of the array. The number of array elements was either $P = 8$ or $P = 16$.

The array input SINR is defined as

$$SINR_{in} = \frac{tr(\mathbf{R}_S)}{tr(\mathbf{R}_I) + tr(\mathbf{R}_N)} \tag{5.40}$$

with $\mathbf{R}_S, \mathbf{R}_I, \mathbf{R}_N$ denoting the spatial covariance matrices for the desired signal, interference and noise, respectively, and $tr()$ the matrix trace operation. The noise was spatially uncorrelated and the input SINR was fixed at $10dB$ for all cases. For an arbitrary array weight vector $\mathbf{w}$ the output SINR is defined as

$$SINR_{out} = \frac{\mathbf{w}^\dagger \mathbf{R}_S \mathbf{w}}{\mathbf{w}^\dagger (\mathbf{R}_I + \mathbf{R}_N) \mathbf{w}} \tag{5.41}$$

The array gain is defined as the ratio of the array output SINR to the array element input SINR, or

$$Gain_{SINR} = \frac{SINR_{out}}{SINR_{in}} \tag{5.42}$$

Similar expressions were used to compute the gain in the array SNR and INR.

The beamsteering, LCMV, maximum SINR, and 0th and 1st order nulling techniques were investigated using the spatial covariance matrices for the Jakes 'circular ring' geometry and the Laplacian AOA models. The results for the Jakes model are presented first, followed by the results for the Laplacian AOA model.

Figure 5.1 shows the results for the Jakes spatial covariance model, beamsteering method and a $P = 8$ element circular array. Since this method is non-adaptive with respect to the interference, the INR reduction is determined by the sidelobe level of the array response, the proximity of the angle of arrival of the interferer with respect to nulls in the array response and the angular spread of the interference. From the figure it is seen that for $R = 0m$ there is significant reduction in the INR when the angle of arrival of the interference corresponds to a null in the array response. However, the INR reduction is significantly degraded as the scattering radius is increased. The gain in the array SNR is observed to be independent of the angular separation of the desired mobile and interferer, as expected, since this method is non- adaptive with respect to the interference. Note that there is a slight degradation of the SNR gain as the scattering radius is increased. This effect is caused by loss of signal energy for angles of arrival outside the main lobe of the array response. The beamsteering method produces the largest SNR gain of any of the methods investigated.

Figure 5.2 shows the results for the Jakes spatial covariance model, LCMV method, $P = 8$ element circular array and input SINR=10dB. Note the significant degradation in the SNR gain as the scattering radius is increased. The LCMV method attempts to minimize the total output power of the array subject to a gain constraint at a fixed angle of arrival. Energy arriving from other angles is treated as interference and reduced by the algorithm. In the present case, angular spread
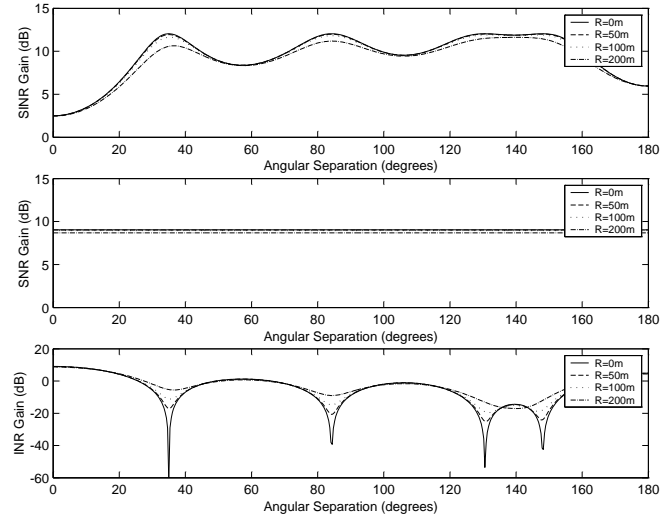
Figure 5.1: Jakes model, circular array, 8 elements with $\lambda/2$ spacing, array input SINR=10dB, beamsteering method. Gain in array SINR, SNR, INR versus angular separation of desired mobile and interferer.

of the signal from the desired mobile results in an effective signal suppression and hence a reduction in the SNR gain. The effect is more pronounced as the scattering radius R is increased. Figure 5.3 illustrates this effect. The array response for the LCMV method is shown for an angle of arrival of the desired mobile of $0°$ and $60°$ for the interferer. Note that while the gain constraint of unity is maintained at an angle of arrival of $0°$ for all cases, the increased sidelobe level of the array response as the scattering radius is increased results in suppression of the desired signal. The width of the mainlobe of the array response is also observed to decrease as the scattering radius is increased. The signal suppression effect depends significantly on the input SINR. Figure 5.4 shows the results for the Jakes model, LCMV method, $P = 8$ element circular array, but with input SINR=0dB. For this case the signal suppression effect is considerably reduced.
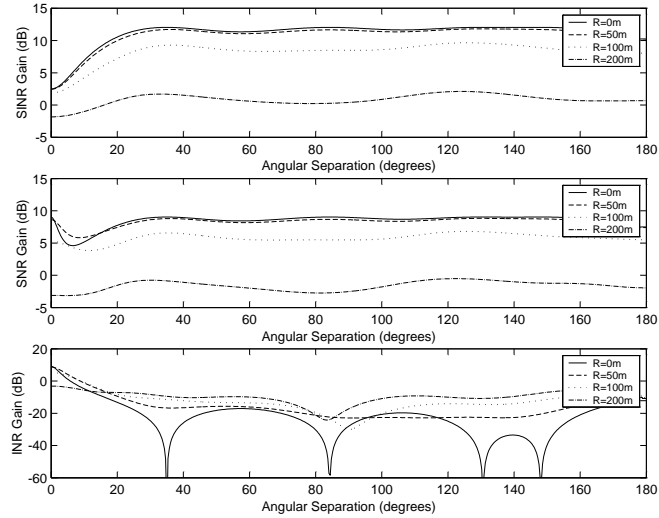
114

Figure 5.2: Jakes model, circular array, 8 elements with $\lambda/2$ spacing, array input SINR=10dB, LCMV method. Gain in array SINR, SNR, INR versus angular separation of desired mobile and interferer.

Signal cancellation effects due to array calibration errors and errors in the estimate of the direction of arrival of the desired source have been reported for the LCMV method. See [61],[62],[63],[49] for further details. It is worthwhile to note that the results presented here indicate that even with perfect knowledge of the spatial covariance matrix and the pointing direction, the signal suppression effect can be observed due to angular spread of the desired signal.

Figure 5.5 shows the results for the Jakes spatial covariance model, maximum SINR method and a $P = 8$ element circular array. For this case the SINR gain shows a slight reduction as the scattering radius is increased. Note that for zero scattering radius the SINR gain produced by the LCMV and maximum SINR methods is equivalent. The maximum SINR method produces the largest SINR gain of any of the methods investigated.

115

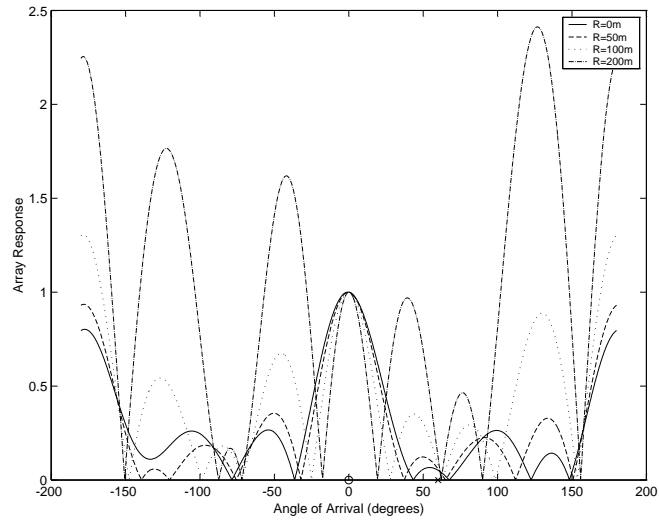Figure 5.3: Jakes model, circular array, 8 elements with $\lambda/2$ spacing, array input SINR=10dB, LCMV method. Array response versus angle of arrival. Desired mobile at $0°$ and interferer at $60°$.
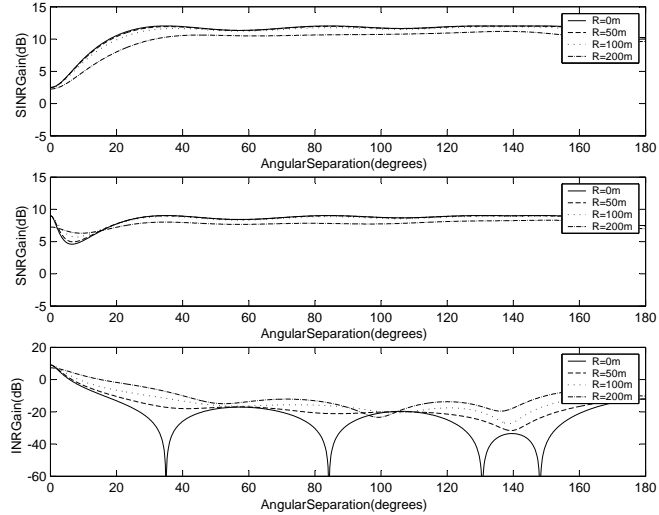

Figure 5.4: Jakes model, circular array, 8 elements with $\lambda/2$ spacing, array input SINR=0dB, LCMV method. Gain in array SINR, SNR, INR versus angular separation of desired mobile and interferer.

Figure 5.5: Jakes model, circular array, 8 elements with $\lambda/2$ spacing, array input SINR=10dB, maximum SINR method. Gain in array SINR, SNR, INR versus angular separation of desired mobile and interferer.

Figure 5.6 shows the results for the Jakes spatial covariance model, 0th order nulling method and a $P = 8$ element circular array. From the plot showing the INR gain it is clear that this method is capable of effectively eliminating interference for zero scattering radius regardless of the angle of arrival, subject to the numerical precision of MATLAB. The method is considerably less successful at reducing interference which is spread in angle, however. The plot showing the SNR gain illustrates that there is substantial variation in the gain as a function of the angular separation of the desired mobile and the interferer. This effect is discussed in more detail following the presentation of the results for 1st order nulling.

Figure 5.7 shows the results for the Jakes spatial covariance model, 1st order nulling method and a $P = 8$ element circular array. This method is also capable of effectively eliminating interference for zero scattering radius regardless of the
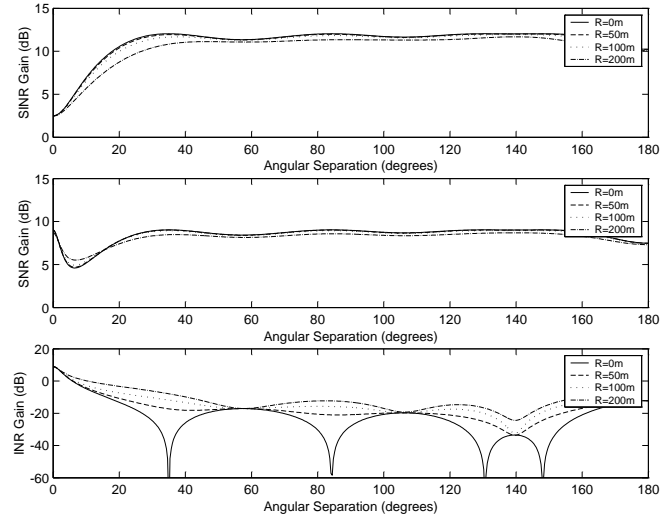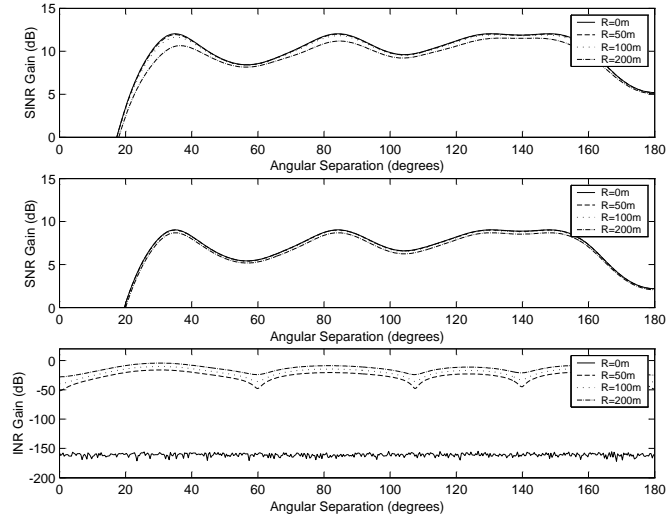
Figure 5.6: Jakes model, circular array, 8 elements with $\lambda/2$ spacing, array input SINR=10dB, 0th order nulling method. Gain in array SINR, SNR, INR versus angular separation of desired mobile and interferer.

angle of arrival, and is more capable of reducing interference that is spread in angle compared to 0th order nulling. However, there is also significant variation in the SNR gain as a function of the angular separation of the desired mobile and the interferer for this case. The effect is caused by perturbation of the array response due to the addition of a null at the angle of the interferer. Recall that the nulling algorithms minimize the mean-square error of the achieved array response with respect to the beamsteering response while simultaneously constraining the array response to be zero in the direction of interference sources. For the 1st order nulling algorithm the derivative of the array response is also constrained to be zero in the direction of interferers. Thus, the achieved mean-square error is a measure of the deviation between the nulling response and the beamsteering response. Figure 5.8 shows the mean-square error of the array response for 0th and 1st order nulling as

a function of the angular separation of the desired mobile and the interferer for a circular array with $P = 8$ elements. The array response for beamsteering is also shown for reference. Note that mean-square error for 1st order nulling exceeds that for 0th order nulling for all values of angular separation between the desired mobile and the interferer. Also apparent is the dominance of the nulling constraint for values of angular separation that place the interferer in the main lobe response of the array. This effect is more pronounced for 1st nulling and highlights the fact that interference sources close to the angle of arrival of the desired mobile cannot be effectively nulled without also nulling the signal. From Figure 5.8, the local minima of the mean-square error occur at the nulls of the beamsteering response for 0th order nulling. For this case the array weights for nulling and beamsteering are identical, as expected, since the beamsteering response exhibits a null at the angle of the interferer. With reference to Figure 5.6, local maxima of the SNR gain correspond to local minima of the mean-square error. Also, the local minima of the SNR gain correspond roughly to the local maxima of the mean-square error. For all cases the achievable gain in SNR for both 0th and 1st order nulling is upper bounded by the SNR gain for beamsteering.

In order to mitigate the perturbation of the array response due to the placement of nulls, alternative optimization criteria may be considered. For example, rather than require the array response to be identically zero in the direction of interferers, the response may be constrained to be no larger than a prescribed threshold. The array weight vector that satisifes this optimization criteria must be found using numerical techniques since a closed-form solution is not available. This topic is currently being investigated.

Figures 5.9 through 5.13 show the results for the Jakes spatial covariance model

Figure 5.7: Jakes model, circular array, 8 elements with $\lambda/2$ spacing, array input SINR=10dB, 1st order nulling method. Gain in array SINR, SNR, INR versus angular separation of desired mobile and interferer.

Figure 5.8: Circular array, 8 elements with $\lambda/2$ spacing. Mean-square error of the array response for 0th and 1st order nulling versus angular separation of desired mobile and interferer. Also shown is the array response for beamsteering.
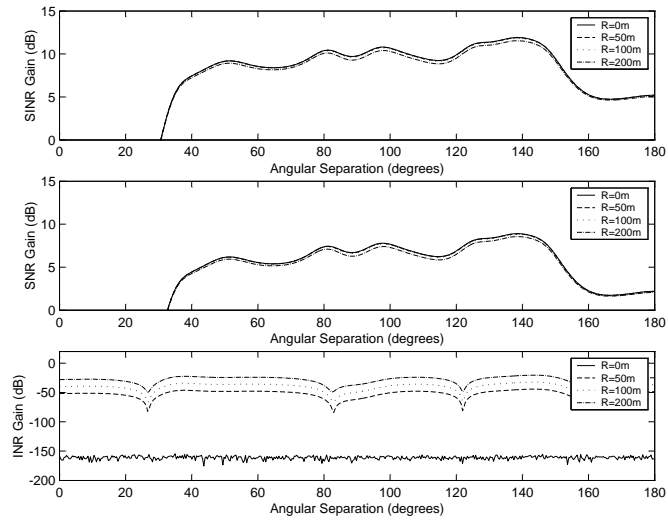
Figure 5.9: Jakes model, circular array, 16 elements with $\lambda/2$ spacing, array input SINR=10dB, beamsteering method. Gain in array SINR, SNR, INR versus angular separation of desired mobile and interferer.

and a $P = 16$ element circular array. With reference to Figure 5.9, the maximum achievable SNR gain, expressed in decibels, is bounded above by $10\log_{10}P$. The maximum SNR gain is achievable with beamsteering for a point source for the desired mobile, but not generally for an angularly spread source. From Figure 5.10 the signal suppression effect associated with the LCMV method is exacerbated for $P = 16$ array elements as compared to $P = 8$ array elements. With fixed element spacing, a larger number of array elements produces a narrower main lobe width thus causing the algorithm to reject the signal from the desired mobile for relatively small values of scattering radius.

Figures 5.14 through 5.18 show the results for the Laplacian AOA covariance model and a $P = 8$ element circular array and Figures 5.19 through 5.23 show the results for a $P = 16$ element circular array.

Figure 5.10: Jakes model, circular array, 16 elements with $\lambda/2$ spacing, array input SINR=10dB, LCMV method. Gain in array SINR, SNR, INR versus angular separation of desired mobile and interferer.
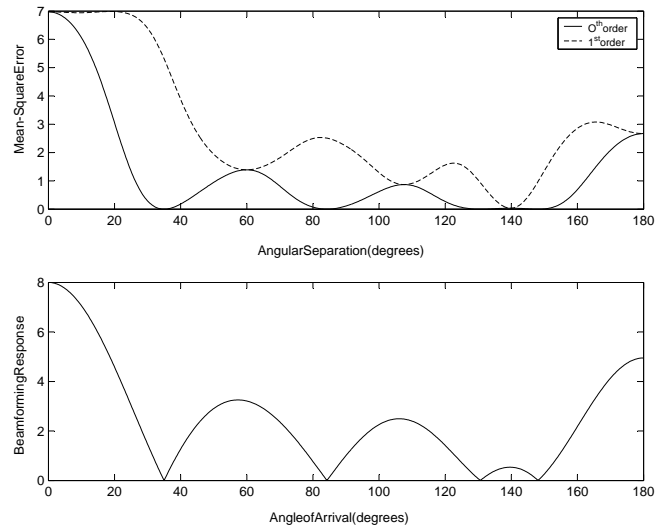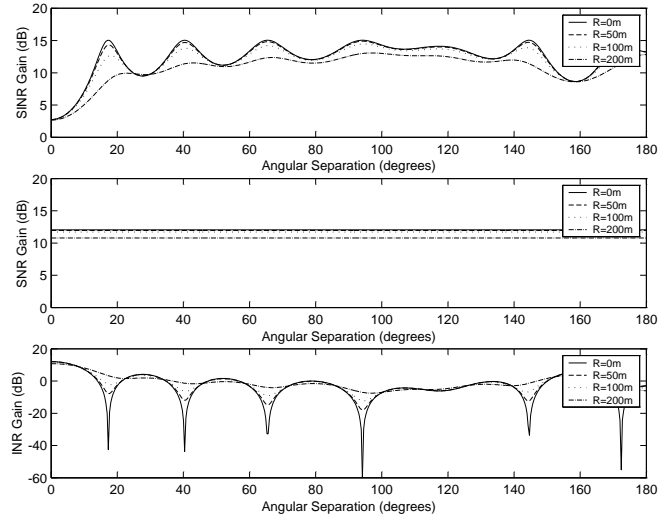

Figure 5.11: Jakes model, circular array, 16 elements with $\lambda/2$ spacing, array input SINR=10dB, maximum SINR method. Gain in array SINR, SNR, INR versus angular separation of desired mobile and interferer.

Figure 5.12: Jakes model, circular array, 16 elements with $\lambda/2$ spacing, array input SINR=10dB, 0th order nulling method. Gain in array SINR, SNR, INR versus angular separation of desired mobile and interferer.

Figure 5.13: Jakes model, circular array, 16 elements with $\lambda/2$ spacing, array input SINR=10dB, 1st order nulling method. Gain in array SINR, SNR, INR versus angular separation of desired mobile and interferer.

Figure 5.14: Laplacian AOA model, circular array, 8 elements with $\lambda/2$ spacing, array input SINR=10dB, beamsteering method. Gain in array SINR, SNR, INR versus angular separation of desired mobile and interferer.
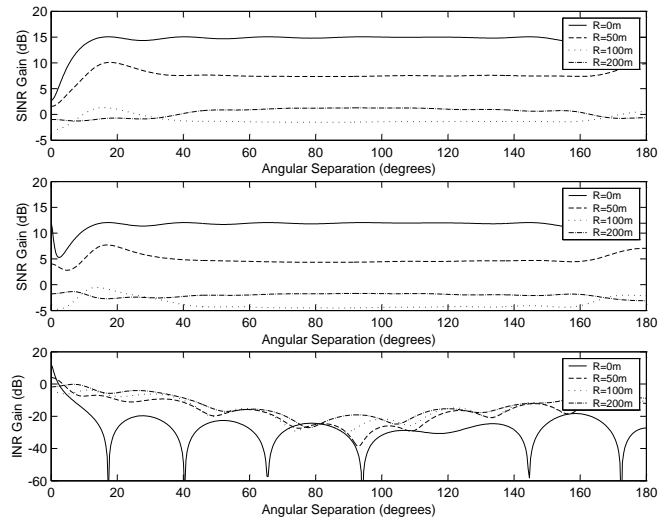

Figure 5.15: Laplacian AOA model, circular array, 8 elements with $\lambda/2$ spacing, array input SINR=10dB, LCMV method. Gain in array SINR, SNR, INR versus angular separation of desired mobile and interferer.
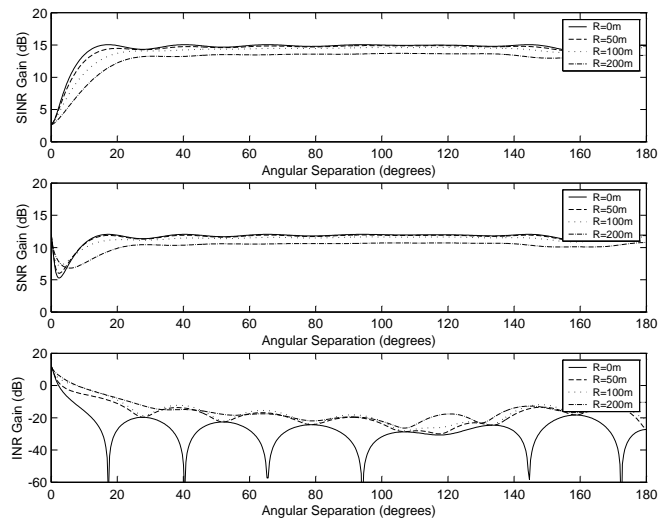
Figure 5.16: Laplacian AOA model, circular array, 8 elements with $\lambda/2$ spacing, array input SINR=10dB, maximum SINR method. Gain in array SINR, SNR, INR versus angular separation of desired mobile and interferer.
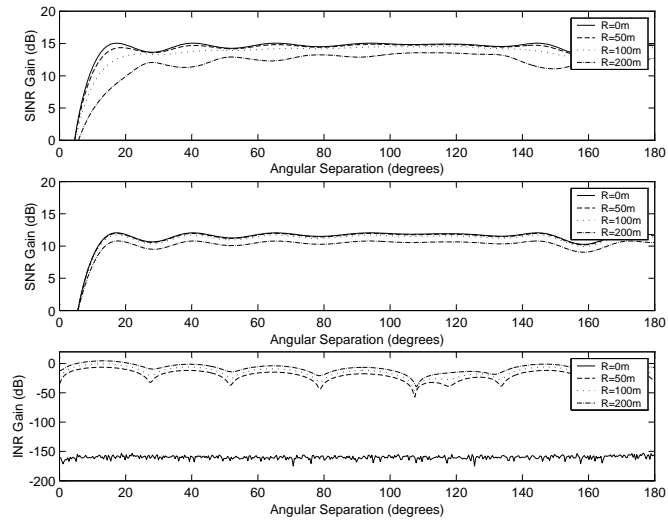

Figure 5.17: Laplacian AOA model, circular array, 8 elements with $\lambda/2$ spacing, array input SINR=10dB, 0th order nulling method. Gain in array SINR, SNR, INR versus angular separation of desired mobile and interferer.
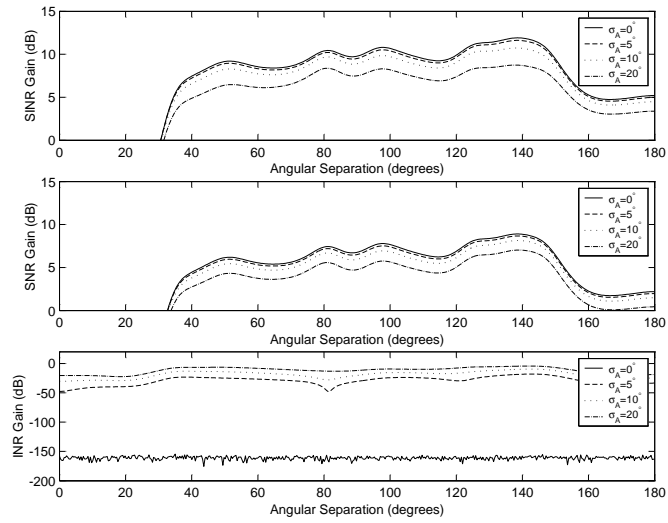
Figure 5.18: Laplacian AOA model, circular array, 8 elements with $\lambda/2$ spacing, array input SINR=10dB, 1st order nulling method. Gain in array SINR, SNR, INR versus angular separation of desired mobile and interferer.
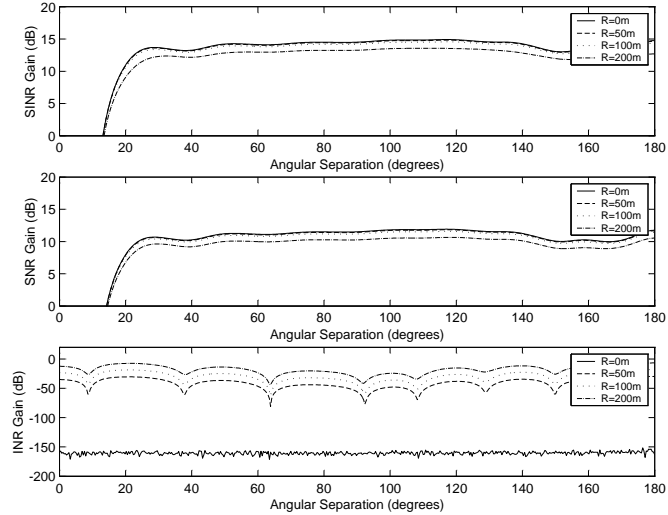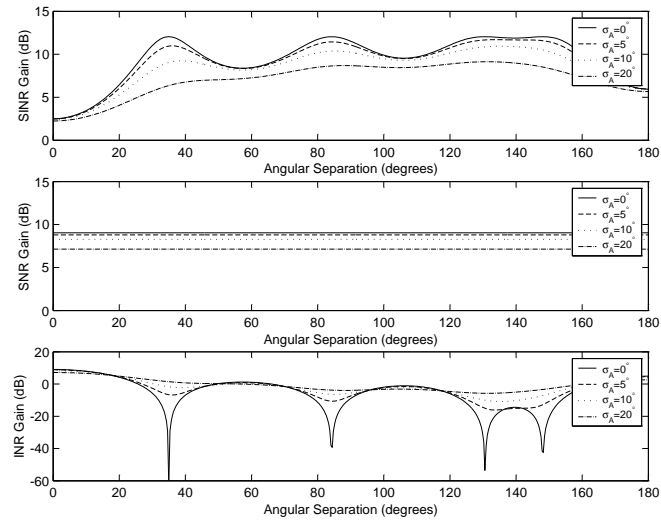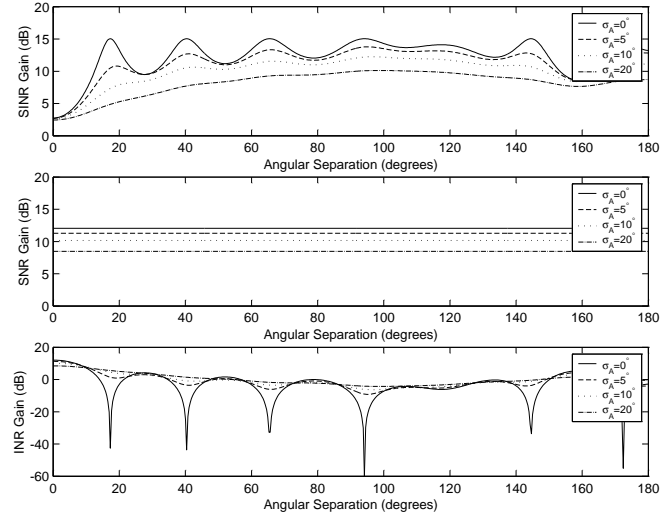

Figure 5.19: Laplacian AOA model, circular array, 16 elements with $\lambda/2$ spacing, array input SINR=10dB, beamsteering method. Gain in array SINR, SNR, INR versus angular separation of desired mobile and interferer.
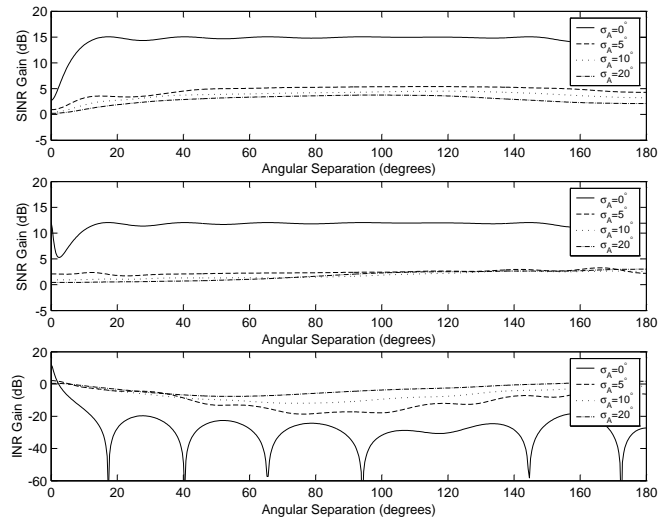
Figure 5.20: Laplacian AOA model, circular array, 16 elements with $\lambda/2$ spacing, array input SINR=10dB, LCMV method. Gain in array SINR, SNR, INR versus angular separation of desired mobile and interferer.
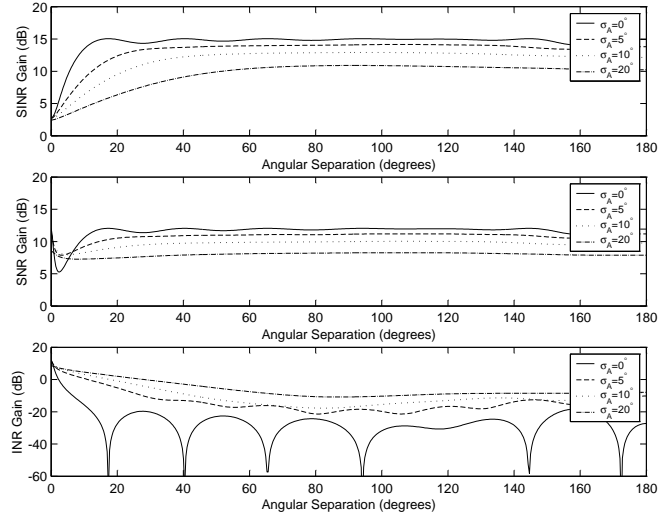
Figure 5.21: Laplacian AOA model, circular array, 16 elements with $\lambda/2$ spacing, array input SINR=10dB, maximum SINR method. Gain in array SINR, SNR, INR versus angular separation of desired mobile and interferer.
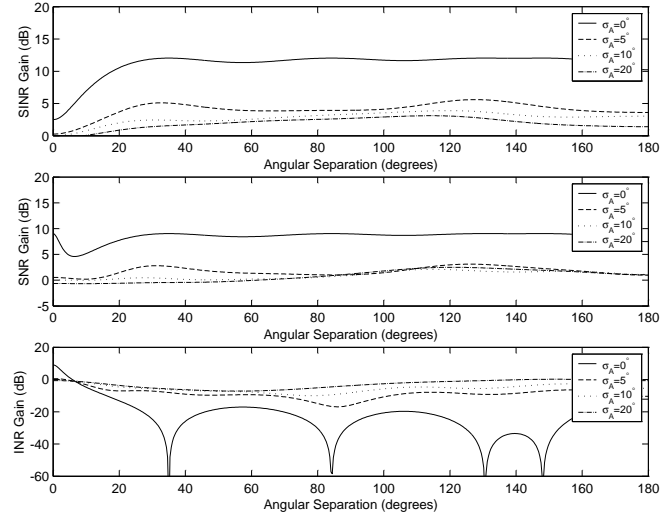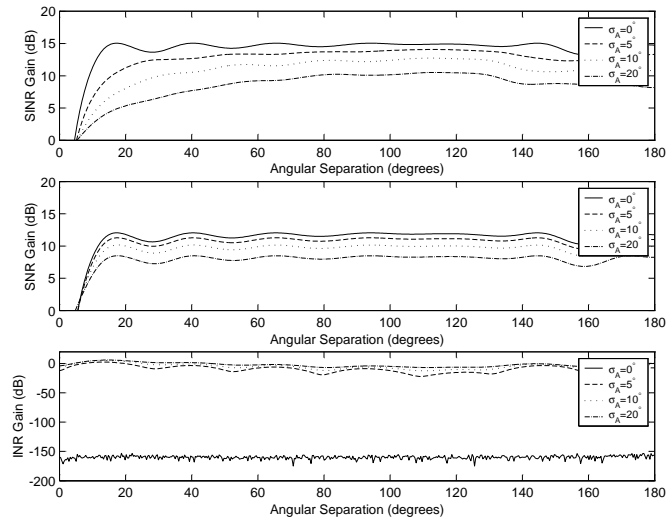
Figure 5.22: Laplacian AOA model, circular array, 16 elements with $\lambda/2$ spacing, array input SINR=10dB, 0th order nulling method. Gain in array SINR, SNR, INR versus angular separation of desired mobile and interferer.
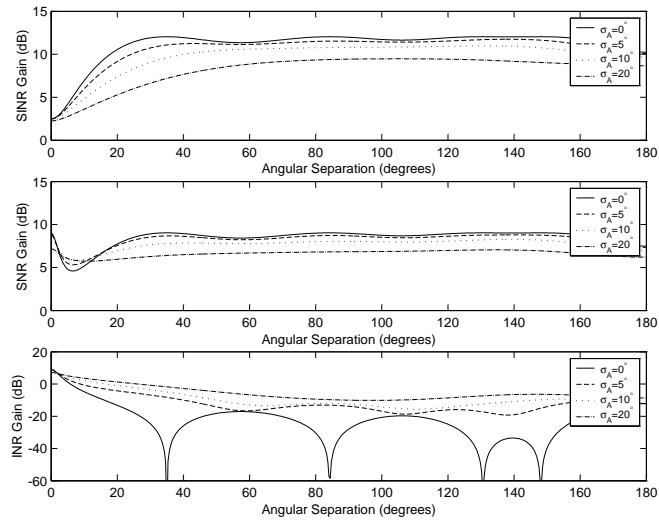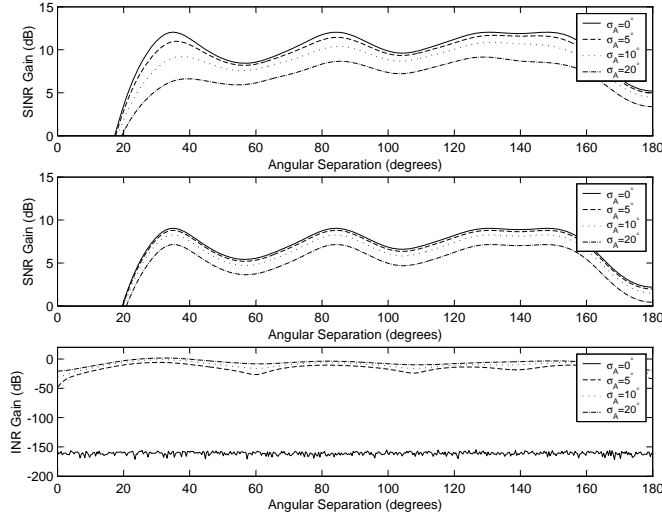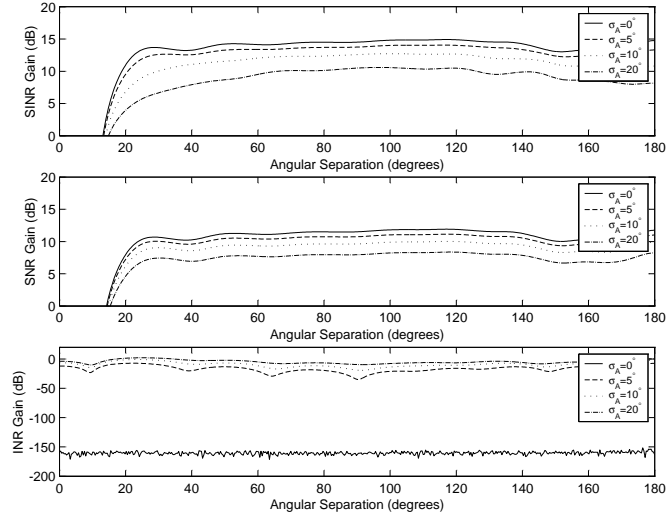

Figure 5.23: Laplacian AOA model, circular array, 16 elements with $\lambda/2$ spacing, array input SINR=10dB, 1st order nulling method. Gain in array SINR, SNR, INR versus angular separation of desired mobile and interferer.

5.4   Chapter Summary

In this chapter we have examined several spatial processing techniques for use on the uplink of a wireless communications systems. We have quantified the effectiveness of such techniques for reducing co-channel interference when the signals from the desired source and interferer experience angular spread due to multipath. Numerical results were presented for the Jakes 'circular ring' scatterer model and the Laplacian angle of arrival model.

Chapter 6

Conclusions and Future Research

In this thesis we have proposed a general space-time covariance model and used it to evaluate the performance of space-time block coding and beamforming techniques for spatially and temporally correlated wireless channels.

The space-time covariance model is applicable to arbitrary scatterer geometry, arbitrary transmit and receive array geometry and includes temporal effects resulting from mobile motion. We applied the covariance model to the 'circular ring' scattering geometry and the two-dimensional Gaussian scattering geometry that is based on recent field measurements. We developed simplified results for the spatial-only case for several commonly-used angle of arrival probability densities and approximations for small angular spread.

In order to evaluate the performance of the proposed transmit diversity techniques, we determined the union bound on the block error probability for arbitrary space-time block codes based on the exact pairwise probability. In addition, we determined the exact symbol error probability for orthogonal space-time block codes and the quasi-static channel. We also determined the exact symbol error probability for maximum ratio transmission with perfect feedback and beamsteering. Using these results and the space-time covariance model that we developed,

we presented extensive numerical results to illustrate the performance of several transmit diversity techniques for the two-dimensional Gaussian scatterer model. Some conclusions from these numerical results are as follows.

The error performance of space-time block coding was found to be significantly dependent on the spatial and temporal characteristics of the wireless channel. To achieve performance comparable to the ideal channel (uncorrelated in space and time) under worst-case scattering geometry, the transmit antennas must be widely separated in space, typically tens of wavelengths. In an actual implementation this may be difficult to achieve due to practical restrictions on antenna placement, for example. In any case, the results presented in this thesis have quantified the error performance of several space-time codes for a realistic channel model and varying degrees of spatial and temporal correlation.

When considering the effects of feedback of the channel state information to the transmitter, our results indicate that a substantial improvement in performance can be realized for perfect feedback. However, for imperfect feedback we determined that slight decorrelation of the feedback channel response resulted in significant performance degradation. Most notable was a reduction in the achieved diversity order. The requirements for timely feedback of the channel state information were found to be considerably relaxed for pedestrian applications as compared to vehicular applications.

Based on the results of this dissertation, there are several potential areas of future research. First, we have assumed that the receiver has perfect knowledge of the channel response and ignored issues associated with channel estimation. Open issues are the design of optimal training sequences and the evaluation of estimator performance considering the spatial and temporal characteristics of the channel.

The estimation scheme must balance statistical confidence in the channel estimates with adaptability to time-varying channel conditions. The numerical results presented here indicate that the best-case wireless channel for space-time block coding is uncorrelated in space and time. However, from a channel estimation viewpoint, it is difficult to estimate the channel response if the channel itself is changing rapidly with time. Such issues must be considered in an objective assessment of the overall performance of transmit diversity techniques.

Second, traditional space-time code design is based upon maximizing the diversity gain and coding gain assuming a spatially uncorrelated channel. As the numerical results presented in this thesis have demonstrated, there is a substantial degradation in code performance for spatially correlated wireless channels. In many cases it may be practically infeasible to achieve the antenna spacing required to spatially decorrelate the channel response. It is therefore useful to consider how the design of space-time block codes could be improved based upon knowledge of the spatial and temporal characteristics of the channel. One possible approach is to employ a parameterized space-time covariance model of the channel response, such as that developed in this thesis, in the code design process. Parameters of the model could be estimated by the receiver and fed back to the transmitter to determine the appropriate space-time code to use. Of course, issues such as robustness and adaptability to varying channel conditions must be addressed in such approaches.

Third, significant research effort has been expended on the design of transmit diversity techniques to improve system performance in fading channels. Issues such as the reduction of co-channel interference, both at the transmitter and the receiver, have not received as much attention. In conventional space-time block

coding, for example, the base station transmitter radiates energy omnidirectionally without regard for the actual location of the mobile receiver. This creates co-channel interference for unintended users and has the potential to limit achievable performance. There is a significant volume of research on spatial processing techniques for reducing interference that has not been applied to wireless communication systems. Ideally, such techniques should address both goals of achieving diversity gain and minimizing co-channel inteference.

Appendix A

Characteristic Function of the Norm of a Complex Gaussian Random Vector

We determine the characteristic function of the Frobenius norm of a complex Gaussian random vector. Specifically, we prove

$$\phi(s) = \mathrm{E}\left[\exp\left(s\|\mathbf{y}\|^2\right)\right] \tag{A.1}$$
$$= \frac{1}{\det\left(\mathbf{I} - s\mathbf{R}\right)}$$

where the vector $\mathbf{y}$ is complex Gaussian with zero mean vector and covariance matrix $\mathbf{R}$ and $\|\mathbf{y}\|^2 = \mathbf{y}^\dagger\mathbf{y}$. A related result appears in [44]. For completeness, we provide a proof of this property here.

If the matrix $\mathbf{R}$ is positive definite then there exists a non-singular matrix $\mathbf{Q}$ such that $\mathbf{Q}^\dagger\mathbf{R}\mathbf{Q} = \mathbf{\Lambda}$ and $\mathbf{Q}^\dagger\mathbf{Q} = \mathbf{I}$, where $\mathbf{\Lambda}$ is diagonal with entries λ_n corresponding to the eigenvalues of $\mathbf{R}$ [64].

Let $\mathbf{y} = \mathbf{Q}\mathbf{\Lambda}^{1/2}\bar{\mathbf{y}}$ where the matrix $\mathbf{\Lambda}^{1/2}$ is diagonal with entries $\sqrt{\lambda_n}$. We have

$$\mathbf{y}^\dagger\mathbf{y} = \left(\mathbf{Q}\mathbf{\Lambda}^{1/2}\bar{\mathbf{y}}\right)^\dagger\left(\mathbf{Q}\mathbf{\Lambda}^{1/2}\bar{\mathbf{y}}\right) \tag{A.2}$$

$$= \bar{\mathbf{y}}^\dagger\mathbf{\Lambda}^{1/2}\left(\mathbf{Q}^\dagger\mathbf{Q}\right)\mathbf{\Lambda}^{1/2}\bar{\mathbf{y}}$$

$$= \bar{\mathbf{y}}^\dagger\mathbf{\Lambda}\bar{\mathbf{y}}$$

$$= \sum_{n=1}^N \lambda_n|\bar{y}_n|^2$$

where

$$\bar{\mathbf{y}} = \begin{pmatrix} \bar{y}_1 & \bar{y}_2 & \dots & \bar{y}_N \end{pmatrix}'. \tag{A.3}$$

Also,

$$\mathrm{E}\left[\bar{\mathbf{y}}\bar{\mathbf{y}}^\dagger\right] = \mathrm{E}\left[\left(\mathbf{\Lambda}^{-1/2}\mathbf{Q}^\dagger\mathbf{y}\right)\left(\mathbf{\Lambda}^{-1/2}\mathbf{Q}^\dagger\mathbf{y}\right)^\dagger\right] \tag{A.4}$$

$$= \mathbf{\Lambda}^{-1/2}\left(\mathbf{Q}^\dagger\mathbf{R}\mathbf{Q}\right)\mathbf{\Lambda}^{-1/2}$$

$$= \mathbf{I}.$$

So, $\bar{y}_n$ are i.i.d. complex Gaussian random variables with zero mean and unit variance. Therefore,

$$\mathrm{E}\left[\exp\left(s\mathbf{y}^\dagger\mathbf{y}\right)\right] = \mathrm{E}\left[\exp\left(s\sum_{n=1}^N \lambda_n|\bar{y}_n|^2\right)\right] \tag{A.5}$$

$$= \prod_{n=1}^N \mathrm{E}\left[\exp\left(s\lambda_n|\bar{y}_n|^2\right)\right]$$

$$= \prod_{n=1}^N \frac{1}{1 - s\lambda_n}$$

since $|\bar{y}_n|^2$ are i.i.d. χ^2 random variables with 2 degrees of freedom. Because

$\det(\mathbf{Q}^\dagger)\det(\mathbf{Q}) = 1$, we have

$$\prod_{n=1}^{N} (1 - s\lambda_n) = \det(\mathbf{I} - s\mathbf{\Lambda}) \tag{A.6}$$

$$= \det\left(\mathbf{Q}^\dagger\mathbf{Q} - s\mathbf{Q}^\dagger\mathbf{R}\mathbf{Q}\right)$$

$$= \det\left(\mathbf{Q}^\dagger\right)\det\left(\mathbf{I} - s\mathbf{R}\right)\det\left(\mathbf{Q}\right)$$

$$= \det\left(\mathbf{I} - s\mathbf{R}\right) .$$

Finally,

$$\phi(s) = \mathrm{E}\left[\exp\left(s\mathbf{y}^\dagger\mathbf{y}\right)\right] \tag{A.7}$$

$$= \prod_{n=1}^{N} \frac{1}{1 - s\lambda_n}$$

$$= \frac{1}{\det\left(\mathbf{I} - s\mathbf{R}\right)} .$$

BIBLIOGRAPHY

[1] M. Abramowitz and I.E. Stegun, *Handbook of Mathematical Functions*, National Bureau of Standards, December 1972.

[2] W.C. Jakes, *Microwave Mobile Communications*, IEEE-Press, 1974.

[3] N. Seshadri and J.H. Winters, "Two Signaling Schemes for Improving Error Performance of Frequency-Division Duplex (FDD) Transmission Systems using Transmitted Antenna Diversity," *Int. Journal Wireless Information Networks*, Vol. 1, No. 1, January 1994.

[4] J.H. Winters, "The Diversity Gain of Transmit Diversity in Wireless Systems with Rayleigh Fading," *IEEE Transactions of Vehicular Technology*, Vol. 47, No. 1, February 1998.

[5] R.H. Clarke, "A Statistical Theory of Mobile-Radio Reception," *Bell System Technical Journal*, pp.957-1000, July-Aug. 1968.

[6] T.A. Chen et al. "A Space-Time Model for Frequency Nonselective Rayleigh Fading Channels with Applications to Space-Time Modems," *IEEE Journal on Selected Areas in Communications*, Vol. 18, No. 7, July 2000.

[7] D.S. Shiu et al. "Fading Correlation and Its Effect on the Capacity of Multi-element Antenna Systems," *IEEE Transactions on Communications*, Vol. 48, No. 3, March 2000.

[8] A. Abdi, M. Kaveh "A Space-Time Correlation Model for Multielement Antenna Systems in Mobile Fading Channels," *IEEE Journal on Selected Areas in Communications*, Vol. 20, No. 3, April 2002.

[9] Z. Safar and K.J.R. Liu "Space-Time Correlation of MIMO Flat Rayleigh Fading Channels," in *EUSIPCO 2002*, Toulouse France, Sept. 2002.

[10] K. Pedersen, P. Mognesen, and B. Fleury, "A Stochastic Model of the Temporal and Azimuthal Dispersion Seen at the Base Station in Outdoor Propagation Environments," *IEEE Transactions on Vehicular Technology*, Vol. 49, No. 2, pp. 437-447, Mar. 2000.

[11] K. Pedersen, P. Mognesen, and B. Fleury, "Power Azimuth Spectrum in Outdoor Environments," *Electronics Letters*, Vol. 33, No. 18, pp. 1583-1584, Aug. 1997.

[12] K. Pedersen, P. Mognesen, and B. Fleury, "Spatial Channel Characteristics in Outdoor Environments and their Impact on the BS Antenna System Performance," in *IEEE Vehicular Technology Conf.*, 1998, pp. 719-723.

[13] R. Janaswamy, "Angle and Time of Arrival Statistics for the Gaussian Scatter Density Model," *IEEE Transactions on Wireless Communications*, Vol. 1, No. 3, July 2002.

[14] S-T Kim, J-H Yoo and H-K Park, "A Spatially and Temporally Correlated Fading Model for Array Antenna Applications," *IEEE Transactions on Vehicular Technology*, Vol. 48, No. 6, pp. 1899-1905, Nov. 1999.

[15] J. Fuhl and A. Molisch, "Capacity Enhancement and BER in a Combined SDMA/TDMA System," in *IEEE Vehicular Technology Conf.*, 1996, pp.1481-1485.

[16] J. Fuhl, A. Molisch and E. Bonek, "Unified channel model for mobile radio systems with smart antennas," *IEE Proc.-Radar, Sonar Navig.*, Vol. 145, No. 1, Feb. 1998.

[17] M. Kalkan and R. H. Clarke, "Prediction of the Space-Frequency Correlation Function for Base Station Diversity Reception," *IEEE Transactions on Vehicular Technology*, Vol. 46, No. 1, pp. 176-184, Feb. 1997.

[18] J. Salz and J. Winters, "Effect of Fading Correlation on Adaptive Arrays in Digital Mobile Radio," *IEEE Transactions on Vehicular Technology*, Vol. 43, No. 4, pp. 1049-1057, Nov. 1994.

[19] M. Jacobson, "Space-Time Correlation in Spherical and Circular Noise Fields," *The Journal of the Acoustical Society of America*, Vol. 34, No. 7, pp.971-978, Jul. 1962.

[20] B. Cron and C. Sherman, "Spatial-Correlation Functions for Various Noise Models," *The Journal of the Acoustical Society of America*, Vol. 34, No. 11, pp.1732-1736, Nov. 1962.

[21] B. Fleury, "First- and Second-Order Characterization of Direction Dispersion and Space Selectivity in the Radio Channel," *IEEE Transactions on Information Theory*, Vol. 46, No. 6, pp. 2027-2044, Sep. 2000.

[22] K. Pedersen, P. Mognesen, and B. Fleury, "Power Azimuth Spectrum in Outdoor Environments," *Electronics Letters*, Vol. 33, No. 18, pp. 1583-1584, Aug. 1997.

[23] K. Pedersen, P. Mognesen, and B. Fleury, "Spatial Channel Characteristics in Outdoor Environments and their Impact on the BS Antenna System Performance," in *IEEE Vehicular Technology Conf.*, 1998, pp. 719-723.

[24] T. Trump and B. Ottersten, "Estimation of nominal direction of arrival and angular spread using an array of sensors," *Signal Processing*, Vol. 50, pp. 57-69, 1996.

[25] O. Besson and P. Stoica, "Decoupled Estimation of DOA and Angular Spread for a Spatially Distributed Source," *IEEE Transactions on Signal Processing*, Vol. 48, No. 7, July 2000.

[26] J. Wang, M.K. Simon, M.P. Fitz and K. Yao, "On the Performance of Space-Time Codes over Correlated Rayleigh Fading Channels," *IEEE Transactions on Communications*, to appear.

[27] T. Lo, "Maximum Ratio Transmission," *IEEE Transactions on Communications*, Vol. 47, No. 10, October 1999.

[28] J. K. Cavers, "Single-User and Multiuser Adaptive Maximal Ratio Transmission for Rayleigh Channels," *IEEE Transactions on Vehicular Technology*, Vol. 49, No. 6, November 2000.

[29] G. Jongren et al., "Combining Beamforming and Orthogonal Space-Time Block Coding," *IEEE Transactions on Information Theory*, Vol. 48, No. 3, March 2002.

[30] S. Zhou and G. Giannakis, "Optimal Transmitter Eigen-Beamforming and Space-Time Block Coding Based on Channel Mean Feedback," *IEEE Transactions on Signal Processing*, Vol. 50, No. 10, Oct. 2002.

[31] S. Zhou and G. Giannakis, "Optimal Transmitter Eigen-Beamforming and Space-Time Block Coding Based on Channel Correlations," *IEEE Transactions on Information Theory*, Vol. 49, No. 7, July 2003.

[32] S. Alamouti, "A Simple Transmit Diversity Technique for Wireless Communications," *IEEE Journal on Selected Areas in Communications*, Vol. 16, No. 8, October 1998.

[33] V. Tarokh et al., "Space-Time Block Coding for Wireless Communications: Performance Results," *IEEE Journal on Selected Areas in Communications*, Vol. 17, No. 3, March 1999.

[34] V. Tarkokh et al., "Space-Time Block Codes from Orthogonal Designs," *IEEE Transactions on Information Theory*, Vol. 45, No. 5, July 1999.

[35] M.O. Damen, K. Abed-Meraim and J.-C. Belfiore, "Diagonal Algebraic Space-Time Block Codes," *IEEE Transactions on Information Theory*, Vol. 48, No. 3, pp. 628-636, March 2002.

[36] B.M. Hochwald and W. Sweldens, "Differential Unitary Space-Time Modulation," *IEEE Transactions on Communications*, Vol. 48, No. 12, pp. 2041-2052, December 2000.

[37] B.L. Hughes, "Differential Space-Time Modulation", *IEEE Transactions on Information Theory*, Vol. 46, pp. 2567-2578, November 2000.

[38] V. Tarokh and H. Jafarkhani, "A Differential Detection Scheme for Transmit Diversity," *IEEE Journal on Selected Areas in Communications*, Vol. 18, pp. 1169-1174, July 2000.

[39] W. Su and X.-G. Xia, "On Space-Time Block Codes from Complex Orthogonal Designs," *Wireless Personal Communications*, Vol. 25, No. 1, pp. 1-26, 2003.

[40] W. Su, Z. Safar and K.J.R. Liu, "Space-Time Signal Design for Time-Correlated Rayleigh Fading Channels," in *Proceedings of the IEEE International Conference on Communications*, Vol. 5, pp. 3175-3179, May 2003.

[41] S.M. Kay, *Fundamentals of Statistical Signal Processing, Volume II*, Prentice-Hall, 1998.

[42] J.W. Craig, "A New, Simple and Exact Result for Calculating the Probability of Error for Two-Dimensional Signal Constellations," in *IEEE MILCOM Conf. Rec.*, Boston, MA, 1991.

[43] G.L. Turin, "The Characterisitic Function of Hermitian Quadratic Forms in Complex Normal Variables," *Biometrika*, pp. 199-201, 1960.

[44] S. Siwamogsatham, M.P. Fitz and J.H. Grimm, "A New View of Performance Analysis of Transmit Diversity Schemes in Correlated Rayleigh Fading," *IEEE Transactions on Information Theory*, Vol. 48, No. 4, Apr. 2002.

[45] H. Shin and J. Lee, "Exact Symbol Error Probability of Orthogonal Space-Time Block Codes," *IEEE Global Telecommunications Conference*, Taipei Taiwan, Nov. 2002.

[46] H. Shin and J. Lee, "On the Error Probability of Binary and M-ary Signals in Nakagami-m Fading Channels,"

[47] X. Li et al., "A Squaring Method to Simplify the Decoding of Orthogonal Space-Time Block Codes," *IEEE Transactions on Communications*, Vol. 49, No. 10, October 2001.

[48] W.H. Beyer, *CRC Standard Mathematical Tables*, CRC Press, 1978.

[49] M. Biguesh et al., "BER Improvement in a TDMA/FDMA Cellular System Using Antenna Array," in *Asilomar Conference on Signals, Systems, and Computers*, Vol. 1, Oct. 1999.

[50] B. Noble and J.W. Daniel, *Applied Linear Algebra*, Prentice-Hall, 1988.

[51] Hans Steyskal, "Synthesis of Antenna Patterns with Prescribed Nulls," *IEEE Transactions on Antennas and Propagation*, Vol. AP-30, Mar. 1982.

[52] J. Capon, "High-Resolution Frequency-Wavenumber Spectrum Analysis," *Proceedings of the IEEE*, Vol. 37, Aug. 1969.

[53] D.H. Johnson and D.E. Dudgeon, *Array Signal Processing*, Prentice-Hall, 1993.

[54] R. Monzingo and T. Miller, *Introduction to Adaptive Arrays*, J. Wiley & Sons, 1980.

[55] S. Haykin, *Adaptive Filter Theory*, Prentice-Hall, 2002.

[56] J. Winters, "Optimum Combining in Digital Mobile Radio with Cochannel Interference," *IEEE Journal on Selected Areas in Communications*, Vol. SAC-2, No. 4, pp. 528-539, July 1984.

[57] J. Winters, "Signal Acquisition and Tracking with Adaptive Arrays in the Digital Mobile Radio System IS-54 with Flat Fading," *IEEE Transactions on Vehicular Technology*, Vol. 42, No. 4, pp. 377-384, Nov. 1993.

[58] J. Winters, J. Salz and R. Gitlin, "The Impact of Antenna Diversity on the Capacity of Wireless Communication Systems," *IEEE Transactions on Communications*, Vol. 42, No. 2, pp. 1740-1751, Feb. 1994.

[59] J. Winters and J. Salz, "Upper Bounds on the Bit Error Rate of Optimum Combining in Wireless Systems," in *IEEE Vehicular Technology Conference*, Vol. 2, pp.942-946, 1994.

[60] D. Luenberger, *Optimization by Vector Space Methods*, J. Wiley & Sons, 1969.

[61] J. Yang and A. Swindlehurst, "The Effects of Array Calibration Errors on DF-Based Signal Copy Performance," *IEEE Transactions on Signal Processing*, Vol. 43, No. 11, Nov. 1995.

[62] F. Qian and B. Van Veen, "Quadratically Constrained Adaptive Beamforming for Coherent Signals and Interference," *IEEE Transactions on Signal Processing*, Vol. 43, No. 8, 1995.

[63] H. Cox, "Resolving Power and Sensitivity to Mismatch of Optimum Array Processors," *Journal of the Acoustic Society of America*, Vol. 54, No. 3, 1973

[64] P. Lancaster and M. Tismenetsky, *The Theory of Matrices with Applications*, Academic Press, 1985.

[65] L. Younkins, W. Su and K.J.R. Liu, "On the Robustness of Space-Time Coding for Spatially and Temporally Correlated Wireless Channels," *IEEE Wireless Communications and Networking Conference*, 2004.

[66] L. Younkins, W. Su and K.J.R. Liu, "On the Performance of Orthogonal Space-Time Block Codes for Spatially and Temporally Correlated Wireless Channels," *IEEE Vehicular Technology Conference*, 2004.

[67] L. Younkins, W. Su and K.J.R. Liu, "On the Robustness of Space-Time Coding Techniques Based on a General Space-Time Covariance Model," *IEEE Transactions on Vehicular Technology*, accepted for publication.

[68] L. Younkins, W. Su and K.J.R. Liu, "A Comparison of Space-Time Coding and Beamforming Techniques for Wireless Communications," *IEEE Transactions on Vehicular Technology*, submitted.